

**POLITECNICO DI TORINO**



Corso di Laurea Magistrale in Ingegneria Aerospaziale

Tesi di Laurea Magistrale

# **Design and development of a fluid system for a resonant igniter**

**Advisor**

Prof. Dario Giuseppe Pastrone

**Supervisor**

M. Sc. Paul Lungu

**Author**  
Simone Elia





# Masterarbeit

## Design and development of a fluid system for a resonant igniter

**Author:** Elia, Simone

**Supervisor:** Lungu, Paul, M. Sc.

**Issued:** 19.03.2018

**Submitted:** 16.10.2018



## Declaration of Authorship

Name: **Elia Simone**

I hereby declare that this thesis is my own work prepared without the help of a third party. No other than the listed literature and resources have been used. All sources transferred literally or analogously to this work have been labeled accordingly.

Additionally, I hereby certify that this thesis has not been underlain in any other examination procedure up to the present.

.....  
Date, Sign



# Abstract

The purpose of this thesis is the design process and development of a fluid system dedicated to supply a resonance igniter for use in satellite and upper stage propulsion applications. First of all, an overview of the main characteristics and fundamentals of resonance ignition is pointed out. Secondly, a test campaign is analysed with regards to the main parameters affecting resonance ignition. According to experimental results and igniter design data, a blowdown calculation model for the fluid system design and sizing is presented. Particular attention is paid on assumptions taken and equations used in order to dimension blowdown tanks. Afterwards results of a blowdown test campaign conducted are considered, aiming to validate the calculation model previously addressed. Based on this, an improved model is obtained, with whom the final fluid system blowdown tanks are designed. Furthermore the tanks filling issue is discussed. Finally, considering resonance ignition future improvements, a possible integration solution of the designed fluid system in a spacecraft is proposed.

# Contents

<b>1</b>	<b>Introduction</b>	<b>1</b>
<b>2</b>	<b>Resonance Ignition</b>	<b>2</b>
2.1	Fundamentals . . . . .	2
2.1.1	Resonance main parameters . . . . .	5
2.2	Preceding igniter developments . . . . .	7
2.3	Resonance Igniter Design for GCH <sub>4</sub> /GOX . . . . .	9
2.3.1	Cold Flow . . . . .	12
2.3.2	Hot Flow . . . . .	13
2.4	Pressure regulated test campaign . . . . .	14
2.4.1	Experimental set-up: pressure regulated supply system . . . . .	14
	Control sequence . . . . .	15
2.4.2	Pressure regulated Cold Flow test campaign . . . . .	18
2.4.3	Pressure regulated Hot Flow test campaign . . . . .	21
2.4.4	Pressure regulated Cold Flow test campaign after resonant repair . . . . .	23
<b>3</b>	<b>Fluid system design</b>	<b>25</b>
3.1	Feed systems . . . . .	25
3.2	Blowdown: variation of properties in a vessel discharge . . . . .	30
3.2.1	Mathematical procedure . . . . .	31
	Flow equations depending on time . . . . .	33
3.2.2	Preliminary Blowdown output . . . . .	35
3.3	Blowdown system sizing . . . . .	37
3.4	Tanks sizing . . . . .	44
3.4.1	Propellants Properties . . . . .	44
	Size and Shape of propellant Tanks . . . . .	44
	Mathematical analysis in the sizing of spherical tanks . . . . .	45

---

<b>4</b>	<b>Blowdown test campaign</b>	<b>54</b>
4.1	Experimental setup: blowdown supply system . . . . .	54
4.1.1	Control sequence . . . . .	56
4.2	Blowdown Cold Flow test campaign . . . . .	58
4.3	Calculation model validation with experiments . . . . .	61
	Oxygen validation . . . . .	61
	Methane validation . . . . .	63
	Isothermal model: losses addition . . . . .	65
4.3.1	Oxidizer to fuel ratio calculation . . . . .	66
<b>5</b>	<b>Tank design for spacecraft</b>	<b>71</b>
5.1	Tank optimisation . . . . .	71
5.1.1	Results check . . . . .	75
<b>6</b>	<b>Tank heating and filling</b>	<b>78</b>
<b>7</b>	<b>Conclusions and future prospects</b>	<b>84</b>
<b>A</b>	<b>Appendix</b>	<b>89</b>
A.1	Function for Cold Flow Blowdown calculations - Adiabatic Model . . . . .	89
A.2	Function for Cold Flow Blowdown calculations - Isothermal Model . . . . .	93
A.3	Function for tanks sizing calculations - Isothermal Model . . . . .	98
A.4	Function for Heating calculations . . . . .	102

# List of Figures

2.1	Original resonator experiment by Sprenger [1]	3
2.2	Classical nozzle-resonator configuration with resonator cavity and underexpanded nozzle flow [2]	3
2.3	Achievable heating rates for various types of gases [3]	5
2.4	Rocketdyne reference design for a resonance igniter [4]	7
2.5	Kerosene/oxygen resonance igniter implemented by Kessaev. Et. Al. [5]	8
2.6	Coaxial hydrogen/oxygen resonance igniter [6]	9
2.7	Z1 resonance igniter [2]	10
2.8	Z2 resonance igniter	11
2.9	Pressure regulated supply system for tests	14
2.10	Pressure regulated supply system symbols legend	15
2.11	Resonator temperature dependent on time	18
2.12	Thermocouple position	19
2.13	Resonator maximum temperature over supply pressure for various $s/d$ ratio	19
2.14	Resonator temperature over time for different values of oxygen supply pressure	20
2.15	Chamber pressure (a) and resonator temperature (b) during a Hot Flow test	22
2.16	Resonator temperature over time - $s/d = 1.525$	23
2.17	Resonator maximum temperature dependent on $s/d$ ratio	24
3.1	Simplified design of the rocket engine fluid system	27
3.2	Fluid systems device legend	28
3.3	Igniter fluid system design	29
3.4	Properties over time	35
3.5	Nozzle pressure ratio over time	36
3.6	Pressure comparison	36
3.7	Pressure over time OXYGEN: time ignition and upstream pressure	38
3.8	Pressure over time METHANE: time ignition and upstream pressure	38
3.9	Pressure over time	40

---

3.10	Temperature over time . . . . .	41
3.11	Gas mass over initial pressure in the tank . . . . .	42
3.12	Volume over initial pressure in the tank . . . . .	43
3.13	Pressure forces distribution in a spherical shape [25] . . . . .	45
3.14	Agent pressure on half spherical cap [25] . . . . .	46
3.15	Effect of pressure on structural mass for various materials - OXYGEN . . .	49
3.16	Effect of pressure on structural mass for various materials - METHANE . .	49
3.17	Effect of volume on structural mass for various materials - OXYGEN . . .	50
3.18	Effect of volume on structural mass for various materials - METHANE . .	50
3.19	Effect of pressure on wall thickness for various materials - OXYGEN . . . .	51
3.20	Effect of pressure on wall thickness for various materials - METHANE . . .	51
3.21	Effect of volume on tank radius - OXYGEN . . . . .	52
3.22	Effect of volume on tank radius - METHANE . . . . .	52
4.1	Blowdown supply system for tests . . . . .	55
4.2	Blowdown supply system symbols legend . . . . .	55
4.3	Resonator temperature over time . . . . .	58
4.4	Pressure over time - experimental data . . . . .	59
4.5	Resonator maximum temperature over measured pressure . . . . .	60
4.6	Blowdown models comparison with experimental data - $P_0 = 35 \text{ bar}$ . . . .	61
4.7	Blowdown models comparison with experimental data - $P_0 = 26 \text{ bar}$ . . . .	63
4.8	Pressure over time - experimental data . . . . .	64
4.9	Pressure over time - models comparison plus losses: oxygen . . . . .	65
4.10	Pressure over time - models comparison plus losses: methane . . . . .	65
4.11	Oxygen mass flow comparison . . . . .	67
4.12	Methane mass flow comparison . . . . .	68
4.13	Pressure over time during igniter operation time . . . . .	69
4.14	Oxidizer to fuel ratio over time . . . . .	69
5.1	Temperature over time . . . . .	72
5.2	Pressure over time for different $P_0$ . . . . .	72
5.3	Pressure over time - igniter operation time . . . . .	73
5.4	Oxidizer to fuel ratio . . . . .	74
5.5	Gas mass over initial tank pressure . . . . .	76
5.6	Structural mass over initial tank pressure . . . . .	76
5.7	Tank volume over initial tank pressure . . . . .	77
6.1	Extract from fluid system . . . . .	78

---

6.2	Thermal power over time - $t_h = 10\text{ s}$ . . . . .	81
6.3	Thermal power over time - $t_h = 10\text{ s}$ . . . . .	81
6.4	Thermal power over pressure . . . . .	82
6.5	Thermal power over pressure . . . . .	82
6.6	Thermal power over LOX temperature - $t_h = 10\text{ s}$ . . . . .	83
6.7	Thermal power over LCH4 temperature - $t_h = 10\text{ s}$ . . . . .	83

# List of Tables

2.1	Igniter design data . . . . .	12
2.2	Pressure regulated Cold Flow sequence . . . . .	16
2.3	Pressure regulated Hot Flow Sequence . . . . .	17
2.4	Pressure regulated Hot Flow test results . . . . .	21
2.5	Resonator maximum temperature measured in Kelvin - $t_{ph} = 5 s$ . . . . .	24
3.1	Pressure and time constraint values . . . . .	39
3.2	Optimum values . . . . .	42
3.3	Materials properties [7] . . . . .	48
3.4	Structural optimum values . . . . .	53
4.1	Experimental setup values . . . . .	54
4.2	Blowdown Cold Flow sequence . . . . .	56
4.3	Maximum resonator temperature for initial pressure in the blowdown tank	59
4.4	O/F calculation parameters . . . . .	67
4.5	Igniter supply pressure values . . . . .	70
5.1	Tanks design values . . . . .	75
5.2	Tanks design values - Thickness correction . . . . .	77
6.1	Liquid propellant characteristics . . . . .	80
6.2	Heating results - $t_h = 10 s$ . . . . .	80

# Nomenclature

## List of Symbols and Variables

$s/d$	[—]	Resonator distance divided by the nozzle diameter
$s$	[ $mm$ ]	Distance between resonator and cavity
$d$	[ $mm$ ]	Diameter nozzle
$O/F$	[—]	Oxidizer to fuel ratio
$p_e$	[ $bar$ ]	Downstream nozzle static pressure
$p_e$	[ $bar$ ]	Upstream nozzle static pressure
$T_{BMVO}$	[ $K$ ]	Temperature Before Methane Valve Opening
$d_{CH_4}$	[ $mm$ ]	Methane nozzle diameter
$P_{O_2}$	[ $bar$ ]	Oxygen supply pressure
$P_{CH_4}$	[ $bar$ ]	Methane supply pressure
$t_{ph}$	[ $s$ ]	Preheating time
$P_{chamber}$	[ $bar$ ]	Chamber pressure
$A_t$	[ $mm^2$ ]	Nozzle throat area
$P^*$	[—]	Dimensionless pressure
$P_{cri}^*$	[—]	Dimensionless critical pressure
$T^*$	[—]	Dimensionless temperature
$\rho^*$	[—]	Dimensionless density
$P_e^*$	[—]	Dimensionless downstream pressure
$\dot{m}^*$	[—]	Dimensionless mass flow rate
$t^*$	[—]	Dimensionless time
$t_{char}^*$	[—]	Characteristic time
$k$	[—]	Specific heat ratio
$R$	[ $J/Kg/K$ ]	Gas constant
$C_p$	[ $J/Kg/K$ ]	Specific heat
$P_{up}$	[ $bar$ ]	Nozzle upstream pressure

## NOMENCLATURE

---

$t_{up}$	[s]	Upstream time referred to the nozzle upstream pressure
$C_D$	[—]	Discharge orifice coefficient
$P_0$	[bar]	Initial pressure in the tank
$T_0$	[K]	Initial temperature in the tank
$\rho_0$	[kg/m <sup>3</sup> ]	Initial density in the tank
$V_0$	[L]	Tank volume
$M$	[g]	Gas mass in the tank
$M_{structural}$	[g]	Structural mass of the tank
$th$	[mm]	Thickness of the tank walls
$r$	[mm]	Tank radius
$S_y$	[—]	Safety factor
$\sigma_y$	[MPa]	Ultimate yield stress
$\rho_{material}$	[Kg/m <sup>3</sup> ]	Material density
$T_{MAX}$	[K]	Maximum resonator temperature
$T_{res}$	[K]	Resonator temperature
$\Delta h$	[J]	Enthalpy
$T_f$	[K]	Final temperature
$T_i$	[K]	Initial temperature
$m_p$	[g]	Propellant mass
$TP$	[Watt]	Thermal Power
$T_{liquid}$	[K]	Liquid propellant temperature
$T_{boiling}$	[K]	Boiling temperature @ 20 bar
$t_h$	[s]	Heating time
$\Delta H_{evap}$	[J/K]	Latent Heat of Evaporation
$T_{design}$	[K]	Design temperature

## Abbreviations

MMH	Monomethylhydrazine
TUM	Technische Universität München
LTF	Institute for Flight Propulsion
NPR	Nozzle pressure ratio
GOX	Gaseous Oxygen
LOX	Liquid Oxygen
LCH <sub>4</sub>	Liquid Methane
GCH <sub>4</sub>	Gaseous Methane
JIM	Jet Instability Mode
JRM	Jet Regurgitant mode
JSM	Jet Screech Mode
NPR	Nozzle Pressure Ratio
MVN1	Magnetic Valve Nitrogen directly after pressure regulator
MVO1	Magnetic Valve Oxygen directly after pressure regulator
MVF1	Magnetic Valve Methane directly after pressure regulator
MVN2	Magnetic Valve Nitrogen referred to main valve with actuator
MVO2	Magnetic Valve Oxygen referred to main valve with actuator
MVF2	Magnetic Valve Methane referred to main valve with actuator
PR	Pressure Ratio
CPR	Critical Pressure Ratio
EU REACH	European Regulation
Z1	Igniter 1 (Configuration 2)
Z2	Igniter 2
StD	Strength to density ratio

# Chapter 1

## Introduction

In-orbit propulsion systems based on Hydrazine and its derivatives have been used for more than 50 years [8]. Since MMH is found to be a substance with a high toxic content, has been named by the EU REACH framework as a "substance of very high concern" [8]. As a consequence of this, the European space industry has started to look for new "green" solutions, as well as new combinations of propellants able to replace the current ones with good performance. This represents a great challenge because, as far as they are toxic substances, they have high reliability and excellent storability [9].

Although alternative, storable high-performance bipropellants exist, a number of key issues have to be resolved before system integrators are able to adapt this new technology [9]. One of the main challenges common to all green bipropellants is their need for a dedicated ignition system. Therefore, the Institute for Flight Propulsion (LTF) investigates Resonance Ignition methods, as these have the potential to create a passive, lightweight and extremely reliable ignition system. Furthermore various aspects of the propellants LOX/LCH<sub>4</sub> for use in satellite and upper stage propulsion applications are investigated. Previous testing campaigns have been conducted at the Technische Universität München (TUM) providing promising results. An operational envelope was defined and validated for the ignition system called Z1, allowing reliable ignitions with delay times below 150 ms [2]. In addition, a smaller igniter, called Z2, is currently being studied. This is how the need to design and develop a fluid system capable of powering this type of ignition systems arises. This thesis therefore aims to propose a suitable feed supply system based on the requirements of the igniter Z2, suggesting a possible implementation within a spacecraft. The design and development of such a fluid system aims to be done in the simplest, most reliable and lightest way. A blowdown supply system meets these requirements, therefore a blowdown calculation model is used in this thesis and it is validated with the help of a blowdown test campaign.

## Chapter 2

# Resonance Ignition

Within the field of study of methane oxygen mixtures for space propulsion as green propellants, the need for a dedicated ignition system arises, as they are not able to self-ignite. For satellite propulsion systems with mission durations of more than 10 years and millions of engine cycles the options are very limited [5]. To meet this requirement a valid ignition system is represented by a device called resonant igniter, or by an ignition system that uses the effect of resonance heating to heat a gas mixture up to the ignition temperature. So, in the present chapter, the basis of resonance heating are explained and a short overview of historical resonance ignition developments is given, which provides some context for the current developments [5].

## 2.1 Fundamentals

During pitot-tube pressure-measurements in under-expanded free-stream jets Hartmann discovered, that strong pressure oscillations inside a tube can be started at certain nozzle-tube distances [10]. This mechanism was later used for high power sound producing systems [11] and became known as the Hartmann-Whistle. Discovered in 1922, it is still subject to research for use as powerful ultrasonic actuator in modern active flow control employments.

After that Sprenger discovered, that the Hartmann-Whistle are also able to produce relevant thermal effects, if cavities are built with low conductivity material [1]. In the simple but demonstrative experiment shown in figure 2.1 he demonstrated that cavities constituted of wood can quickly be ignited with pressurized air. This type of configuration was later named Hartmann-Sprenger Tube. The dissipative heating produced is attributed, like Hartmann suggested, to shockwaves traveling inside the cavity. Other researchers concluded that wall friction can make a considerable contribution to the heating effect, but a

complete description of the flow phenomena has to be found yet [5].

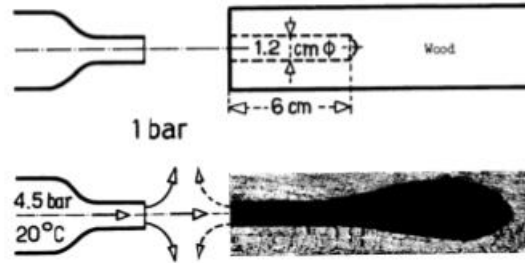


**Figure 2.1:** Original resonator experiment by Sprenger [1]

Consequently the main principle of resonance ignition systems consists of a pressurized gas flowing through a nozzle generating an under-expanded jet directed towards a resonator cavity to generate a Mach disk at the inlet of the cavity in which resonance occurs [2], as shown in figure 2.2.

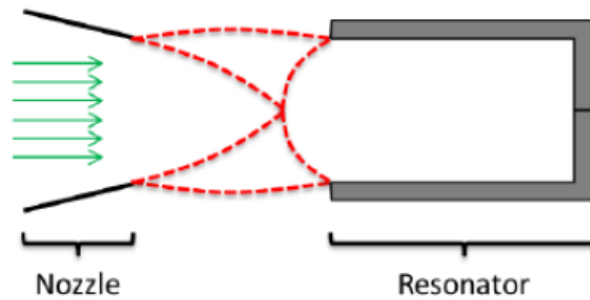


**Figure 2.2:** Classical nozzle-resonator configuration with resonator cavity and underexpanded nozzle flow [2]

As regards to oscillation, one of the most conclusive studies has been conducted by Sarohia and Back [12], who identified the main oscillation types occurring inside the resonator cavity.

They identify three oscillation modes which imply different macroscopic thermal effects. The first one is the **Jet Instability Mode (JIM)** which only occurs at subsonic nozzle pressure ratios and is related to vortex shedding originating from the nozzle lip. Since neither large heating effects nor relevant pressure amplitudes are generated it is not of further interest [8].

Then in **Jet Regurgitant Mode (JRM)** a series of weak compression waves enters the cavity. If the resonator is long enough these can coalesce and form strong shocks, with pressures exceeding the nozzle total pressure and falling below ambient pressure. This

causes almost complete emptying and re-filling of the cavity during a single flow cycle. Although this cycle is characterized by the fundamental frequency of the resonator, in- and outflow phases have different durations. A portion of the fluid near the closed end of the tube remains in the resonator and is repeatedly compressed and expanded, causing gradual heating through irreversible effects. Consequently, no considerable heating rates can be observed for short resonators, as weak compression waves compress and expand the gas almost isentropically [8].

The **Jet Screech Mode (JSM)** is characterized by relatively weak pressure oscillations at frequencies considerably higher than the fundamental frequency of the resonator. Compared to JRM mass exchange between cavity and surrounding fluid is strongly reduced. Often an almost normal shock between resonator and nozzle can be observed, axially oscillating at high frequencies. Under certain conditions and for short resonators strong heating at local node points can be observed, suggesting that standing waves are present within the cavity. In JSM Sarohia and Back observed considerable gas heating only for short resonators, longer resonators remained at almost ambient temperatures. This observation has been confirmed by investigations at LTF, but currently no satisfying explanation for this behavior exists [8].

### 2.1.1 Resonance main parameters

Among the most important influences on the oscillation mode there are the geometrical parameters of a resonance system: Nozzle diameter  $d$ , distance between resonator and nozzle  $s$ , resonator geometry (form, diameter, length), and thermodynamic properties of the operating gas: Speed of sound, heat capacity, density and supply pressure. From these values, two important non-dimensional properties are deduced: The  $s/d$  ratio (resonator distance divided by the nozzle diameter) and the nozzle pressure ratio (NPR). The NPR is defined in equation 2.1, where  $p_e$  is the downstream static pressure and  $p_n$  is the feed pressure upstream of the nozzle or the total pressure in the nozzle exit plane, assuming isentropic expansion [2].

$$NPR = \frac{p_n}{p_e} \quad (2.1)$$

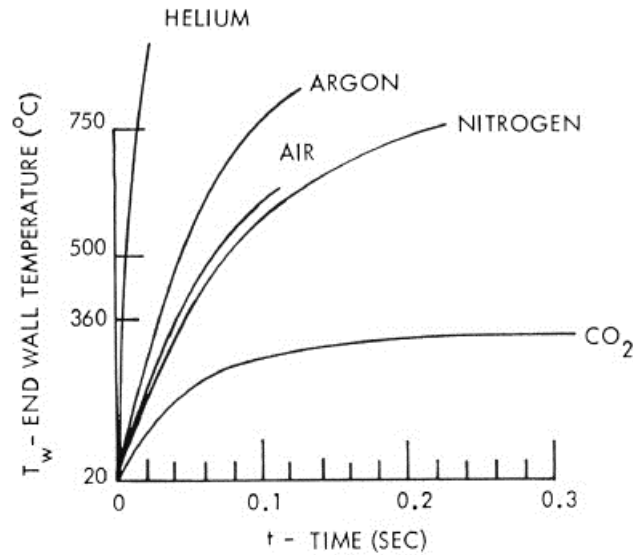


**Figure 2.3:** Achievable heating rates for various types of gases [3]

The severe impact of the operating gas on the heating process is exemplified in figure 2.3 [3].

When the NPR is increased beyond the critical limit, an underexpanded free-stream jet with the typical diamond or barrel-shock structure is generated. Under these conditions, depending on the nozzle-resonator distance  $s$ , a transition to the Jet Regurgitant Mode (JRM) is possible, which can be characterized by two distinct phases [9]. During the inflow phase the free-stream enters the cavity almost unobstructed, creating a series of pressure waves which travel inside the cavity towards the closed end. Given sufficient cavity length, these waves coalesce to a single shockwave, which is reflected at the closed resonator end.

When this shock reaches the open cavity end, strong expansion waves start traveling into the cavity, marking the transition to the outflow phase. During this period the gas leaves the resonator with considerable velocity, displacing the nozzle free-stream upstream. Once the cavity has been emptied, a new inflow cycle starts. It is worth noting that the static pressure inside the cavity can exhibit values exceeding the total pressure of the nozzle and fall below ambient pressure. These strong oscillations occur with approximately the acoustic fundamental frequency of the cavity, but strong non-linear effects can lead to considerable deviations. If the cavity is long enough, a small fraction of the resonance gas remains in the cavity, undergoing repeated compressions and expansions, causing gradual heating due to irreversible effects. If the NPR or nozzle-resonator distance is changed a sudden switch to Jet Screech Mode (JSM) can occur [9].

## 2.2 Preceding igniter developments

Even though the details of the flow phenomena occurring inside Hartmann-Sprenger Tubes are far from completely understood, a wealth of experimental studies allows selecting proven parameter combinations and thus designing practical applications.

**A. Rocketdyne, 1973** During the pre-development phase for the Space Shuttle this principle was applied for designing a resonance igniter for a possible hydrogen/oxygen based Auxiliary Propulsion System. A considerable number of investigations in this direction pursued [13] [14] [15] [4], concluding that resonance igniters offer considerable weight savings compared to electrical spark igniters. Even though the reference igniter design was quite advanced and reliable ignition at cryogenic conditions was demonstrated, the program was later discontinued. Their design, depicted in Figure 2.4, featured a simple convergent nozzle, generating an underexpanded hydrogen free-stream jet impinging on a stepped cavity resonator.

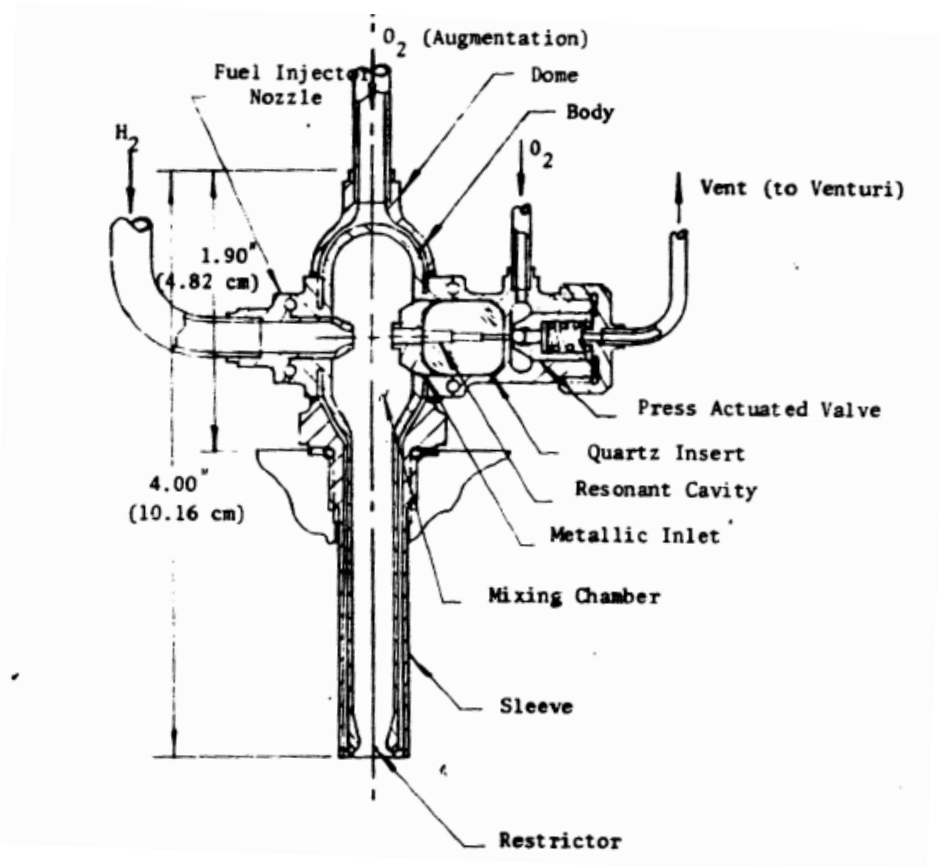
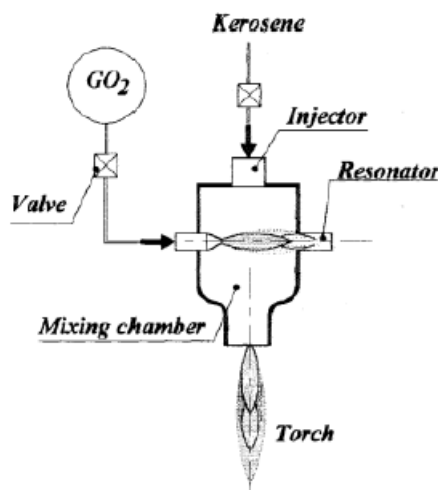


Figure 2.4: Rocketdyne reference design for a resonance igniter [4]

When enough hot hydrogen is produced by resonant heating at the cavity bottom, oxygen would be introduced through a pressure-actuated valve, starting the combustion and generating a torch sufficiently strong for igniting the main combustion chamber. This "staggered" introduction of the propellants became common for all later developments. The restrictor orifice was designed to maintain sonic conditions during resonant heating, which was necessary for maintaining a constant NPR by decoupling the mixing chamber from the downstream combustion chamber. This increased however the required supply pressure, requiring additional, rechargeable high-pressure tanks for pump-fed engines, while the pressure-actuated valve in the high-temperature region of the resonator reduced the reliability of the otherwise completely passive device [5].

**Kessaev et. Al., 2000** In an effort to create an igniter for a restartable rocket engine the group around Kessaev developed, implemented and tested a "staggered" resonance torch igniter for GOX/Kerosene [5], a concept proposed by him in a book chapter [16]. In contrast to earlier designs oxygen is used as resonance gas, which supposedly requires more sophisticated cavity designs, due to the lower heating rates compared to those of hydrogen.



**Figure 2.5:** Kerosene/oxygen resonance igniter implemented by Kessaev. Et. Al. [5]

Additionally, kerosene is not introduced directly into the resonator, but perpendicular to the oxygen jet. This not only solves the problem of requiring a fragile valve in the hot region of the resonator, but also allows for considerably smaller fuel feed pressures. Reliable ignition was achieved for oxygen inlet pressures as low as 0.8 MPa and igniter preparation times of 0.1 s. However, ignition at these low inlet pressures suggests, that the torch outlet was not implemented as sonic throat, making the igniter susceptible to disturbances intro-

duced through the main combustion chamber. This may cause problems when integrated into the startup sequence of an actual thruster, since changing backpressures caused by purge or chilldown flows may potentially de-tune the system and lead to Failure or delayed ignition [5].

**C. Song et. Al., 2005** Intended for use in a hydrogen/oxygen based orbital maneuvering system for the Chinese space station, a coaxial resonance igniter was developed, built and tested [5] [6] [17]. Due to its compact design, the igniter was to be implemented directly into the thruster faceplate. After hydrogen is heated sufficiently in the tapered resonator, oxygen is introduced in the core of the free-stream jet, leading to ignition. Ground tests with mixture ratios around 0.7 showed ignition delays below 0.2 s. However, no data regarding operation at cryogenic conditions is available.

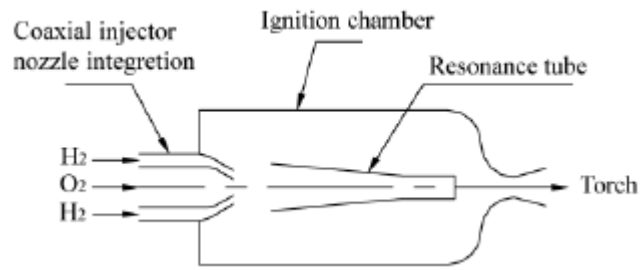


**Figure 2.6:** Coaxial hydrogen/oxygen resonance igniter [6]

Due to the low mass flow rate of the corresponding thruster, the entire hydrogen mass flow was introduced through the igniter, re-using this assembly as injector element, after ignition is achieved. Several variations of this igniter were implemented, spawning a number of patents, including some for air-breathing applications [5].

## 2.3 Resonance Igniter Design for GCH<sub>4</sub>/GOX

Although previous investigations [18], [19], [6] have clearly demonstrated successful resonance ignition, none of these concepts have never been used in actual flight missions.

One reason for this neglect may be the relatively strong sensitivity of the resonator oscillation mode to variations of the nozzle pressure ratio. For this reason, earlier studies investigated possible measures to stabilize the mode of operation for sufficiently large NPR ranges [8], [20]. It could be shown that special nozzle designs can sustain resonant oscillations over a large range of pressure ratios. These investigations have resulted in a novel design for a resonance igniter operated with gaseous oxygen and methane. Details can be

found in [5], where it is designated as 'Configuration 2'. The general concept of a coaxial torch igniter is selected, due to its compact construction. Since the research focus at LTF is concentrated on methane/oxygen rocket engines, the same propellant combination is also selected for the igniter.

Two configurations are investigated at the Institute for Flight Propulsion (LTF) at the Technische Universität München (TUM): a test campaign on the igniter 'Configuration 2', which is actually the Z1 igniter, has been conducted, delivering promising results. An operational envelope was defined and validated at a specific resonator-nozzle distance for the ignition system Z1, allowing reliable ignitions with delay times below 150 ms [2]; the second configuration called Z2 is currently under investigation and a test campaign conducted is presented in the next section.

The design characteristics of the Z1 igniter (Configuration 2) are quite similar to Z2 igniter. They consist of a coaxial injection nozzle (1) for oxygen on the outer and methane on the inner part. A tapered resonator (2) within the igniter pilot chamber is aligned with the injection nozzle as seen in figure 2.7 [2] and figure 2.8, where additionally the nozzle-resonator distance  $s$  and nozzle diameter  $d$  are specified.

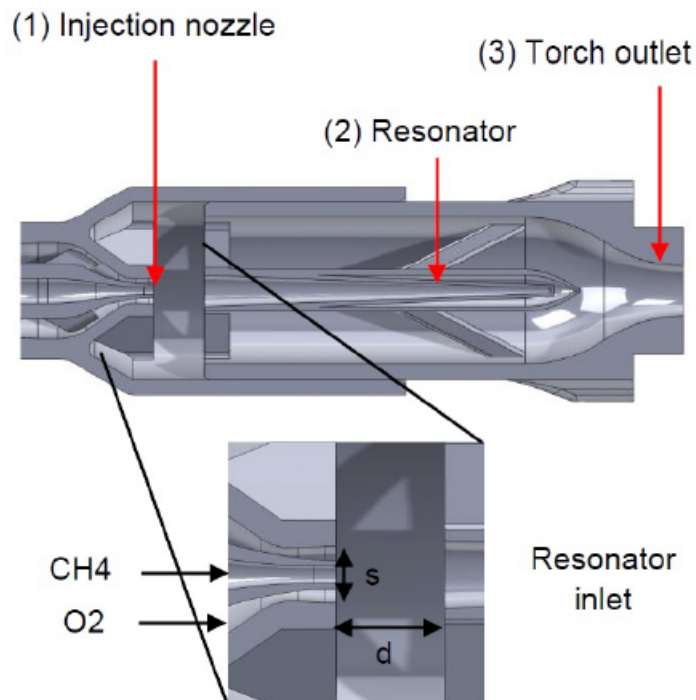


**Figure 2.7:** Z1 resonance igniter [2]

Methane and oxygen nozzle cross sections are designed for ambient pressure during the resonant heat-up process. In the original configuration the oxygen supply pressure and torch outlet (3) were designed to maintain roughly ambient pressure inside the igniter

torch prior to ignition coupling the igniter chamber to the downstream conditions [2]. In  $Z1$  igniter (Configuration 2) and in the  $Z2$  igniter the injection nozzle for  $O_2$  is designed in such a way as to have a choking conditions during operation: this makes the nozzle insensitive to downstream disturbances. With regards to  $Z1$  igniter (Configuration 2), the feed pressure for  $O_2$  is set to have choked cold flow. In addition, the  $Z2$  presented in 2.8, the design and the supply pressures are such as to have choked flow through injection nozzle and through the chamber throat. Since combustion chamber is choked during operation, it allows to get a constant NPR independent of the supply pressure and so that laboratory tests can also be reproduced in vacuum.

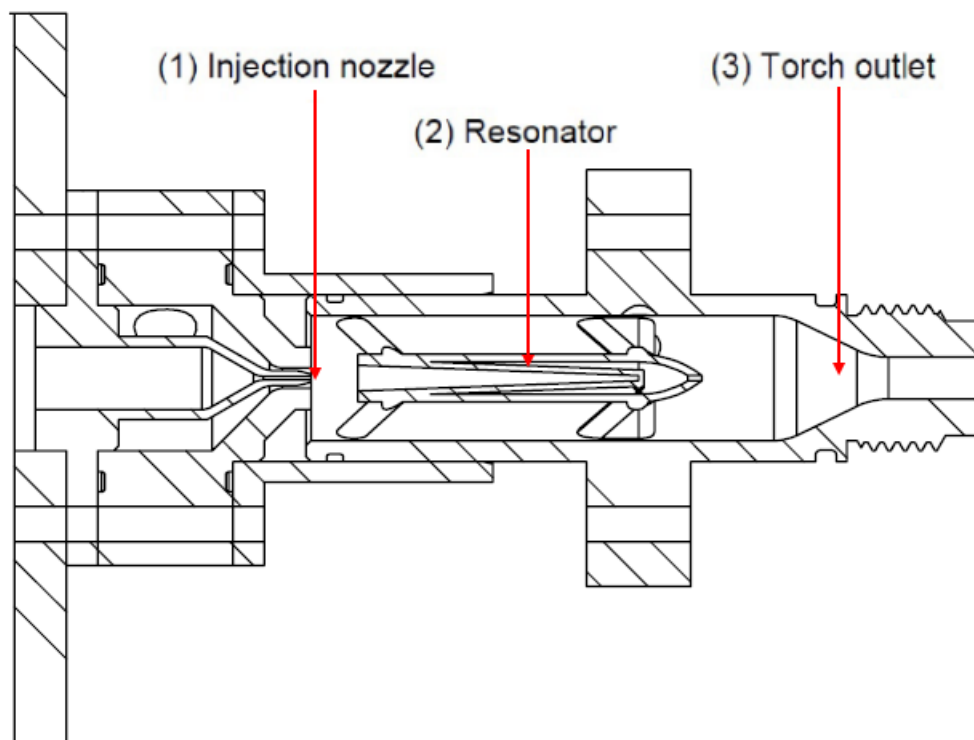


**Figure 2.8:**  $Z2$  resonance igniter

For operation, oxygen is first introduced through the nozzle into the resonator at supersonic velocity. This leads to resonant heating of the oxygen, predominantly near the closed resonator end. Subsequently, methane flows into the resonator, mixes there with the hot oxygen and finally ignition occurs [2].

With reference to these two drawings and in particular to the design parameters, a fluid system can be designed and developed to support these igniters. The design parameters of the  $Z2$  are shown in the table 2.1 and the sizing of the fluid system is done with reference to those parameters as the  $Z2$  is currently under investigation.

To understand which are the basic parameters that affect the design of the fluid supply

system, it is necessary to analyse which parameters are determined in the Cold Flow and Hot Flow phases.

**Table 2.1:** Igniter design data

IGNITER	
$P_{CF} = 200000 [Pa]$	Cold Flow Pressure
$P_{CF} = 550000 [Pa]$	Hot Flow Pressure
$O/F = 30 [-]$	Oxidizer to Fuel ratio
OXYGEN	
$R = 259.8 [J/Kg/K]$	Gas Costant
$T = 298.5 [K]$	Inlet Temperature
$\dot{m} = 6.004548e - 03 [Kg/s]$	Mass Flow Rate
$A_t = 1.562145e - 06 [m^2]$	Throat Area
$k = 1.4 [-]$	Specific Heat Ratio
METHANE	
$R = 518.3 [J/Kg/K]$	Gas Costant
$T = 298.5 [K]$	Inlet Temperature
$\dot{m} = 0.200152e - 03 [Kg/s]$	Mass Flow Rate
$A_t = 1.0557e - 07 [m^2]$	Throat Area
$k = 1.31 [-]$	Specific Heat Ratio

### 2.3.1 Cold Flow

The key to the heating concept is that some of the gas that is trapped within the tube and heated by the first cycle of shock passages will remain in the tube for the second cycle of shock passages etc. Thus, the strength and frequency of the shock waves within the cavity will determine the heating of the indigenous gas. It can be seen that adjusting the cavity relative to the under-expanded jet will produce the variation of temperature. It means that the best distance between resonator and cavity has to be found according to a certain  $NPR$  of the resonating gas ( $O_2$ ). According to this, the Cold Flow aims to define the best  $s/d$  ratio and the oxygen feed pressure that allows to reach in the shortest time possible the ignition temperature through resonance heating. So a Cold Flow test campaign consist to run several Cold Flow with different  $s/d$  ratio and  $P_{O_2}$  with the same injection time and then find the couple  $s/d$  ratio  $P_{O_2}$  that gives the highest temperature. When the best heating performance is achieved, it is assumed that the igniter is operating

in such a condition that the first Mach disk is located around the leading edge of the resonator. This type of situation is precisely sought in Cold Flow test campaign.

### 2.3.2 Hot Flow

Once the boundary conditions were chosen in the cold flow campaign, the next step is to carry out the hot flow. The latter aims to optimize the igniter performance. It consists in determining the minimum preheating time necessary to ignite the  $OX/CH_4$  mixture and the methane supply pressure. An oxidizer to fuel ( $O/F$ ) ratio of 30 has been chosen as nominal since it is sufficiently far away from the lean flammability limit of  $O/F = 36$  but still lean enough so that the resulting hot gas temperatures, compared to rich mixes, allow for a sufficiently long operating time of the ignition system [2].

## 2.4 Pressure regulated test campaign

Before to analyse test campaign results, is presented and explained the experimental set-up of the test rig. This test campaign aims to define the operational envelope of the igniter. The parameter that has to be defined are:

- $s/d$  ratio
- Oxygen supply pressure
- Methane supply pressure
- Preheating time  $t_{ph}$

### 2.4.1 Experimental set-up: pressure regulated supply system

The supply system for the igniter tests shown in figure 2.9 basically consists of the feed lines for the propellants and gaseous nitrogen for purging after the test run.

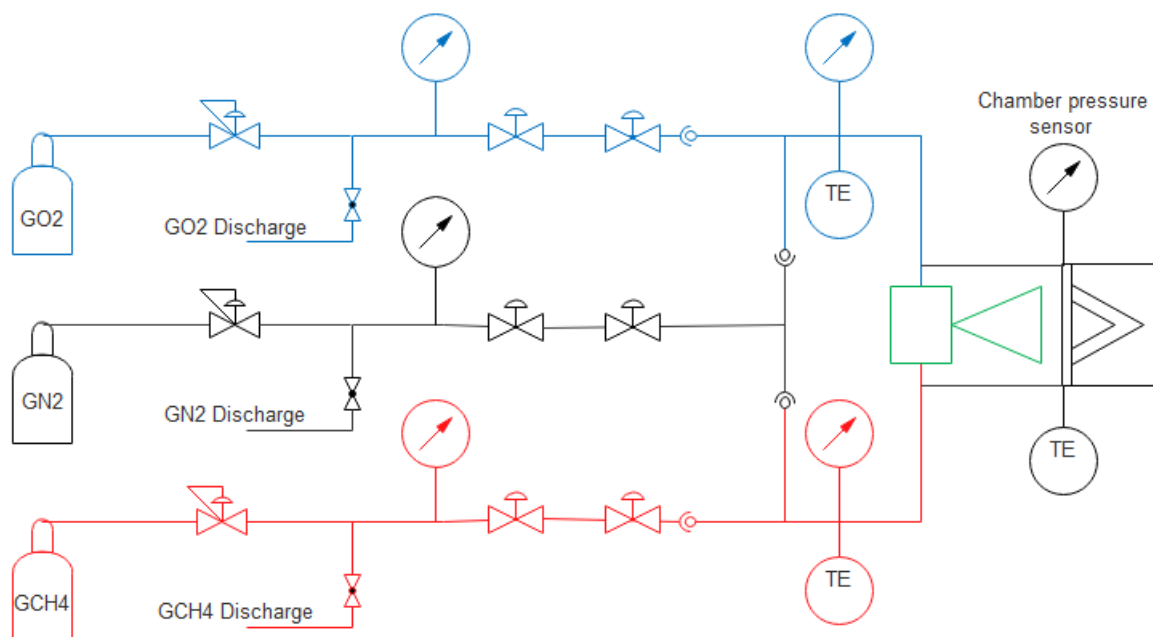


**Figure 2.9:** Pressure regulated supply system for tests

Each line features a pressure regulator with an actuated valve and a downstream valve. The feed line pressure has to be adjusted by the pressure regulators to achieve the desired mass flow rate. These predefined pressures upstream the orifice can variate, due to

boundary layer losses and manufacturing tolerances, which results in a not fully flowed orifice throat. In addition, a discharge valve is located after the pressure regulator in order to de-pressurize every feed line. Check valves prevent the propagation of  $GN_2$  upstream of the feed lines during purge as well as gas flows from one propellant line to the other over the purge line. Temperature and pressure are measured on the oxygen feed line upstream of the injection nozzle, which is designed for choked flow during igniter operation. In addition, a sensor is installed to measure the pressure in the combustion chamber. A thermocouple is installed on the combustion chamber to measure the temperature of the resonator. In figure 2.10 are explained the symbols used in the supply system scheme.

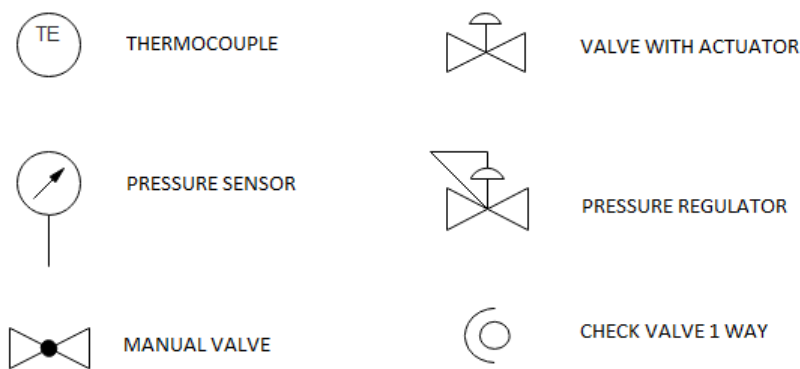


**Figure 2.10:** Pressure regulated supply system symbols legend

### Control sequence

This paragraph aims to a short explanation of the sequence of a cold flow test and an hot flow test. The test sequence is defined by the control of different actuators and valves. The time of action can be set by the GUI of the control program, which allows to set the state of actuators for a given time.

**Cold Flow sequence** In table 2.2 is reported a cold flow sequence example, where it is represented by the use of a binary sequence of 0 and 1. The 0 means closed, while 1 means open.

Below, making reference to acronyms used in table, they correspond to:

- MVN1 = Magnetic Valve Nitrogen directly after pressure regulator
- MVO1 = Magnetic Valve Oxygen directly after pressure regulator
- MVF1 = Magnetic Valve Methane directly after pressure regulator
- MVN2 = Magnetic Valve Nitrogen referred to main valve with actuator

- MVO2 = Magnetic Valve Oxygen referred to main valve with actuator
- MVF2 = Magnetic Valve Methane referred to main valve with actuator

First of all, referring to table 2.2, at  $t = 0$  all valves are closed. Secondly at  $t = 1$  the magnetic valve of oxygen directly after pressure regulator (MVO1) opens and after that also the main valve (MVO2) opens ( $t = 3$ ).

**Table 2.2:** Pressure regulated Cold Flow sequence

Time [s]	MVN1	MVN2	MVO1	MVO2	MVF1	MVF2
0	0	0	0	0	0	0
1	0	0	1	0	0	0
3	0	0	1	1	0	0
8	0	0	1	0	0	0
10	0	0	0	1	0	0
12	1	1	0	0	0	0
14	0	1	0	0	0	0
16	0	0	0	0	0	0

After that, for 5 second they are still open, which is the **preheating** time setted. At  $t = 8$  the main valve (MVO2) is closed and consequently at  $t = 10$  MVO1 is closed and the main valve (MVO2) is opened again to release oxygen. Than the latter is closed and MVN1 and MVN2 are opened at  $t = 12$  to purge the system. Finally at  $t = 14$  MVN1 is closed and consequently at  $t = 16$  MVN2 is closed.

**Hot Flow sequence** In the hot flow sequence nomenclature is equal to cold flow but the steps obviously are different. Now by reference table 2.3, first of all at  $t = 0$  all valves are closed. At  $t = 2$  MVO1 and MVF1 open, and also MVN1 opens in order to have purge ready in case of emergency. Secondly at  $t = 3$  MVN1 remains opened, and MVO2 is opened until  $t = 5$  which represent, as said before, the preheating time which allows oxygen to reach the ignition temperature. After this at  $t = 5$  MVF2 is opened until  $t = 9$  so that ignition takes place: this represent the **burning time**. Than at  $t = 9.5$  also MVO2 is closed. Consequently at  $t = 10$  MVO1 and MVF1 are closed. After at  $t = 11$  MVO2 is opened again to release oxygen and closed at  $t = 13$  when the purge starts (MVN2 opens).

**Table 2.3:** Pressure regulated Hot Flow Sequence

Time [s]	MVN1	MVN2	MVO1	MVO2	MVF1	MVF2
0	0	0	0	0	0	0
2	1	0	1	0	1	0
3	1	0	1	1	1	0
5	1	0	1	1	1	1
9	1	0	1	1	1	0
9.5	1	0	1	0	1	0
10	1	1	0	0	0	0
11	1	0	0	1	0	0
13	1	1	0	0	0	0
14	1	0	0	0	0	1
15	0	1	0	0	0	0
17	0	0	0	0	0	0

Then at  $t = 14$  MVN2 closes, while MVN1 is still open and then close at  $t = 15$ . After that MVN2 ( $t = 15$ ) is opened again to release nitrogen and in the end ( $t = 17$ ) all valves are closed.

## 2.4.2 Pressure regulated Cold Flow test campaign

The cold flow test campaign consist of different run conduced with several value of oxygen pressure for each  $s/d$ , aiming to find optimum in term of supply oxygen pressure and resonator-nozzle distance with 5 second of preheating, analysing the maximum resonator temperature. In figure 2.11 is reported an example of resonator temperature ( $T_{res}$ ) over time. This temperature is detected, as said during the experimental set-up explanation, by a thermocouple inserted up to the external wall of the resonator (see figure 2.12).

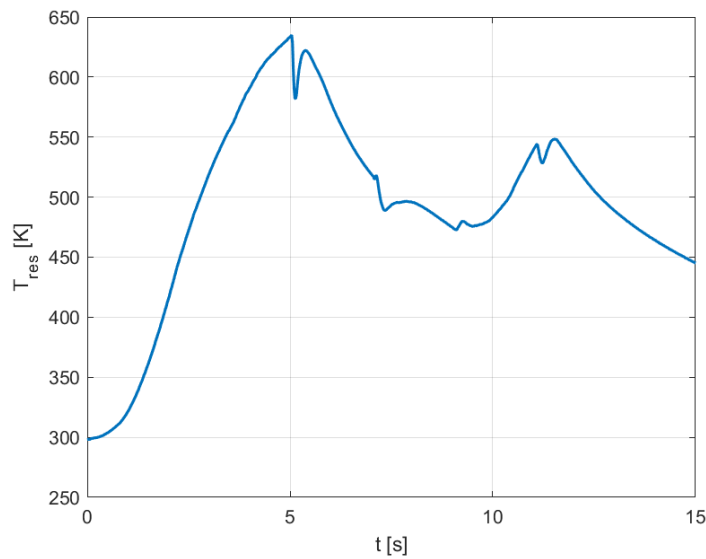


**Figure 2.11:** Resonator temperature dependent on time

The first rise in temperature until the first peak (i.e  $T_{MAX}$ ) represents oxygen injection time which is the preheating time; then there is a fall in temperature due to closing of valve, which causes a back-flow (see figure 2.12) of oxygen from resonator wall to chamber. After that there is a re-raise in temperature due to the fact resonator is still warm and heats the thermocouple up again. Finally it is possible to appreciate a second peak in temperature because of the purge phase.

The test campaign has been conduced with various value of supply pressure from a nominal absolute value of 10 bar to 30 bar, for several resonator-nozzle distances.

From figure 2.13 it is possible to notice the maximum temperature trend: for  $s/d = 1.5$  and  $s/d = 1.625$  are reached the best performance in terms of maximum resonator temperature. Considering the fact that the position of the Mach disk is a factor influencing the heating process it is assumed that it is located approximately at the entrance of the resonator cavity. For bigger value of  $s/d$  heating performance decreasing since Mack disk is assumed moving away from the inlet edge of the cavity.

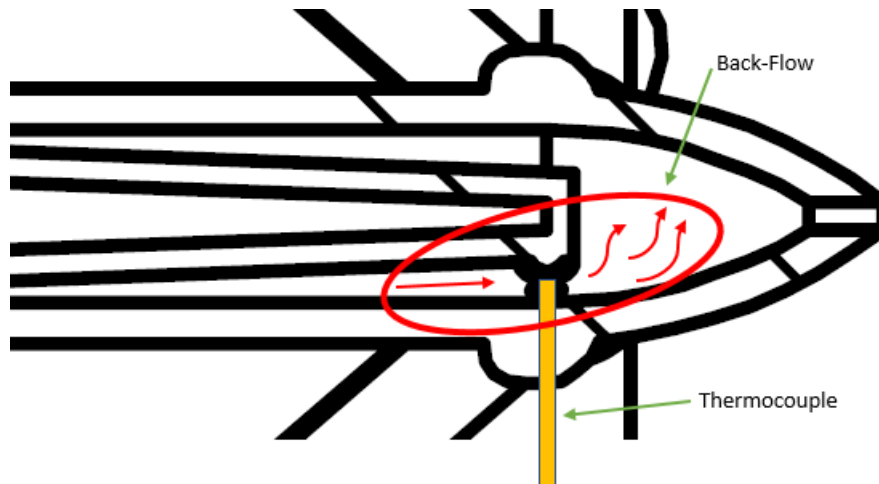


**Figure 2.12:** Thermocouple position

Also for  $s/d$  smaller value performance are worst because, on the contrary, first Mach disk is assumed moving within the cavity. Concluding the optimum is chosen for  $s/d = 1.625$  because it gives the highest temperature, not in absolute terms, but for a wider range of supply pressure values. Figure 2.14 shows that until 15.71 bar of supply pressure, more than 560 Kelvin are not reached.

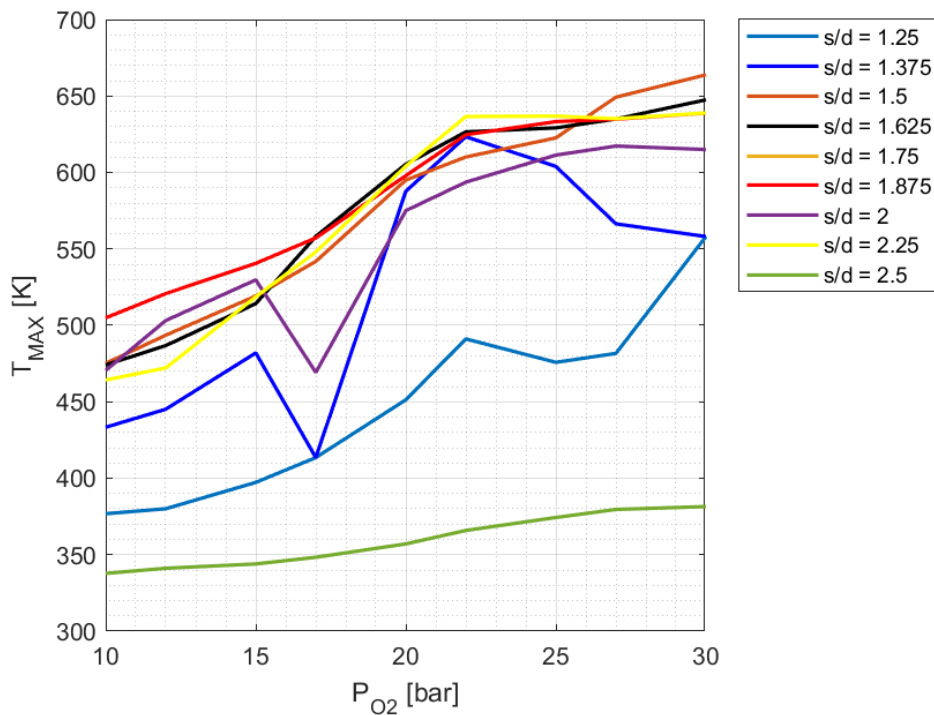


**Figure 2.13:** Resonator maximum temperature over supply pressure for various  $s/d$  ratio

For this chosen value of  $s/d = 1.625$  is plotted in figure 2.14 resonator temperature trend over time for several value of oxygen supply pressure (without the purge effect) in order to see the pressure effect on the heating over time.

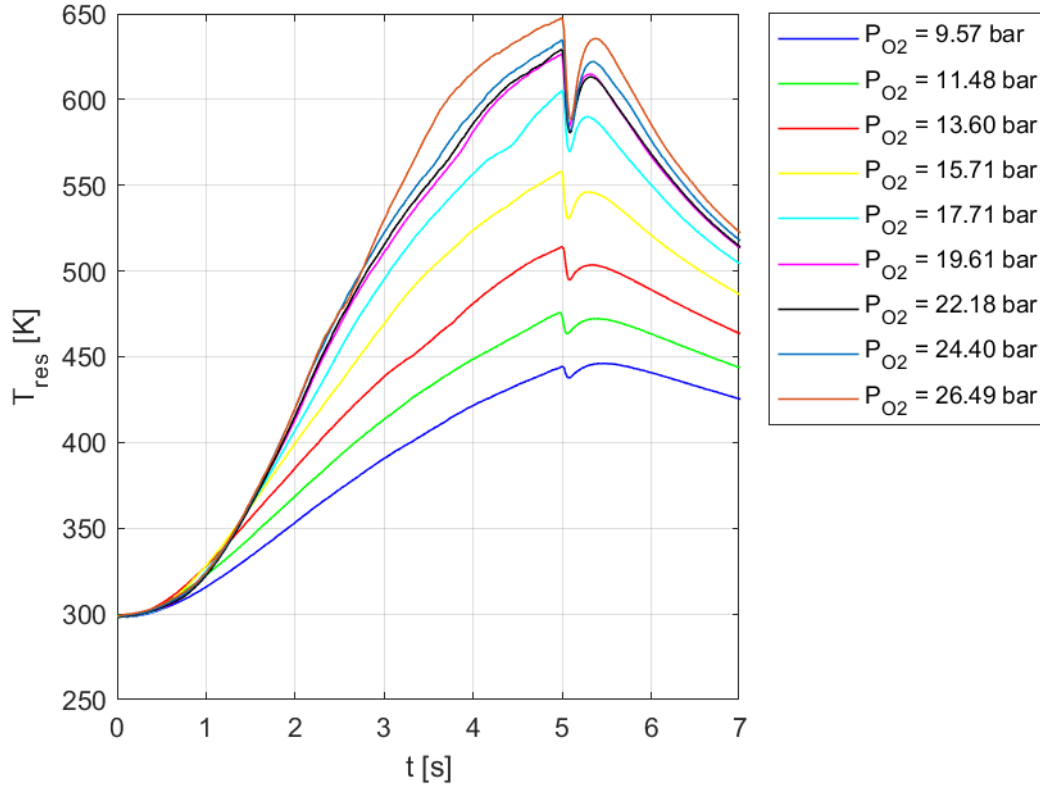


**Figure 2.14:** Resonator temperature over time for different values of oxygen supply pressure

Then, by increasing the oxygen supply pressure, the combustion chamber starts to work in a choking condition, so that the pressure value is such as to allow high temperatures to be reached. For a supply pressure between 19 and 24 bar, the maximum temperature reached is greater than the experimental limit of 600 K for self-ignition. For these pressure values there is then a good heating effect; therefore the oxygen supply pressure is chosen in this range. By further increasing the pressure, the gain in temperature decreases, not leading to any improvement in terms of heating effect.

### 2.4.3 Pressure regulated Hot Flow test campaign

After that an optimum value for the  $s/d$  ratio and the oxygen supply pressure were determined in the last chapter, it is necessary to determine the optimum preheating time for chosen pressures at a certain  $s/d$  ratio. Furthermore it necessary to determinate methane supply pressure in order to obtain the wanted oxidizer to fuel ratio. A methane pressure based on previous tests of 23 bar is chosen, and eleven tests are carried out for this hot fire test campaign.

**Table 2.4:** Pressure regulated Hot Flow test results

Test	$t_{ph}$ [s]	$P_{O_2}$ [bar]	$P_{CH_4}$ [bar]	$P_{chamber}$ [bar]	$T_{BMVO}$ [K]	Ignition
1	10	20	23	4,77	679	Success
2	8	20	23	1,37	677	Failure
3	8	20	23	5,46	678	Success
4	6	20	23	5,40	665	Success
5	6	20	23	5,21	665	Success
6	4	20	23	4,58	614	Success
7	4	20	23	5,78	620	Success
8	3	20	23	1,38	572	Failure
9	3	20	23	1,36	573	Failure
10	2	20	23	1,33	524	Failure
11	2	20	23	1,34	520	Failure

Increasing preheating time results in a rising temperature of the resonance chamber. The test brought up that four seconds of preheating is enough to reach the ignition temperature of the mixture. Successful ignition could be detected seeing the chamber pressure achieved: in fact combustion produce a raise of chamber pressure ( $P_{chamber}$ ) as it is possible to see in figure 2.15a for the test number 1. Furthermore is detected  $T_{BMVO}$  (temperature before methane valve opening - see figure 2.15b) i.e. the temperature reached at the end of preheating time just before methane valve opening. It is assumed that 600 K are enough to have ignition, based on the actual tests results in table 2.5. Concluding for two and three seconds of preheating ignition does not take place because the time is not enough to heat oxygen. It is indeed worthy of mention that ignition Failure has been obtained even if temperature before methane opening valve was over 600 K like test number 2, due to two different reasons. The first is due to a wrong mixing, so new solutions to improve the mixing are under study. The second reason is due to a wrong evaluation of

the  $C_d$  discharge coefficient of the methane orifice. In the Hot Flow test campaign was assumed a far smaller  $C_d$ ; later, during calibration, it was showed that  $C_d$  was bigger, in particular, due to manufacturing tolerance, which for the diameter of the methane nozzle are  $d_{CH_4} = 0.36 + 0.04 \text{ mm}$ , the  $C_d$  value is actually higher than one. Therefore, the mass flow rate of methane introduced into the combustion chamber was higher than expected, leading a too low O/F.

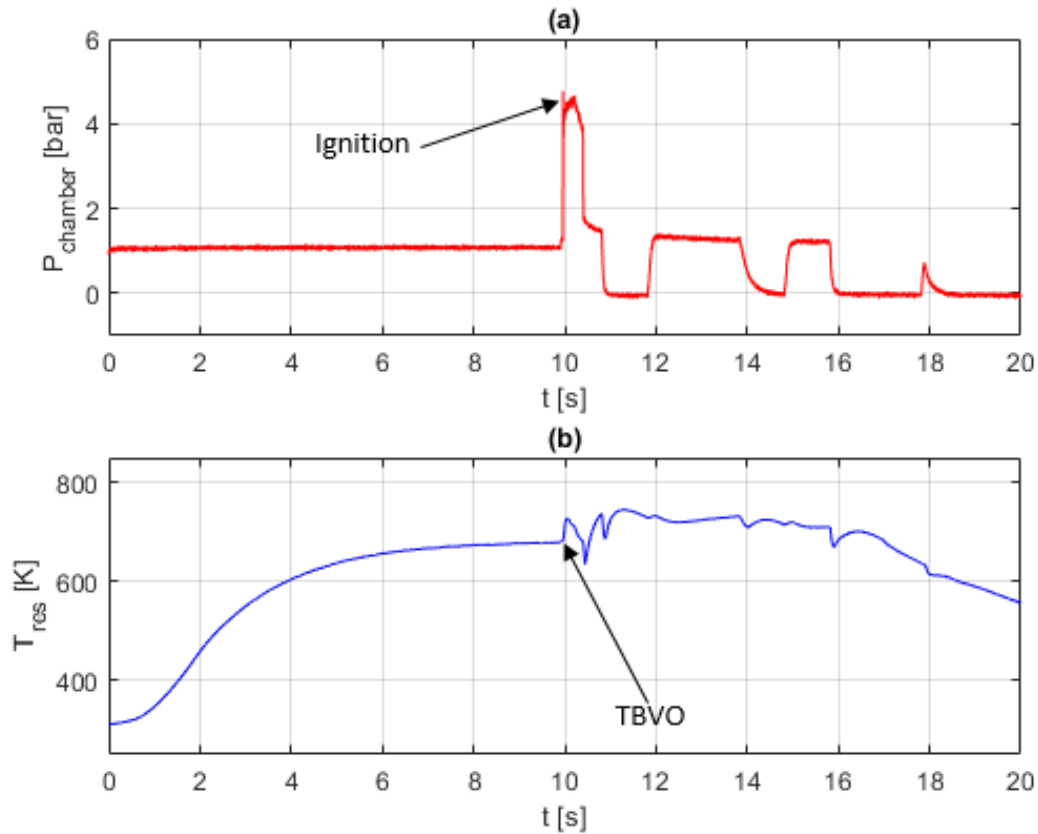


**Figure 2.15:** Chamber pressure (a) and resonator temperature (b) during a Hot Flow test

## 2.4.4 Pressure regulated Cold Flow test campaign after resonant repair

After the Hot Flow test campaign, it has been observed, for the reasons explained before, a damage at the edge entrance of resonator cavity. Basically some material of cavity edge has been cut out. So the resonator entrance edge has been repaired to make it smooth again. Before the damage, the cavity of the resonator was 25 mm, while considering this reduction, it now appears to be 24.2 mm pariah. This leads to a length reduction of 3.2 %.

Consequently a new short Cold Flow test campaign has been carried out, in order to evaluate the resonator performance after the damage and set again the right  $s/d$  value. The solution has been looked for into the igniter operational envelope defined in the previously Cold Flow test campaign. Considering a cavity length reduction of 0.8 millimeter the new optimum will be in the range of:  $s/d = 1.525 \div 1.65$ , with oxygen supply pressure of 22.5 bar, which is in the range of pressure defined after Cold Flow test campaign. Again is evaluated resonator temperature over time, but only for one pressure value and three different distances. Two tests for each distance has been conducted with 5 seconds of preheating.

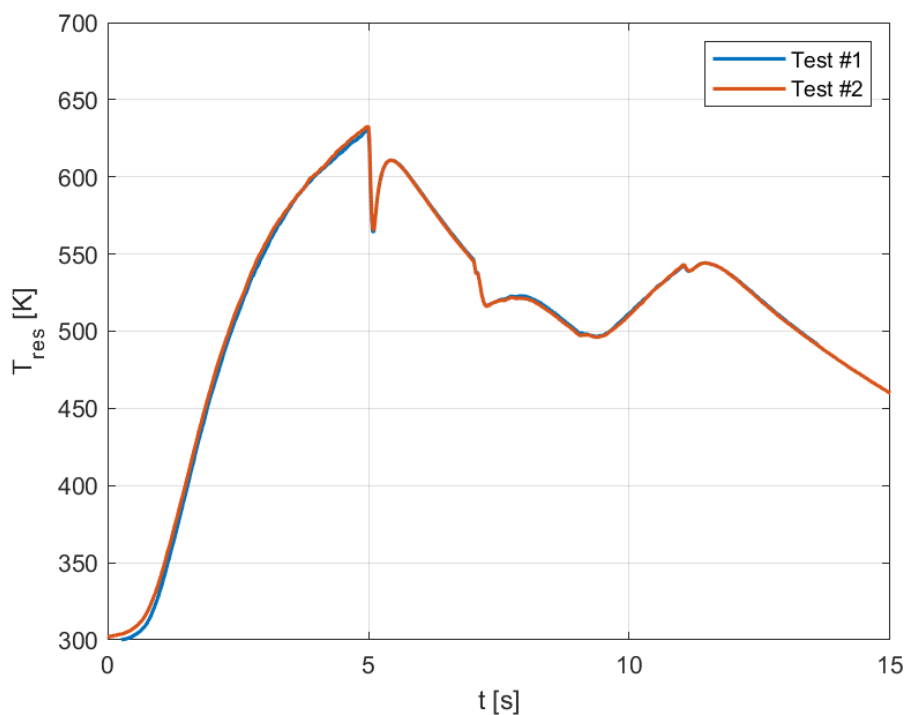


Figure 2.16: Resonator temperature over time -  $s/d = 1.525$

In table 2.5 is shown resonator maximum temperature: it is possible to notice that all three distances give good result in terms of heating. It means that the resonator can still work with oxygen supply pressures already defined, and the optimum in terms of  $s/d$ , as expected after the repair, is in between  $s/d = 1.525$  and  $s/d = 1.65$ .

**Table 2.5:** Resonator maximum temperature measured in Kelvin -  $t_{ph} = 5 s$

$P_{O_2}$	$s/d$		
	1.4	1.525	1.65
22.50 bar	600.49	630.44	622.02
22.50 bar	609.70	632.86	643.09

Referring to this and also seeing what figure 2.17 shows, the maximum temperature in absolute terms is 643 K for  $s/d = 1.65$ . However the optimum is chosen at  $s/d = 1.525$  because it provides maximum temperature values that are close to each other so that allow to assume greater stability in terms of the maximum temperature reached (see figure 2.16).

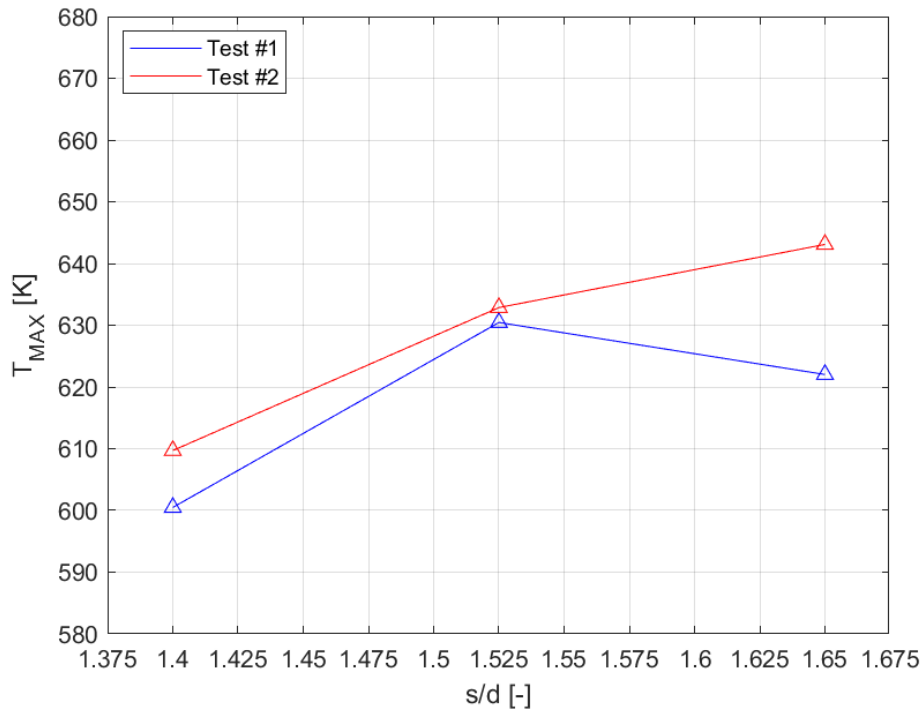


**Figure 2.17:** Resonator maximum temperature dependent on  $s/d$  ratio

## Chapter 3

# Fluid system design

This chapter is going to be focused on the design and development of the fluid system able to feed the previous Z2 described in section 2.3, referring to the design data reported in table 2.1 in section 2.3. Since it has been observed from experimental data that when the ignition has reached 600 K the ignition is generally obtained, it is necessary to dimension a system capable of supplying an adequate feed pressure, so that the resonance heating is provided. For this goal a dedicated supply system is needed and furthermore tanks to store *GO2* and *GCH4*. Before do this are presented the guide lines followed as a result of an investigation in the literature available. This ignition system is investigated for use in satellite and upper stage propulsion applications.

### 3.1 Feed systems

Being that the igniter can be seen as a small combustion chamber same considerations done for a main chamber are took in account.

For the transfer of the rocket propellants from tanks to the thrust chamber at the required flow rates and pressure, a suitable feed system is needed. There is no simple rule for the choice between a pressurized gas feed system or a blowdown feed system [21].

Among the considerations for selection of the type of pressurized gas propellant feed system are:

1. Compatibility of pressurant gases with propellants and tank materials, considering chemical interactions, temperature, solubility, etc.
2. Expected pressurization system reliability and complexity, considering the state of the art of systems components used.

3. Molecular weight of the pressurant gases: lower molecular weight reduces required pressurant weight per unit pressure and per unit tank volume, and thus results in lower vehicle system weight at burnout and thus improved mass ratio.
4. Pressurization system specific weight: i.e. required pressurization system gross weight (including system component), per unit of weight of useful pressurant.

The pressurized system are divided in

- Blowdown system
- Repressurization
- Regulated pressure system

Regulated pressure system are widely used in numerous combinations. The gas is usually stored in a vessel at pressure ranging from 205 *bar* to 345 *bar* and supplied to the propellant feed system at a specified pressure level controlled by a regulator. These systems have achieved a high level of reliability [21]. In general, the most important design requirements for a stored gas system are:

- low molecular weight
- minimum residual gas weight

The igniter system is going to be used for satellite and in-orbit propulsion system, i.e. in-space thrusters, where long mission durations and a high number of ignitions are required [9]. Propulsion system for this kind of spacecraft, in particular spacecraft attitude control and orbital maneuvering thrusters, are almost universally pressure-fed designs. Furthermore these systems are primarily used for space propulsion applications and auxiliary propulsion applications and they require low system pressures and smaller quantities of propellants [22]. On the other hand, the blowdown system is very simple, light and reliable, but pressure decreases over time. On the basis of this the following choices are made:

- Engine → Pressure regulated propulsion system
- Igniter → Blowdown system

The simplified design of the engine with the igniter fluid system is presented in figure 3.1.

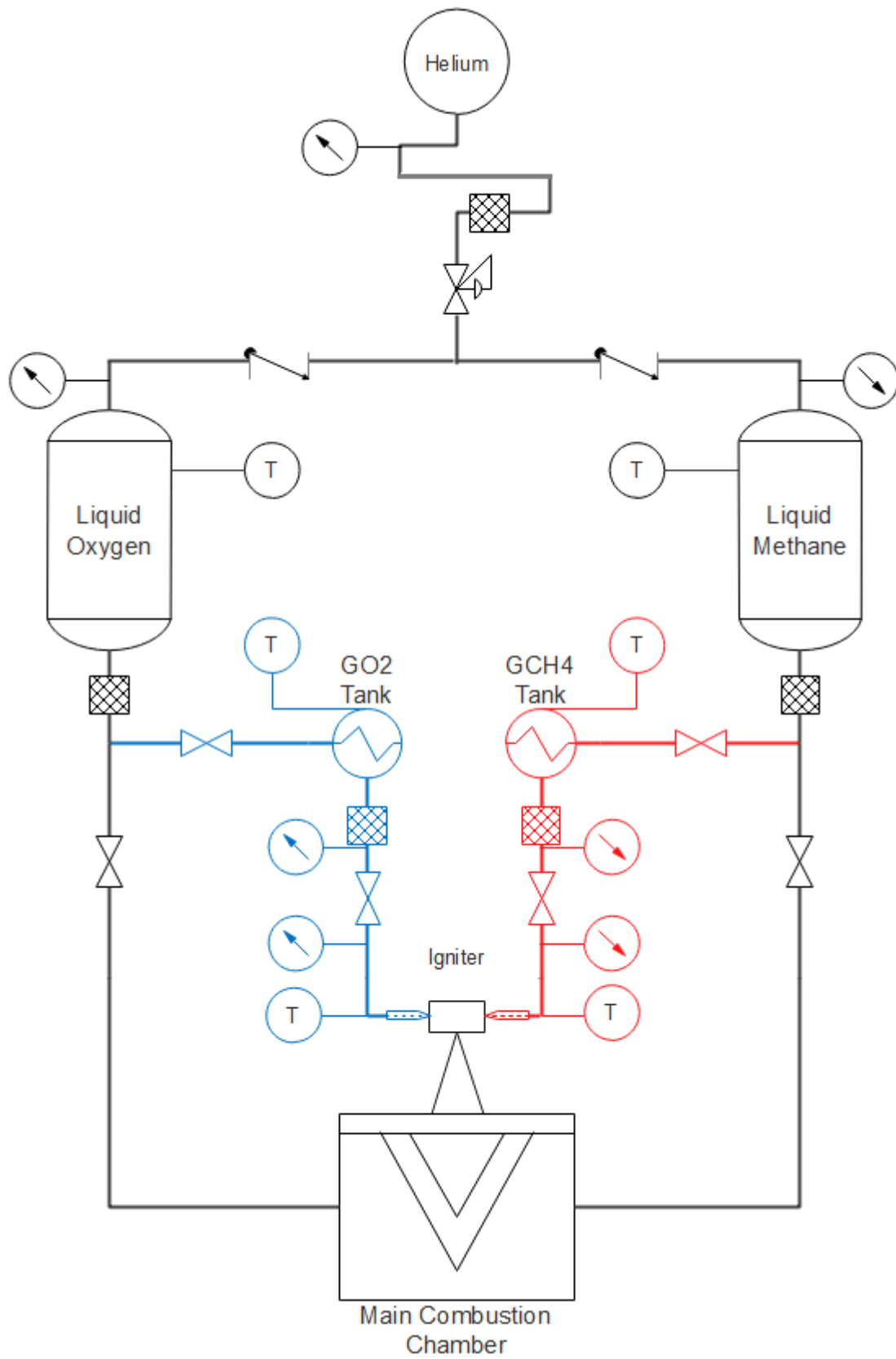


**Figure 3.1:** Simplified design of the rocket engine fluid system

The main feed system consists of a tank containing the pressurized gas, expulsion device to provide energy for the feed system, valves to control the pressure (pressure regulator, latch valve, check valve) and ducting or piping to transfer fluids and flow (also filter device). For reference see the devices legend in figure 3.2.

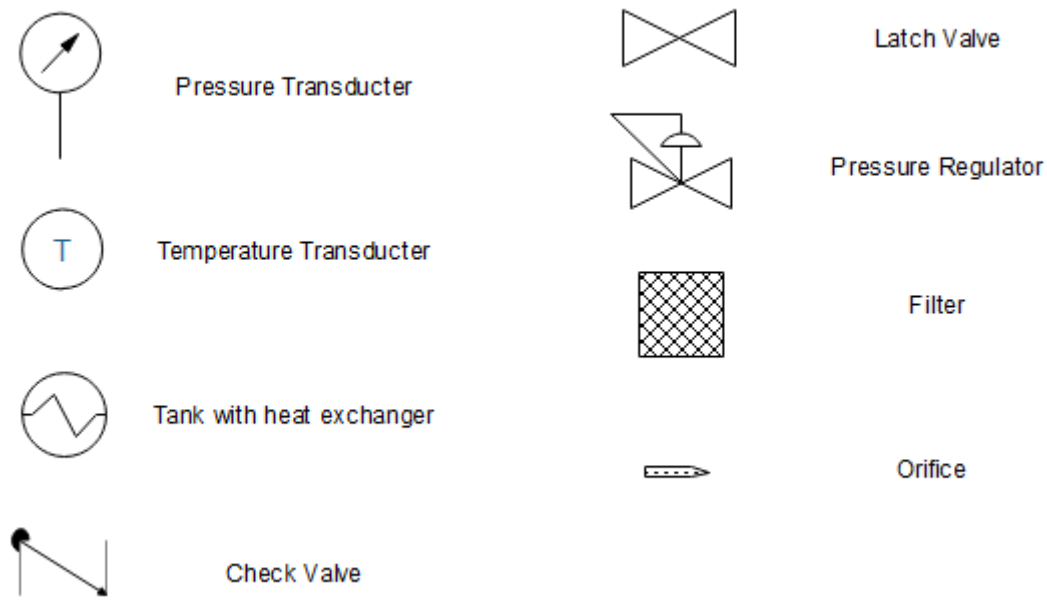


**Figure 3.2:** Fluid systems device legend

The attention of this thesis is going to focus on the igniter feed system which is shown in figure 3.3 aiming to design igniter supply tanks.

The igniter fluid system consist of two supply line: the blue one is Oxygen feed line while the red one is Methane feed line. Both supply lines are formed by a dedicated tank, which is pressurized at a certain pressure. The characteristic and the properties of those vessels are discussed in this chapter, who aims to define those tanks size in order to supply the igniter in a blowdown way. All two tanks are filled from the respective main liquid propellant tanks. The filling process is going to be discussed in chapter 6.

As said in a blowdown system pressure decay over the time, which means that the variation of properties over the time like pressure, temperature, density of the stored gas has to be taken into account.

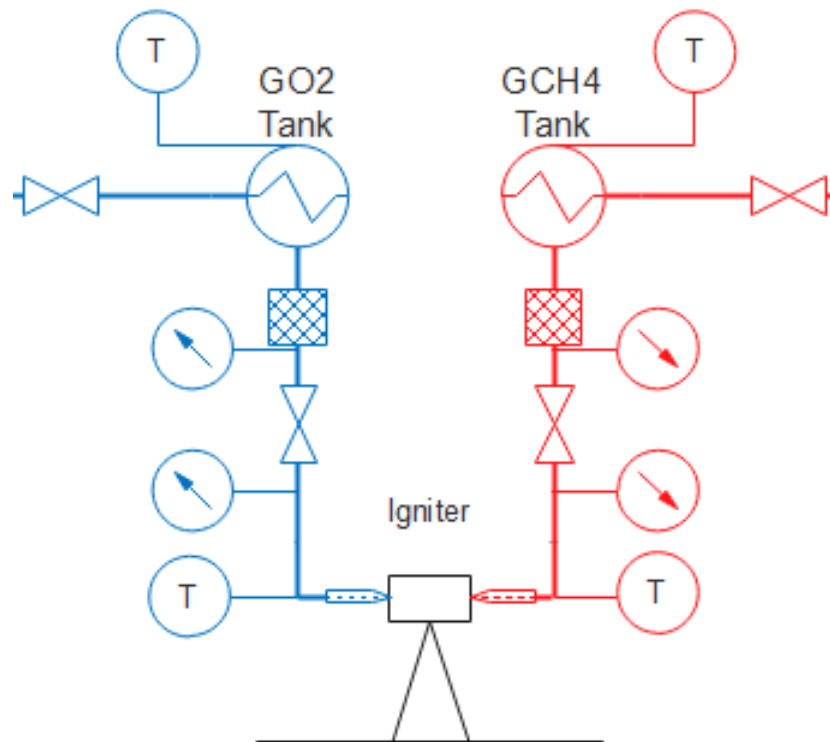


**Figure 3.3:** Igniter fluid system design

So in the next section, first of all, is presented the variation of properties in a vessel discharge in order to find out the key characteristic of blowdown.

## 3.2 Blowdown: variation of properties in a vessel discharge

This section explains a study of a pressurized flow when a closed tank is suddenly opened and the flow passes through an orifice until the tank is at equilibrium with the surroundings [23]. In order to fully characterize the flow, the study analyses the pressure, the temperature, the density, and the mass flow rate during the discharge of the vessel. All of these properties are studied using their own equations in their dimensionless form and later plotted using the math code written with the help of the software Matlab. Given some inputs such as the initial and final dimensionless pressures and the specific heat ratio, it is possible to determine the dimensionless time until the tank is drained and the evolutions of the properties.

In addition, the following assumptions [23] are made:

1. Properties of the gas in the tank are spatially uniform at any instant of time (i.e., quasi-steady or uniform state assumption);
2. Average velocity of the gas in the tank is zero;
3. Opening modeled as an ideal converging or converging-diverging nozzle with isentropic flow to the nozzle throat;
4. One-dimensional flow and properties in the nozzle;
5. Neglect gravitational potential energy;
6. No shear or shaft work for the control volume;
7. Gas is thermally and calorically perfect;
8. Thermodynamic process is either adiabatic ( $\dot{Q} = 0$ ) or isothermal ( $\dot{Q} = \text{constant}$ ).

Two model are analysed and compared, that are the adiabatic model and the isothermal model. The adiabatic assumption would be expected to be a good model for very rapid discharge processes in which case there would be little time for significant heat transfer between the tank walls and the gas. On the other hand, the isothermal assumption is expected to be appropriate for slow vessel discharge processes whereby there is sufficient time for heat transfer to maintain the temperature of the gas in the vessel constant.

In the discharge analysis the gas thermodynamic properties are non-dimensionalized with respect to their initial values [23]. So we have:

$$P^* = \frac{P}{P_i} \quad (3.1)$$

$$T^* = \frac{T}{T_i} \quad (3.2)$$

$$\rho^* = \frac{\rho}{\rho_i} \quad (3.3)$$

$$P_e^* = \frac{P_e}{P_i} \quad (3.4)$$

$$\dot{m}^* = \frac{\dot{m}\sqrt{RT_i}}{P_i A} \quad (3.5)$$

$$t^* = \frac{t}{t_{char}} \quad (3.6)$$

$$t_{char} = \frac{V_i}{P_i a_i} \quad (3.7)$$

### 3.2.1 Mathematical procedure

To describe a flow we need the governing equations, but in this case only two are necessary: the continuity and energy conservation equations. Once these equations are found, it is possible to study the thermodynamic relationships of the fluid to know how the fluid inside the tank expands as it is being drained [23].

#### Continuity equation

$$\frac{\partial}{\partial t} \int_V \rho dV + \int_S \rho V \cdot dS = 0 \quad (3.8)$$

Under the quasi-steady flow assumption (assumption number 1), the density is uniform throughout the control volume and can be pulled out of the integral. Then, as it is a rigid tank (assumption number 8), it is possible to take the volume out from the time derivative, leaving the density which is a function of time. Knowing the definition of mass flow rate,  $\dot{m} = \rho v A$ , the continuity equation becomes [23]:

$$\frac{d\rho}{dt} + \frac{\dot{m}}{V} = 0 \quad (3.9)$$

### Energy equation

$$\dot{Q} - \dot{W} = \frac{\partial}{\partial t} \int_V e \rho dV + \int_S (e + pv) \rho V \cdot dS \quad (3.10)$$

The first and the second term become 0 because of assumptions 7 and 5 respectively. Defining the internal energy as  $e = u + \frac{v^2}{2} + gz$ , substituting it in the third and fourth terms, and simplifying while making assumptions 2 and 4, an expression of continuity depending on the enthalpy is developed. Resolving the integrals it is possible to obtain a final equation [23]:

$$\frac{d}{dt}(\rho u) + \frac{\dot{m}}{V} H = 0 \quad (3.11)$$

### Thermodynamic relation

Combining the equations of continuity and energy in order to remove the mass flow rate and the volume as variables, another equation is obtained. Invoking assumption 7 for an adiabatic flow, the stagnation enthalpy  $H$  is the enthalpy of the fluid in the tank  $h$  [23]. It becomes

$$\frac{d}{dt}(\rho u) - \frac{d\rho}{dt} h = 0 \quad (3.12)$$

Following this simplification, assumption 6 implies some definitions that are helpful, such as the specific heat ratio  $k$  for these type of flows

$$u = C_v T, \quad h = C_p T, \quad k = \frac{C_p}{C_v}; \quad (3.13)$$

Substituting these definitions in the equation 3.12, continuing with the development of it, and introducing the dimensionless variables result in the isentropic relations. That means that when the tank is draining the fluid expands isentropically and the temperature and density can be expressed as a function of pressure as it follows.

$$T^* = (P^*)^{\frac{k-1}{k}} \quad (3.14)$$

$$\rho^* = (P^*)^{\frac{1}{k}} \quad (3.15)$$

### Flow equations depending on time

Due to the high difference of pressures between inside and outside of the tank, the flow will evolve through two different behaviors. These two cases have been studied, and their dimensionless time-dependent equations derived [23].

**Choked flow equations - adiabatic Model** In this case the mass flow rate is expressed by Fliegner's formula which is independent of pressure and dependent on the specific heat ratio of the fluid  $k$ . So, as long as the flow is choked the mass flow rate is a constant  $K=0.6847$  (taking  $k = 1.4$ ) [23].

$$m^* = \sqrt{k} \left[ \frac{k+1}{2} \right]^{\frac{-(k+1)}{2(k-1)}} \quad (3.16)$$

By introducing the dimensional form of the mass flow rate to the continuity equation 3.9, non-dimensionalizing all the variables, and defining the characteristic time, it is possible to reach a simple expression with all the variables of interest.

$$\frac{d\rho^*}{dt^*} + \frac{K}{\sqrt{k}} \frac{P^*}{\sqrt{T^*}} = 0 \quad (3.17)$$

When the variables have been substituted using the isentropic relations and the equation depends only on time and pressure, it is possible to integrate it and arrive at an expression of the pressure depending on the time. Using the isentropic relations again results in temperature and density expressions.

$$P^* = \left[ 1 + \left( \frac{k-1}{2} \right) \left( \frac{k+1}{2} \right)^{\frac{-(k+1)}{2(k-1)}} \cdot t^* \right]^{\frac{-2k}{(k-1)}} \quad (3.18)$$

**Choked flow equations - isothermal Model** For completeness is also given the isothermal Model [24]:

$$P^* = \exp \left[ - \left( \frac{k+1}{2} \right)^{\frac{-(k+1)}{2(k-1)}} \cdot t^* \right] \quad (3.19)$$

**Unchoked compressible flow equation** For determining when the flow becomes unchoked, we used the critical pressure ratio condition [23]:

$$CPR = \frac{P_e^*}{P_{cri}^*} = \left( \frac{2}{k+1} \right)^{\frac{k}{k-1}} \quad (3.20)$$

This expression depends solely on the heat specific ratio, so it is a constant for each value of  $k$ . When the pressure ratio  $PR = \frac{P_e^*}{P^*}$  is lower than that constant, it means that the flow is still choked, and when it becomes greater, it means that the flow is unchoked [23]. As the tank pressure falls toward the back pressure, the nozzle will eventually unchoke. The theoretical results can be extended through the unchoked regime by writing a mass flow expression at the nozzle exit plane, imposing the boundary condition that the nozzle exit static pressure must equal the ambient pressure, substituting this result into the integral continuity equation, and integrating the resulting ordinary differential equation using the unchoking point values  $(P_{unch}^*, t_{unch}^*)$  as the initial condition [23]. Finally the mass flow for an unchoked flow is

$$m^* = \left( \frac{2k}{k-1} \right)^{\frac{1}{2}} \cdot \left[ 1 - \left( \frac{P_e^*}{P^*} \right)^{\frac{k-1}{k}} \right]^{\frac{1}{2}} \cdot \left( \frac{P_e^*}{P^*} \right)^{\frac{1}{k}} \quad (3.21)$$

### 3.2.2 Preliminary Blowdown output

As mentioned previously in order to figure out the main parameters that have to be taken into account, a preliminary study of the blowdown discharge over the time is here presented with the help of the software Matlab.

Using equations 3.18, varying the dimensionless time from 0 to 4.5, it is possible to obtain the blowdown characteristic curve, which is nothing else that the decay pressure over the time in a vessel with dimensionless variables, i.e variables normalized with respect initial conditions in the tank. Figure 3.4 shows the dimensionless properties during a tank discharge.

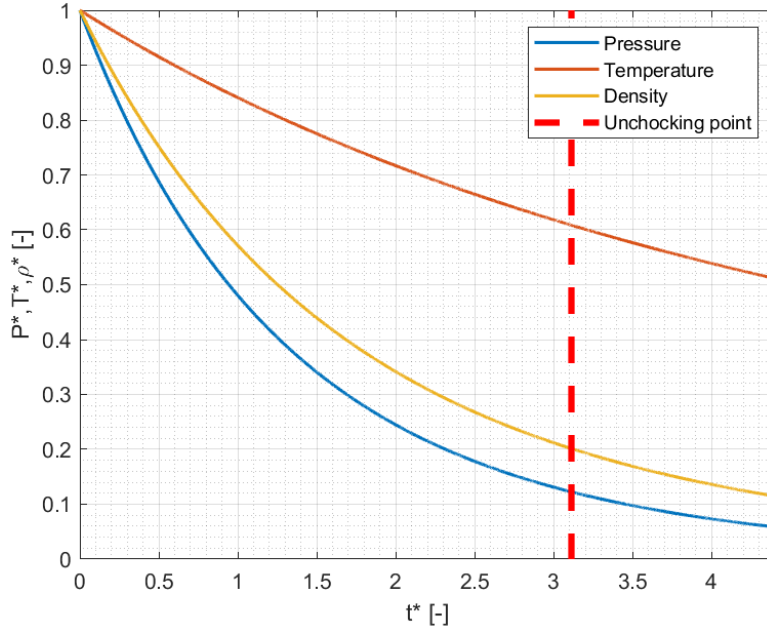


**Figure 3.4:** Properties over time

Pressure decays over the time (blue curve) very fast and consequently temperature decreases like density due to the fact that the gas mass in the tank is reducing. Being that the flow conditions are decided by the value of the pressure ratio  $PR$ , it is important to put on evidence how its value changes over the time. From figure 3.4 it is possible to see that if the pressure ratio  $PR$  is lower than the critical pressure ratio  $CPR$  we are in choking conditions while if it is greater than  $CPR$  the flow results unchoked.

$$\frac{P_e^*}{P^*} < \frac{P_e^*}{P_{cri}^*} \rightarrow \text{Choked flow} \quad (3.22)$$

$$\frac{P_e^*}{P^*} > \frac{P_e^*}{P_{cri}^*} \rightarrow \text{UnChoked flow} \quad (3.23)$$

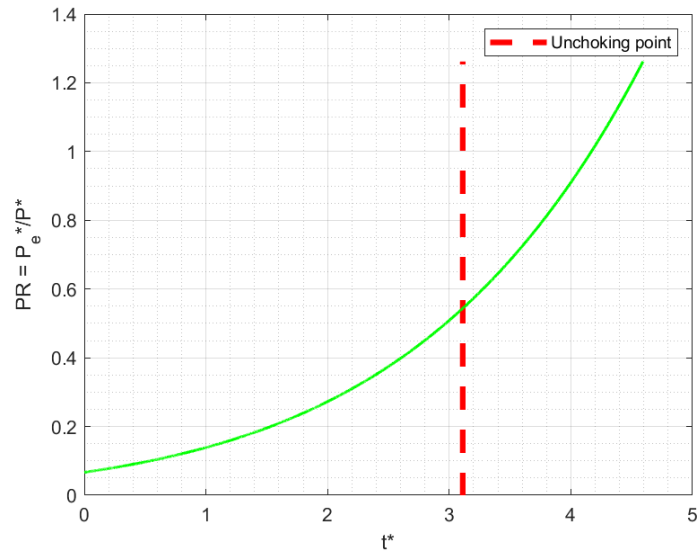


**Figure 3.5:** Nozzle pressure ratio over time

Finally is shown in figure 3.6 a comparison between the adiabatic model and the isothermal model: since the igniter operative time is very short, the adiabatic Model is selected, justified from the fact that the adiabatic model would be expected to be a good model for very rapid discharge processes in which case there would be little time for significant heat transfer between the tank walls and the gas.

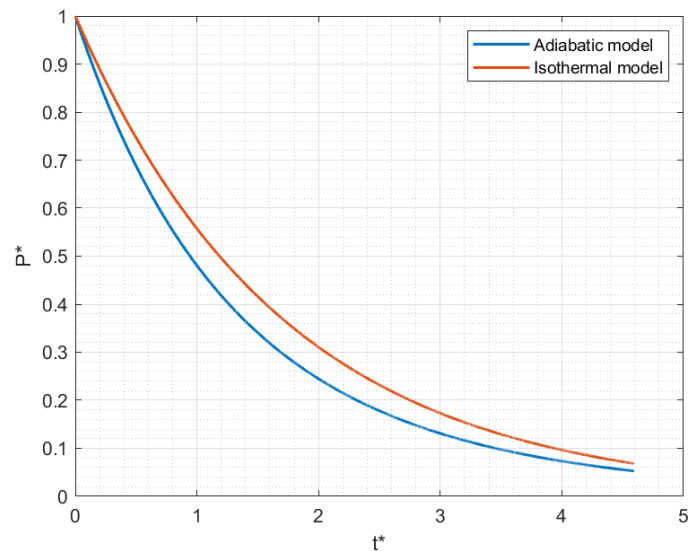


**Figure 3.6:** Pressure comparison

### 3.3 Blowdown system sizing

After the preceding blowdown study, basing on the igniter design data, is it necessary to size the tanks of the feed system in terms of volume, initial pressure in the tank and gas mass. The objective is to find an optimum of the above parameters taking into account the design parameters presented in table 2.1 in section 2.3 for the configuration Z2, currently under investigation at LTF. It is therefore necessary to find the lightest and least bulky tank and at the same time to be able to feed the igniter with the right value of mass flow until is obtained the one O/F such as to ensure ignition. The design strategy used to achieve this objective consists in calculating the pressure upstream of the nozzle that allows to obtain the correct mass flow rate at a predetermined instant of time. In fact, the actual ignition starts after the oxygen has reached the ignition temperature, i.e. after the preheating time. Therefore, for the oxygen from that moment until the ignition is exhausted, the correct value of mass flow must be obtained. For methane, the correct mass flow rate value must be obtained for the ignition time. In order to calculate the design upstream pressure  $P_{up}$  at certain moment of time  $t_{up}$ , the following equations is used

$$\dot{m} = C_D \frac{P_{up} A_t}{\sqrt{RT}} \quad (3.24)$$

in which is assumed isentropic flow, orifice critically flowed and a discharge coefficient  $C_D$  equal to 1.

Now considering the mass flow for a choked flow

$$\dot{m}^* = \frac{\dot{m} \sqrt{RT}}{P_{up} A_t} = \sqrt{k} \left[ \frac{k+1}{2} \right]^{\frac{-(k+1)}{2(k-1)}} \quad (3.25)$$

making clear the pressure is obtained that the upstream absolute pressure is equal to

$$P_{up} = \frac{\dot{m} \sqrt{RT} \left[ \frac{k+1}{2} \right]^{\frac{k+1}{2(k-1)}}}{A_t \sqrt{k}} \quad (3.26)$$

This value is the pressure that has to be achieved at a certain moment that is the upstream time  $t_{up}$ , in order to obtain the mass flow and the Oxidizer to Fuel ratio desired.

Knowing the preheating time for oxygen from the Cold Flow test campaign and the ignition time for methane from the Hot Flow test campaign, is thus identified a couple of point

$(P_{up}, t_{up})$  for both oxygen and methane in the blowdown plot pressure over time as shown in figure 3.7 and 3.8.

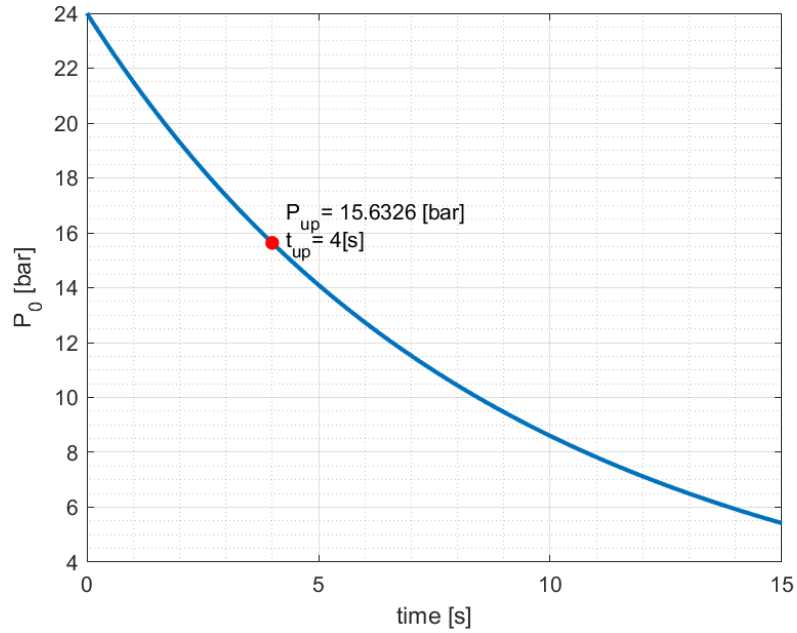


**Figure 3.7:** Pressure over time OXYGEN: time ignition and upstream pressure

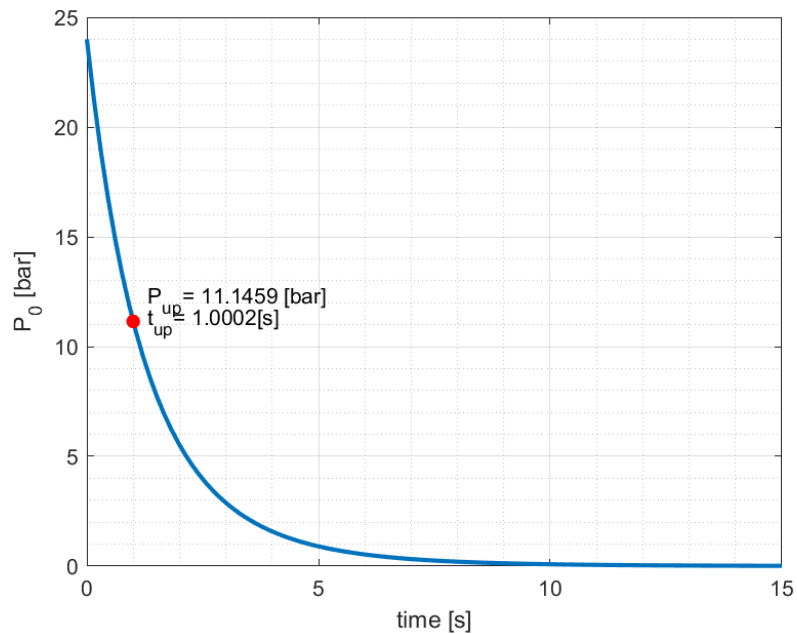


**Figure 3.8:** Pressure over time METHANE: time ignition and upstream pressure

In this way imposing that the blowdown curve intercepts that point, is assured that at a certain time a precise pressure is gained, consequently a precise mass flow: in fact, fixed the other variables, the mass flow is only proportional to the upstream pressure of the orifice

$$\dot{m} \propto P_{up}$$

under the choked and isentropical conditions.

Consequently to this it is possible to choose and to set the initial pressure in the feed tank which allows to have the upstream pressure  $P_{up}$  at the upstream time  $t_{up}$  wanted. In table 3.1 are reported the upstream values chosen. As for the upstream time, 4 seconds of preheating were chosen for the test campaign in chapter 2, while 1 second for methane was chosen to have a slope curve too steep for what will be explained below.

**Table 3.1:** Pressure and time constraint values

		Oxygen	Methane
$P_{up}$	[bar]	15.63	11.14
$t_{up}$	[s]	4	1

Knowing now the initial pressure, assuming ideal gas, it is possible to calculate, with the ideal gas law, the density

$$\rho_0 = \frac{P_0}{RT_0} [Kg/m^3] \quad (3.27)$$

in which the subscript "0" means the initial conditions in the tank.

After that, using the ignition time, it is possible to calculate the mass of gas necessary

$$M = \dot{m} \cdot t_{up} [Kg] \quad (3.28)$$

and being that the specific volume is the inverse of density is obtained the volume

$$V_0 = v_0 \cdot M = \frac{1}{\rho_0} \cdot M [m^3] \quad (3.29)$$

where  $v_0$  is the specific volume.

Now the right mass flow is achieved, so next step is to find an optimum: different initial pressures in the tank have to be investigated. The approach is to vary the initial pressure in the tank, taking into account the constraint of time and pressure: for each initial value of pressure a different blowdown slope is produced as it is possible to see in figure 3.9.

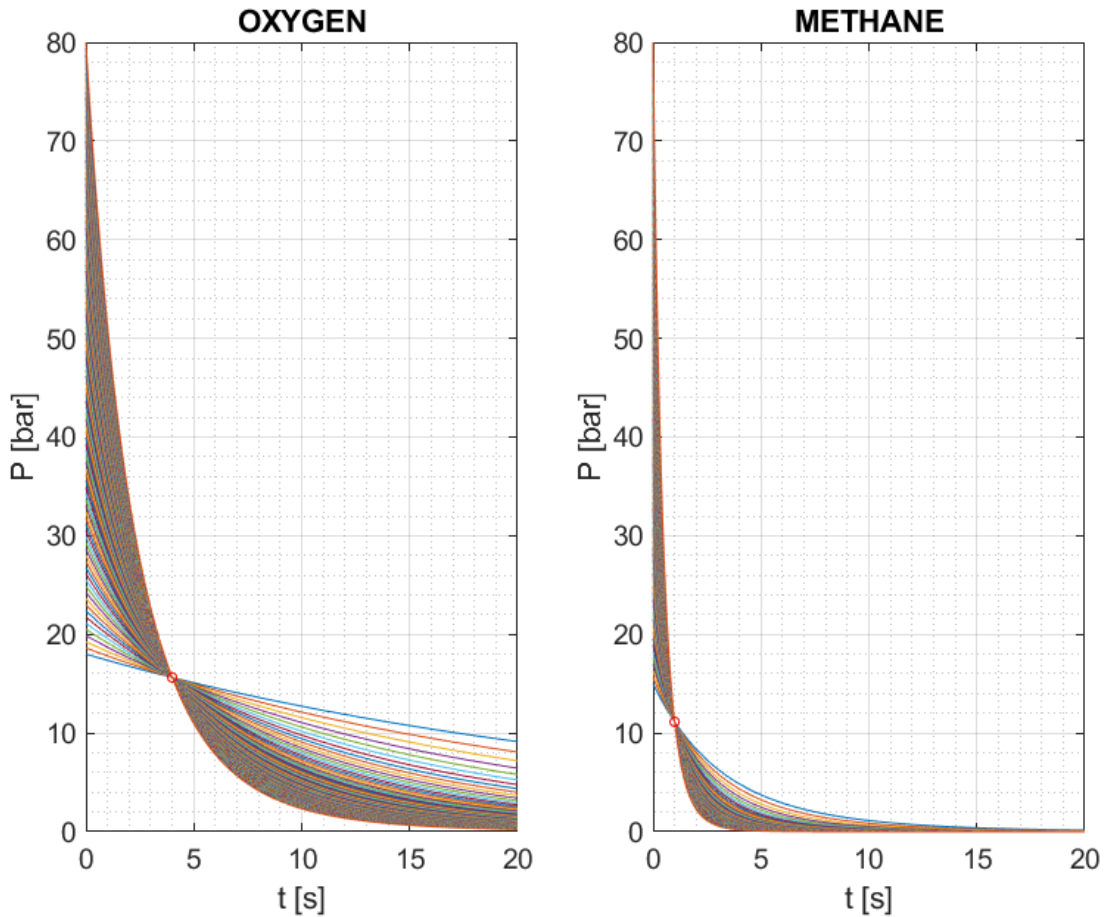


**Figure 3.9:** Pressure over time

Increasing the initial pressure in the tank  $P_0$  the pressure slope becomes steeper due to the fact that, being  $\dot{m} \propto P_0$ , more pressure means more mass flow therefore the discharge is faster. This means that in order to achieve such upstream pressure at such default time is necessary enhance the gas amount inside of tanks. For this reason, when the  $P_0$  is increased, it is required to iterate on the gas mass  $M$  so that the same boundary conditions of upstream pressure and ignition time are kept.

This kind of iteration is obtained with a code written on the software *Matlab* in particular using the function "*BLOWDOWN \_ ADIABATIC \_ CF.m*" reported in appendix A.1. This allowed to plot the beam curves in figure 3.9. Done this is also plotted the temperature over time for the aforesaid  $P_0$  pressure range in figure 3.10.

The temperature over time, in particular is seen that all curves start from the same point, imposed as a boundary condition from the design data, under the assumption of adiabatic flow.

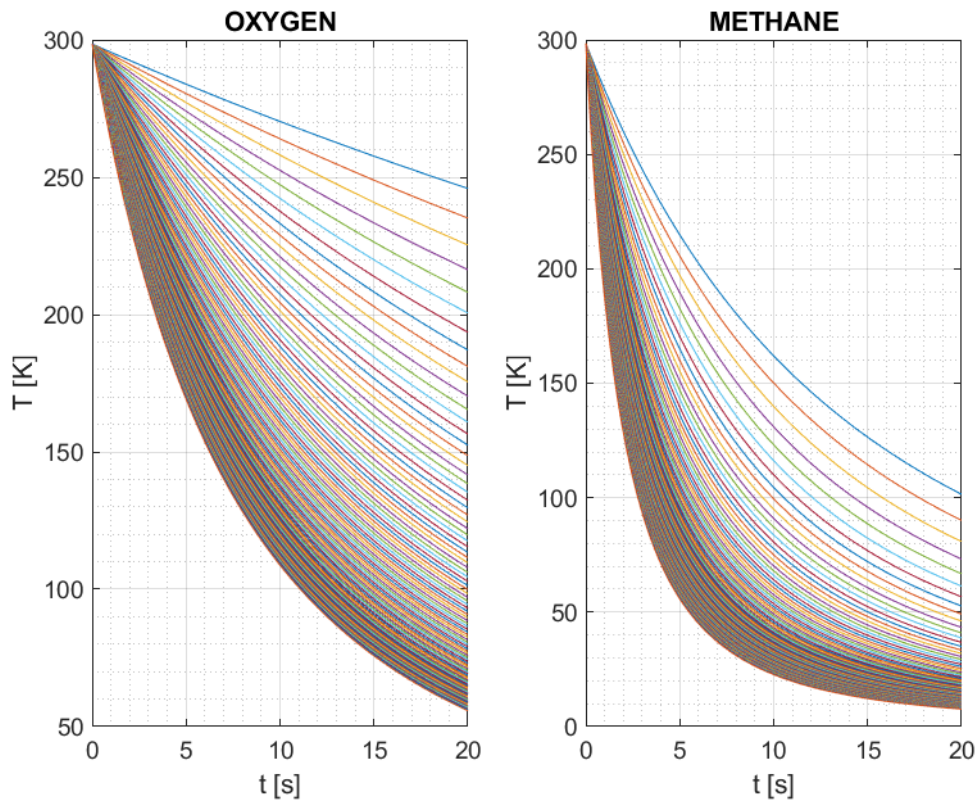


**Figure 3.10:** Temperature over time

Notable is also the difference between oxygen and methane: the first because of the longer use time has roughly slow decay of temperature over time, while methane because of a very short operative time has faster temperature decay and so steeper curves.

The latter consideration results important in the choice of the coupling between the curve oxygen/methane for the igniter supply, because the curves trends have to be as much as possible constant between them in order to guarantee  $O/F$  ratio approximately constant. This is also the reason why in this section 1 second of combustion time was chosen, so as to have a methane curve not too steep for the calculation of  $O/F$ . Now in order to choose the best pressure curve for both oxygen and methane, it is necessary see which one allows to have the minimum volume and the minimum consumption of both gases. For those reasons in figure 3.11 and 3.12 are plotted the gas mass over pressure and the volume over pressure. Again the deep difference between the two is explained from the different time of employment: the oxygen is used to achieve resonance during the preheating time ( $t_{up} = 4\text{ s}$ ); methane is introduced in the igniter only for the ignition time ( $t_{up} = 1\text{ s}$ ), so the mass of the gas needed is deeply different.

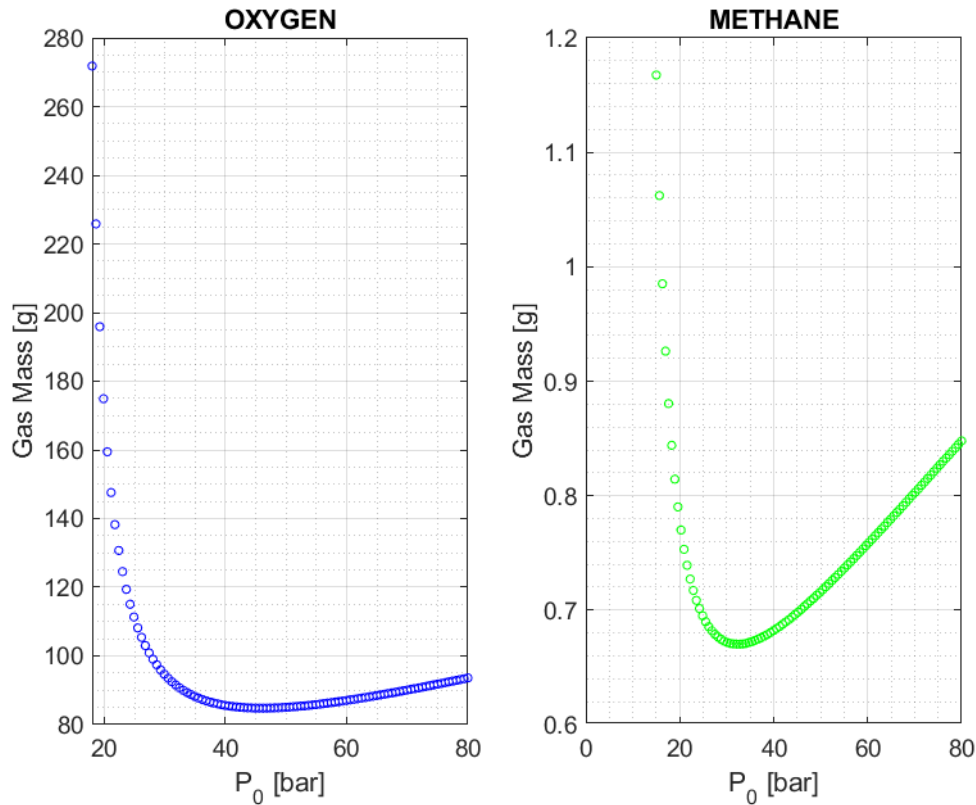


**Figure 3.11:** Gas mass over initial pressure in the tank

As a result of this the volume occupied by the two gas will be very different, which means that also the volume will be very different. It is possible to find this in figure 3.12 in which is shown the trend of volume depending on the initial pressure. Also in this case for high value of pressure the tendency is to a minimum value. Actually from figure 3.12 is not possible see this because that values of pressure are off the scale: in fact such values are very far from the operational envelope achieved in the cold flow test campaign. As a result, the values of excellent pressure, volume and mass of gas, the result of a pure analytical analysis that allow to obtain the correct value of mass flow rate are shown in the table 3.2.

**Table 3.2:** Optimum values

		Oxygen	Methane
$P_0$	[bar]	45	32
$V_0$	[L]	1.44	0.0323
<i>Gas Mass</i>	[g]	84	0.67

The values were chosen on the basis of the criterion of mass saving of gas because it is possible to identify a minimum value, or rather an optimal value.

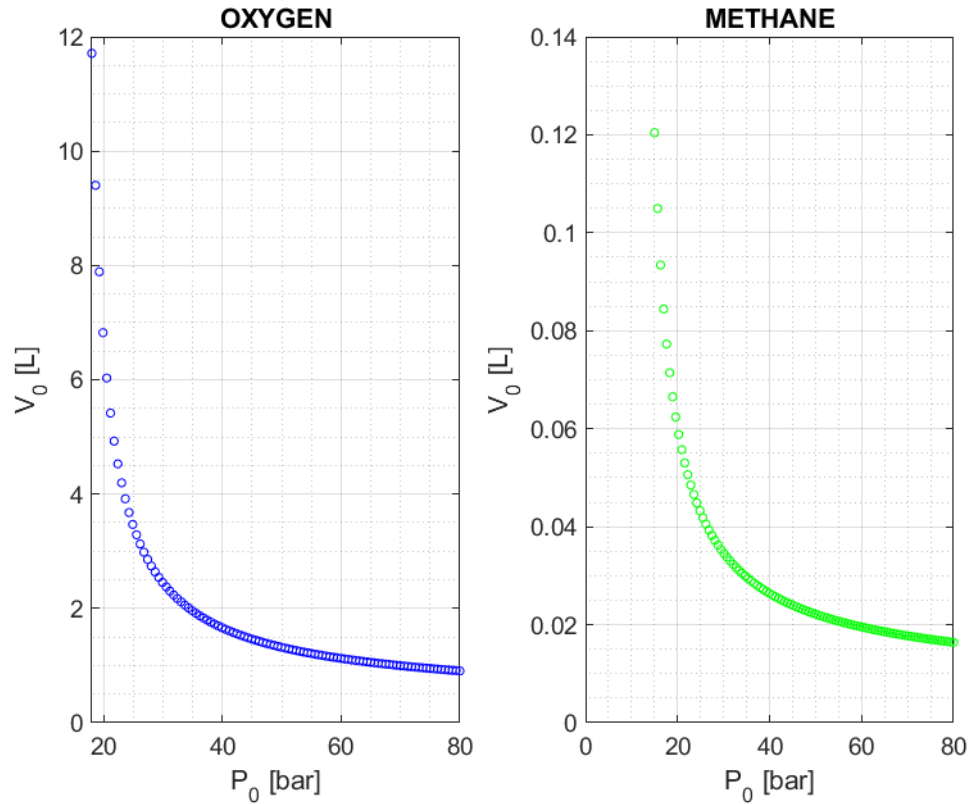


**Figure 3.12:** Volume over initial pressure in the tank

Definitely the solution has to be found in the pressure operational envelope of the igniter, that means to find the best compromise between the latter and the minimum volume occupied. In fact from the values in the table pressure is higher than the supply pressure used in chapter 2 during the blowdown campaign. This is due that, in this chapter, has been done a pure analytical analysis. Therefore, the results should be reviewed after carrying out the blowdown test campaign, which will be discussed in the chapter 4.

## 3.4 Tanks sizing

The tank design is largely influenced by systems optimization within the overall vehicle design. Moreover design details depend greatly upon type of propellants used, from the propulsion system design, mission requirement and available construction materials and manufacturing techniques [21].

### 3.4.1 Propellants Properties

The propellants properties affect design principally by their chemical and physical characteristics. For example storage temperature of propellants in the tanks determinates the operating temperature range. Furthermore the highly reactive and corrosive properties of some propellants strongly limit the choice of tanks materials [21].

#### Size and Shape of propellant Tanks

Tanks for propellants storage are pressurized vessels. Disregarding other factors, the lightest pressure tank for a given volume is a spherical casing, being that it has the smallest surface to volume ratio. The spherical shell has also the smallest structure stress for a given internal pressure.

The coupling of many spheres into generally cylindrical envelope typical for large quantity rocket vehicles causes a substantial volume penalty [21].

Generally vehicle configuration determinates the shape of propellant tanks: for example vehicles of relatively large length-to-diameter ratios and limited space envelopes, cylindrically shaped tanks are employed; on the other side vehicles that use quite high tank pressure and lower stringent conditions, spherical shape is used to best advantage.

Regarding cylindrical shape, the end of the latter could be either ellipsoidal or spherical. In general, normal configurations employ spherical ends because it is lighter than the one with ellipsoidal end. On the other hand ellipsoidal ended vessel has an overall weight lower, when the shorter interstage structure required is considered [21].

Going ahead with fluid system design in the simplest and lightest way, the spherical tanks shape is selected.

After this it is necessary to find out the key parameters of pressurized spherical shapes vessel in order to size them in term of thickness, dimension, material and so on.

First of all in the next sub-paragraph is presented an analytical ease approach and the results.

**Mathematical analysis in the sizing of spherical tanks** As mentioned previously internal stress in a spherical shape vessel is constant, since pressure forces are evenly distributed, as it is shown in figure 3.13.

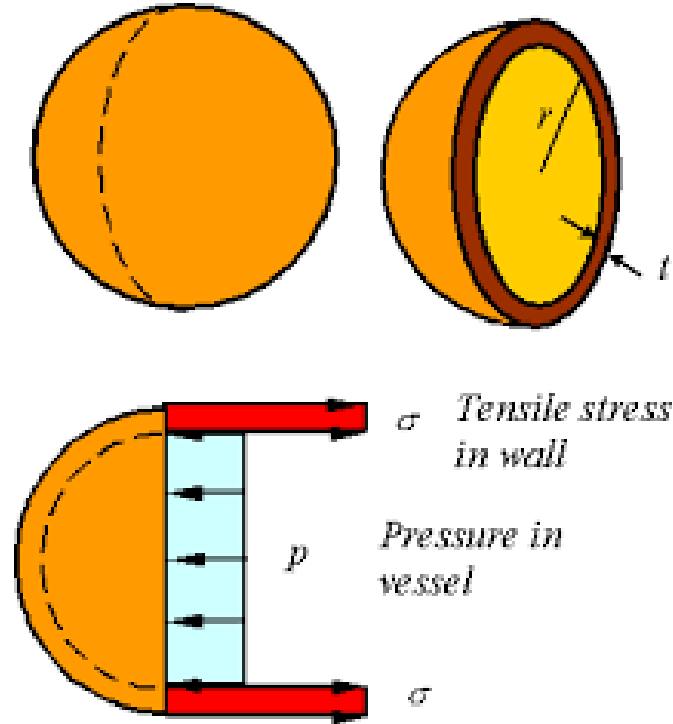


**Figure 3.13:** Pressure forces distribution in a spherical shape [25]

Given the initial pressure in the tank  $P_0$  and the volume  $V_0$ , in necessary to define the thickness of tanks in such a manner that it resists under operative internal pressure. Considering the hypothesis of thin walled vessel, the structural mass is equal to

$$M_{structural} = 4\pi r^2 \cdot th \cdot \rho_{structural} \quad (3.30)$$

where  $th$  is the vessel wall thickness and  $\rho_{structural}$  is the density of the material employed to build such tank.

To evaluate the thickness it is possible to do an equilibrium of agent pressures on half spherical cap, as shown in figure 3.14.

The force due to the internal pressure is

$$F_{internal} = P_0 \pi r^2 \quad (3.31)$$

while the stress on the thin wall is

$$F_{wall} = \sigma \cdot A \quad (3.32)$$

in which  $A = 2\pi r \cdot th$  is the section on whom the stress acts.

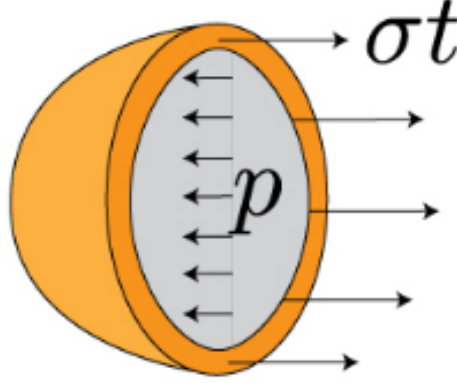


**Figure 3.14:** Agent pressure on half spherical cap [25]

Imposing now that  $\sigma = \sigma_{material}$  and equating the forces is obtained

$$F_{internal} = F_{wall} \rightarrow P_0 \pi r^2 = \sigma_{yield} \cdot 2\pi r \cdot th \quad (3.33)$$

Now dividing with an appropriate Safety Factor  $S_y$  the yield stress  $\sigma_{yield}$ , the 3.33 becomes

$$F_{internal} = F_{wall} \rightarrow P_0 \pi r^2 = \frac{\sigma_{yield}}{S_y} \cdot 2\pi r \cdot th \quad (3.34)$$

Then proceeding to explain the thickness is obtained

$$th = \frac{S_y}{\sigma_{yield}} \cdot \frac{r}{2} \cdot P_0 \quad (3.35)$$

Equation 3.35 permits to calculate how thick has to be the tank, once defined the material, defining only one parameter that is initial tank pressure  $P_0$ .

After that knowing the structural mass

$$M_{structural} = \rho_{material} \cdot V_0 = \rho_{material} \cdot 4\pi r \cdot th \quad (3.36)$$

Replacing equation 3.35 in 3.36 it is possible to write the structural mass as a function of pressure

$$M_{structural} = \rho_{material} \cdot 4\pi r \cdot \frac{S_y}{\sigma_{yield}} \cdot \frac{r}{2} \cdot P_0 = 2\pi r^3 \frac{\rho_{material} \cdot S_y}{\sigma_{yield}} \cdot P_0 \quad (3.37)$$

Now remembering that sphere volume is

$$V_0 = \frac{4}{3}\pi r^3 \quad (3.38)$$

and substituting in 3.37 is given tank structural mass as function of pressure and volume

$$M_{structural} = \frac{3}{2} S_y \frac{\rho_{material}}{\sigma_{yield}} \cdot P_0 \cdot V_0 \quad (3.39)$$

From equation 3.39 and 3.35 it is possible notice importance of material choice in order to define overall structure. In addition to propellants and compatibility considerations and operative rang of pressure, the picking of building materials for tanks is based on their strength-to-density ratio. The lightest tank, for a given operating pressure, will be the one built with the highest ratio of ultimate strength-to-density [21].

As regards to safety factor for propellants tanks design, when calculating allowable-working stresses from the internal pressure, the following correlations are prescribed for different situations:

- no hazard to personnel or vital equipment:

$$- S_W = \sigma_{yield}$$

- special safety device that are provided for personnel

$$- S_W = \frac{\sigma_{yield}}{S_y} \text{ with } S_y = 1.1 \text{ [21]}$$

- hazard to personnel or vital equipment

$$- S_W = \frac{\sigma_{yield}}{S_y} \text{ with } S_y = 1.33 \text{ [21]}$$

where

- $S_W$  is the maximum allowable working stress measured in Pascal: in particular represent the maximum stress due to maximum tank working pressure under normal transient and steady operating conditions [21];
- $\sigma_{yield}$  is the yield strength, in Pascal, of the tank construction material, at operating temperature conditions;
- $S_y$  is the safety factor that is the ratio between the yield strength of the material and the maximum allowable working stress.

Now, in order to choose the appropriate material, a study about how structural properties change with initial pressure  $P_0$  and volume  $V_0$  is investigated. In addition, those properties, are evaluated employing some of the most common materials [7], shown in table 3.3. The tanks sizing calculation have been performed by a Matlab script reported in appendix A.3. The structural properties have been evaluated for each value of initial pressure  $P_0$  and volume  $V_0$  obtained in section 3.3, for each material shown in the table 3.3. It is possible to see that, from the Strength-to-Density ratio, the lightest tank is the one made with titanium, having as said before, the highest value of such ratio.

**Table 3.3:** Materials properties [7]

Material	Density [ $Kg/m^3$ ]	Yield Strength [ $MPa$ ]	StD Ratio
STEEL (quenched and tempered alloy ASTM-A514)	7860	690	0.0878
ALUMINIUM (4.4% Cu 2014-T6)	2800	410	0.1464
TITANIUM ALLOY (6% Al, 4% V)	4460	825	0.1850

Referring to figure 3.15 and figure 3.16 for both oxygen and methane, with increased pressure in the tank, structural mass decreases due to the fact that higher pressures imply a reduction of volume. This decrease is true up to the minimum of the curve, after which the pressure value is so high that the thickness becomes predominant, causing an increase in the weight of the tank. The effect of volume on the overall empty weight of the tank is shown in figure 3.17 and figure 3.18.

The wall thickness over pressure presents an opposite behaviour with respect to tank mass over pressure, i.e with increasing of pressure tank walls are more loaded, consequently walls must be thicker in order to resist to high pressure (see figure 3.19 and figure 3.20). Finally in figure 3.21 and figure 3.22 is shown the trend of the radius over volume, in order to have an idea of overall size of tanks.

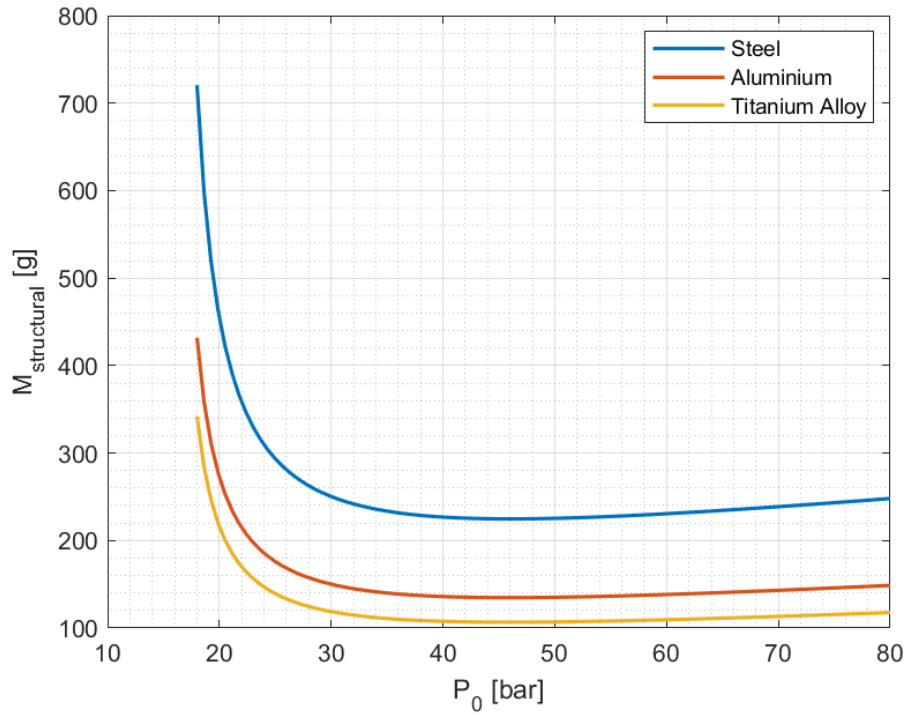


**Figure 3.15:** Effect of pressure on structural mass for various materials - OXYGEN

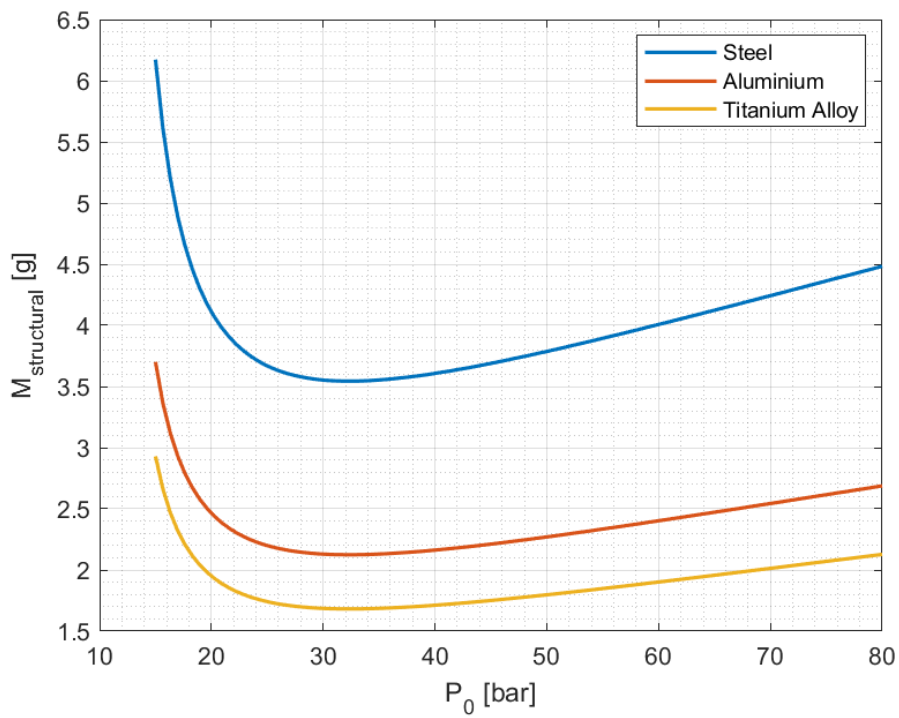


**Figure 3.16:** Effect of pressure on structural mass for various materials - METHANE

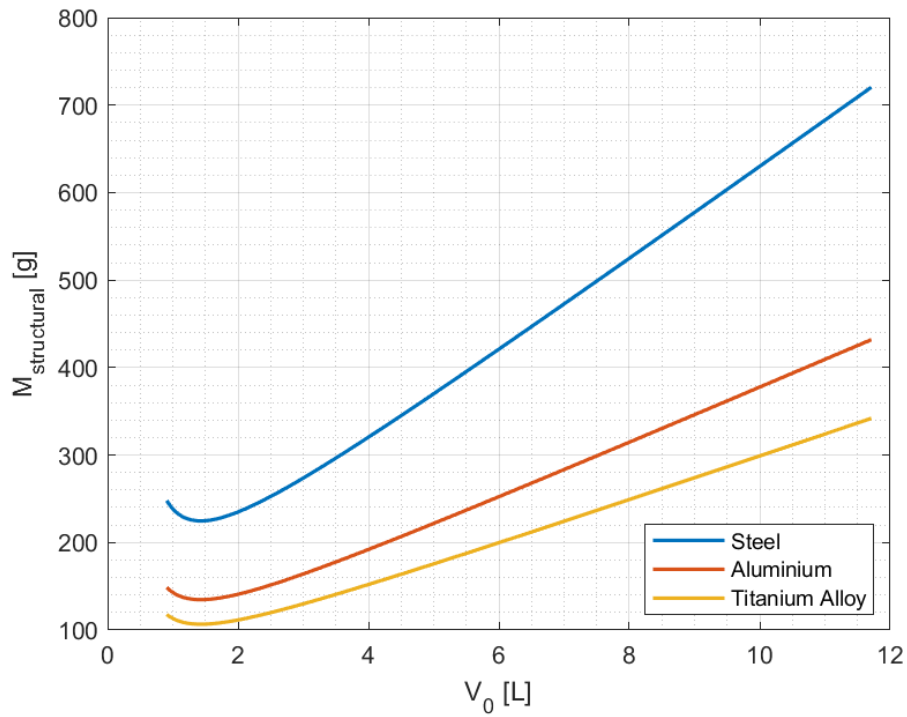


**Figure 3.17:** Effect of volume on structural mass for various materials - OXYGEN

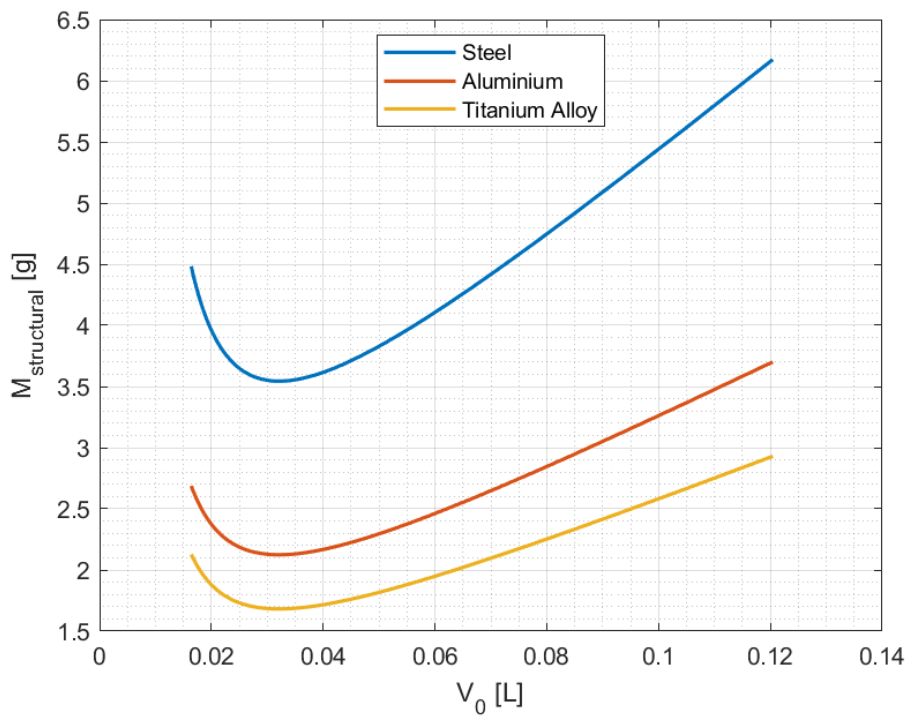


**Figure 3.18:** Effect of volume on structural mass for various materials - METHANE

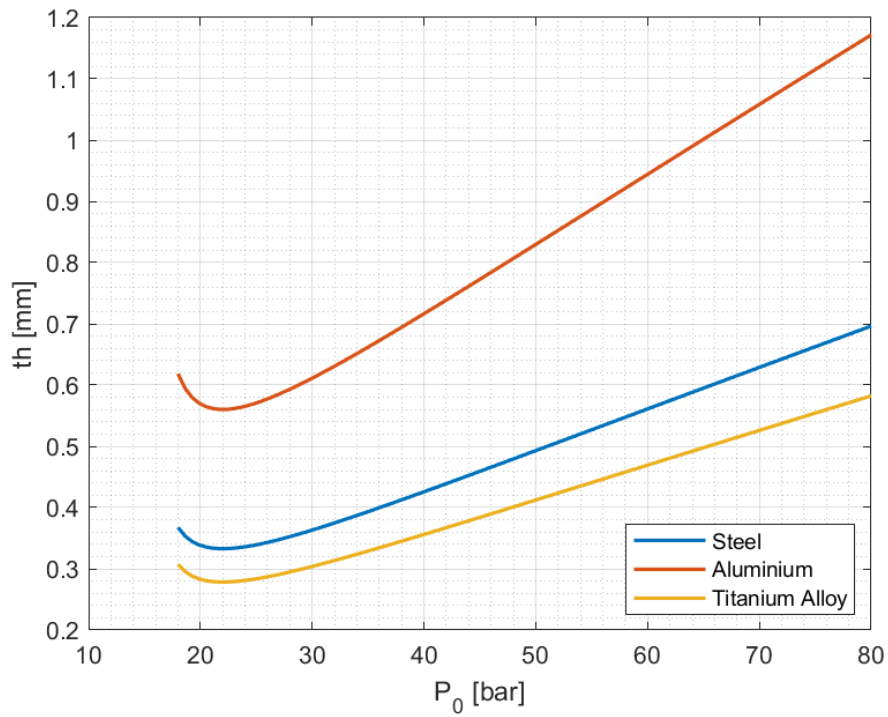


**Figure 3.19:** Effect of pressure on wall thickness for various materials - OXYGEN

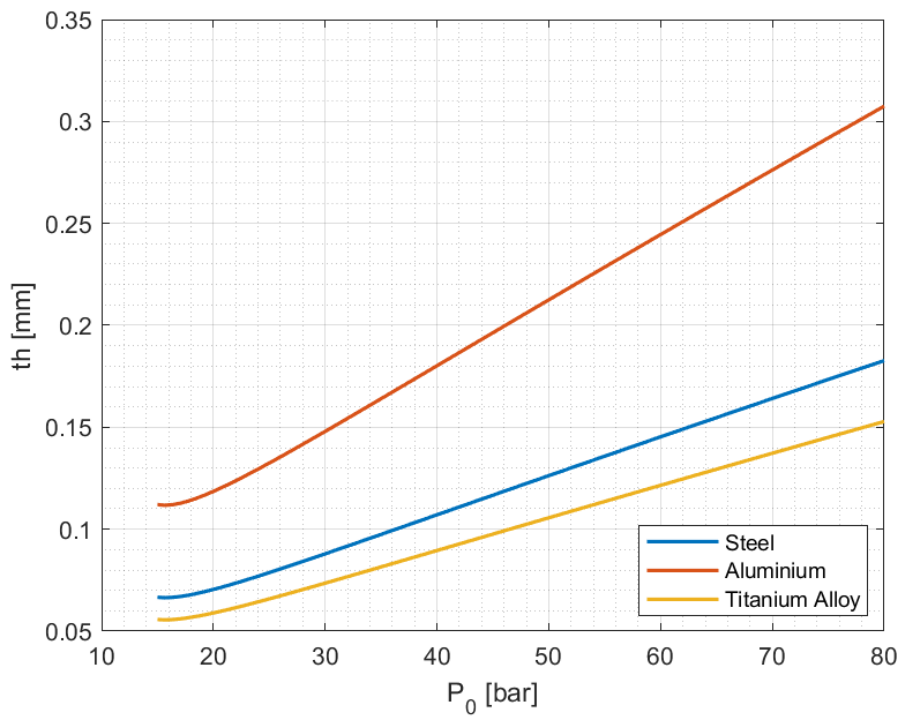


**Figure 3.20:** Effect of pressure on wall thickness for various materials - METHANE

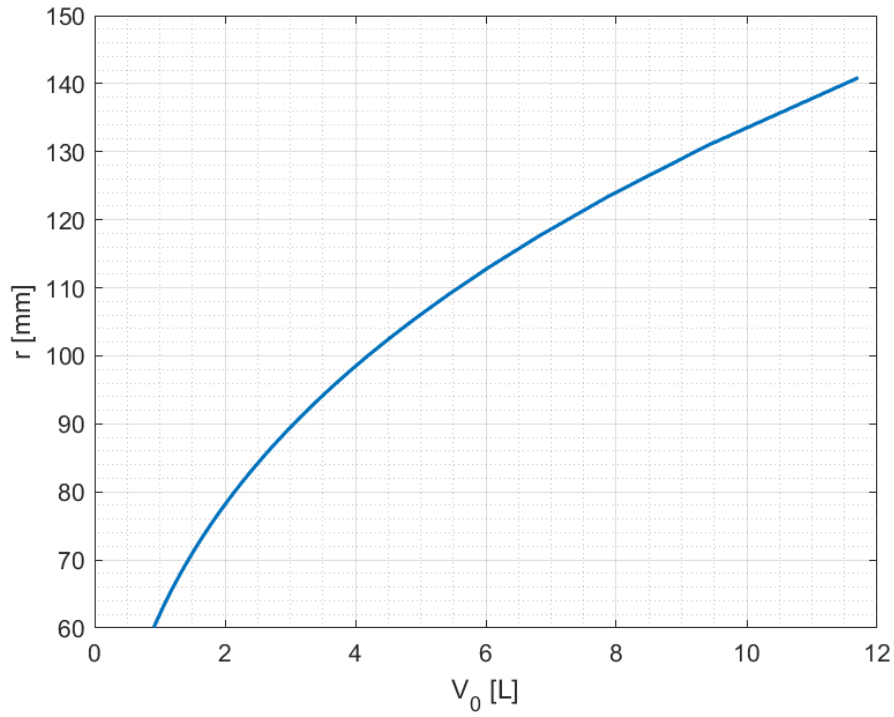


**Figure 3.21:** Effect of volume on tank radius - OXYGEN

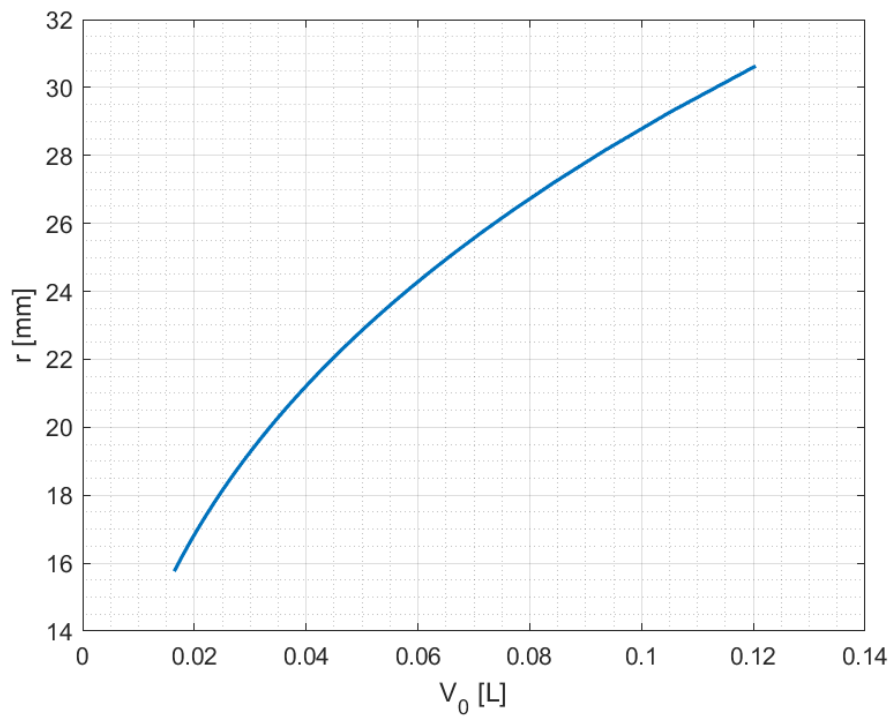


**Figure 3.22:** Effect of volume on tank radius - METHANE

Because titanium alloys have high tensile strength to density ratio, high corrosion resistance [26], fatigue resistance, high crack resistance,[27] and ability to withstand moderately high temperatures without creeping, this material is selected to build the tanks. Furthermore, the titanium 6AL-4V alloy accounts for almost 50% of all alloys used in aircraft applications. Table 3.4 shows the structural characteristics for the tanks selected in the previous section (see table 3.2).

**Table 3.4:** Structural optimum values

		Oxygen	Methane
$M_{structural}$	[g]	106.65	1.68
$th$	[mm]	0.38	0.07
$r$	[mm]	70	19

Referring to the thickness values shown in the table, it is possible to note that these values are such as not to allow their realization. This is due to the fact that the analysis was carried out with a purely analytical approach. Therefore, considering the problem of manufacturing, in order for these tanks to be built, it will be necessary to consider a different value of thickness. This will lead to heavier tanks, but will allow their construction. This is especially important concerning the methane tank since the wall thickness is far lower. However, the methane tank is also smaller, so a higher wall thickness will not add much to the overall mass. Detailed information on manufacturing of advanced titanium propellants tanks can be find in [28].

## Chapter 4

# Blowdown test campaign

This chapter is going to be focused on the blowdown test campaign realized as a validation of theoretical calculations carried out in chapter 3 and in order to obtain experimental data to understand ignition feasibility inside of a blowdown supply system.

## 4.1 Experimental setup: blowdown supply system

The blowdown supply system used is basically the same used for pressure regulated test campaign (see chapter 2 subsection 2.4.1). In figure 4.1 it is possible to see that the only difference is the adding of blowdown tanks, one in the methane line and one in the oxygen line. These are arranged between the two actuating valves: this allows the valve upstream of the tank to be opened and filled; after which the upstream valve is closed and by opening the downstream valve the tank is emptied into a blowdown way (for items legend see figure 4.2). The oxygen blowdown supply tank volume is equal to 3.78 liters since this hardware was available in laboratory. On the other hand, the methane blowdown supply tank volume, instead, is equal to 0.150 liters since methane operation is 2 seconds (1 seconds of requirement), as explained in chapter 3. In table summarises the values used in the experimental tests.

**Table 4.1:** Experimental setup values

	Oxygen	Methane
<i>Run time</i> [s]	10	2
<i>Tank Volume</i> [L]	3.780	0.150

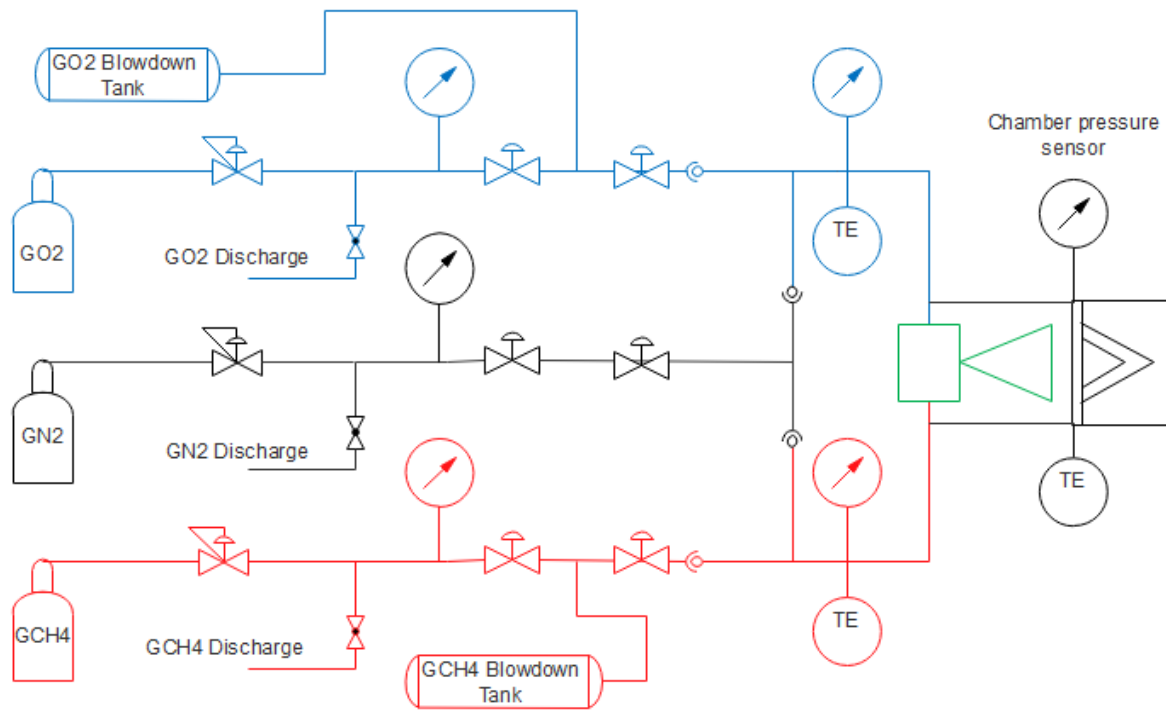


**Figure 4.1:** Blowdown supply system for tests

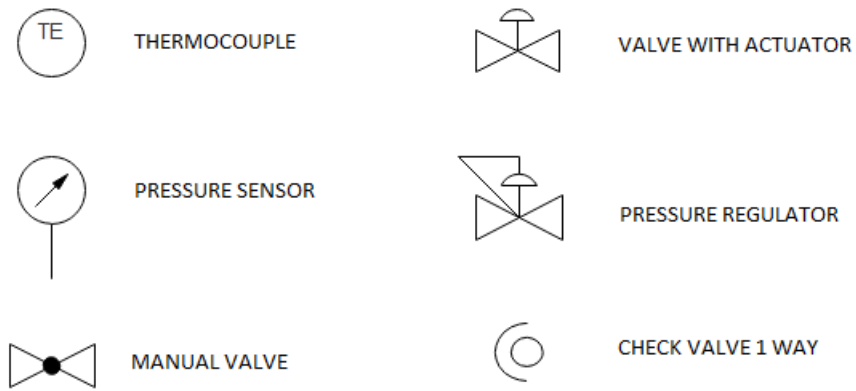


**Figure 4.2:** Blowdown supply system symbols legend

### 4.1.1 Control sequence

As supply system has been modified also control sequence of actuators and valves has to be changed.

**Cold Flow control sequence** The new cold flow control sequence of actuators and valves is shown in figure 4.2 where

- MVN1 = Magnetic Valve Nitrogen directly after pressure regulator
- MVO1 = Magnetic Valve Oxygen directly after pressure regulator
- MVF1 = Magnetic Valve Methane directly after pressure regulator
- MVN2 = Magnetic Valve Nitrogen referred to main valve with actuator
- MVO2 = Magnetic Valve Oxygen referred to main valve with actuator
- MVF2 = Magnetic Valve Methane referred to main valve with actuator

Since it is cold flow, methane line is not used and consequently MVF1 and MVF2 they remain closed for the whole sequence duration.

**Table 4.2:** Blowdown Cold Flow sequence

Time [s]	MVN1	MVN2	MVO1	MVO2	MVF1	MVF2
0	0	0	0	0	0	0
1	0	0	1	0	0	0
6	0	0	0	1	0	0
16	0	0	0	0	0	0
16.5	0	0	0	0	0	0
17	1	1	0	0	0	0
19	0	1	0	0	0	0
21	0	0	0	0	0	0

First of all at  $t = 1$  s the valve just after the pressure regulator opens and the tank starts to fill up until tank pressure is equal to the setted value from upstream pressure

regulator. At  $t = 6$  s MVO1 closes, so the tank is filled. In the same time opens MVO2 and preheating starts for 10 seconds. At  $t = 16$  s preheating is now over and so MVO2 is closed. Now both MVO1 and MVO2 are closed. After that MVN1 and MVN2 open and purge occurs from  $t = 17$  s to  $t = 21$  s. The sequence is thus terminated.

## 4.2 Blowdown Cold Flow test campaign

Based on the pressure regulated cold flow campaign, in particular the one after resonator repair,  $s/d$  value is set to the optimum, which was 1.525. The first test has been run first with 10 seconds of preheating then then has been reduced to 5 seconds. Referring to figure 4.3, comparing 5 seconds to 10 seconds of preheating, it is possible to see that there is not a substantial difference in maximum temperature reached.

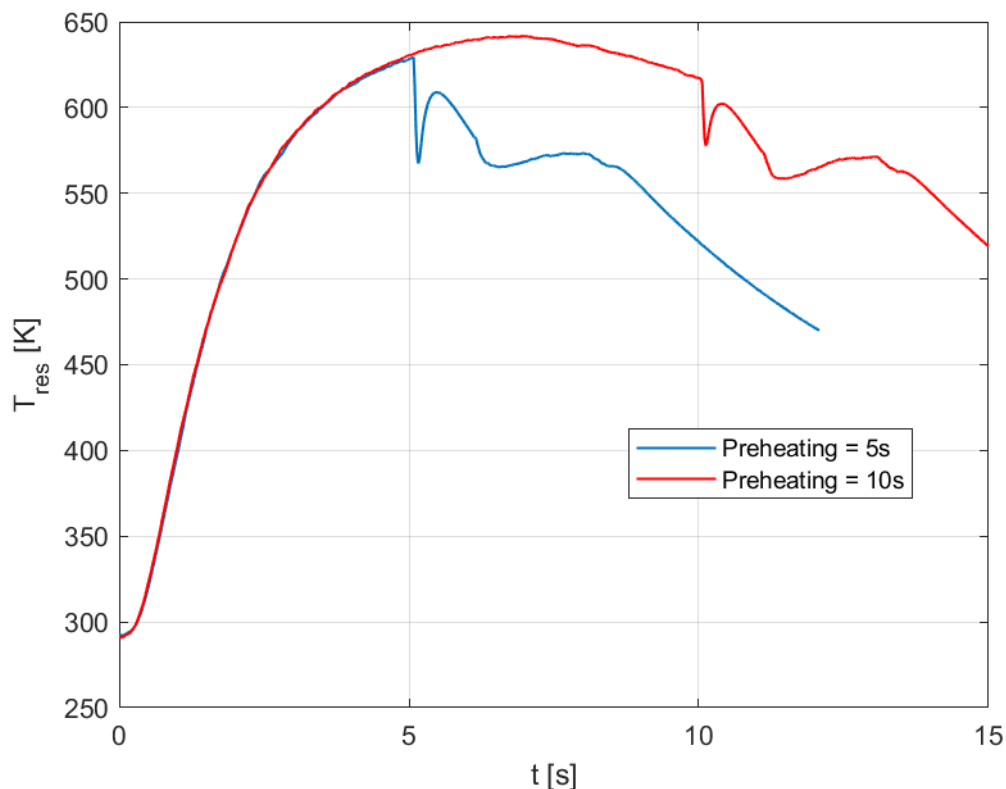


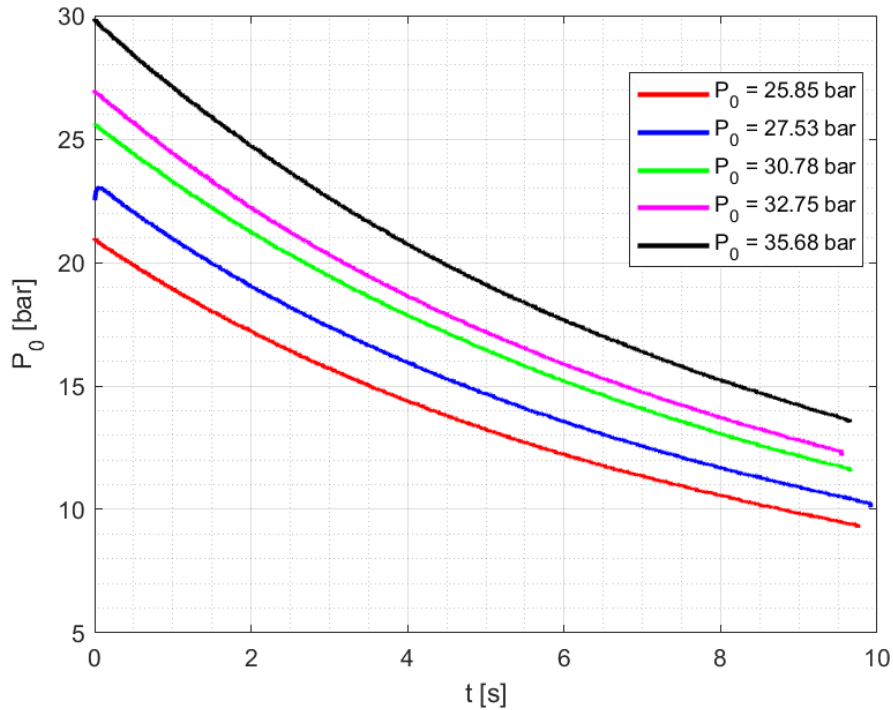
**Figure 4.3:** Resonator temperature over time

The target in terms of maximum temperature is fixed by reference to results obtained in subsection 2.4.2. Table 4.3 shows the maximum temperature values obtained for each initial pressure in the tank set. As can be seen in the figure 4.4, the initial pressure differs from that set in the tank by the pressure regulator, which is shown in the table 4.3. This fact is due to the pressure losses, which will be dealt with in the next section.

**Table 4.3:** Maximum resonator temperature for initial pressure in the blowdown tank

$P_{O_2}$ [bar]	$T_{MAX,5s}$ [K]	$T_{MAX,10s}$ [K]
25.85	598.95	595.36
27.53	611.05	611.82
30.78	622.13	627.08
32.75	628.50	633.10
35.68	629.47	641.75

The campaign starts with an initial tank pressure  $P_0 = 25.85 \text{ bar}$ : is  $T_{MAX} = 598.95 \text{ K}$ , but, with respect value obtained in pressure regulated test campaign before resonator repair, is lower. In fact, here, pressure decreases over time, so starting with 25.85 bar (see red curve in figure 4.4) does not mean having 25.85 bar during the entire preheating, but means lower pressure which are not enough so that  $T_{MAX}$  exceed the assumed value of 600 K, which allows to have ignition. In fact, actually, resonator is working with lower pressures (see figure 4.4), out of the operative envelope of supply pressure defined in subsection 2.4.2.

**Figure 4.4:** Pressure over time - experimental data

As consequence of this initial tank pressure is increased to 27.53 bar (see blue curve in figure 4.4). It results, as expected, in a raise of  $T_{MAX}$  equal to 611.05 K (see table 4.3): it means that nozzle pressure ratio is higher and chamber works in choking conditions for wider time. But comparing to around 630 K reached in pressure regulated test campaign is not still enough.

Increasing even more  $P_0$  in the tank to 30.78 bar (see green curve), due again to an higher nozzle pressure ratio, as expected heating effect is stronger as is highlighted in table 4.3, confirming an upward trend, shown in figure 4.5.

Increasing still more oxygen supply pressure to 32.75 bar and 35.68 bar is obtained a comparable value of maximum temperature with values obtained in the pressure regulated test campaign.

The cold flow test campaign showed that a preheating time of 10 seconds does not bring a substantial gain in terms of the maximum temperature reached by the resonator as it is possible to see in figure 4.5. Moreover, such a long time leads to an excessive waste of oxygen and above all leads to larger tanks than necessary.

As far as the supply pressure is concerned, both because there are pressure losses and because the pressure decreases over time, higher supply pressures are required to achieve maximum resonator temperatures comparable to those obtained with a pressure regulator.

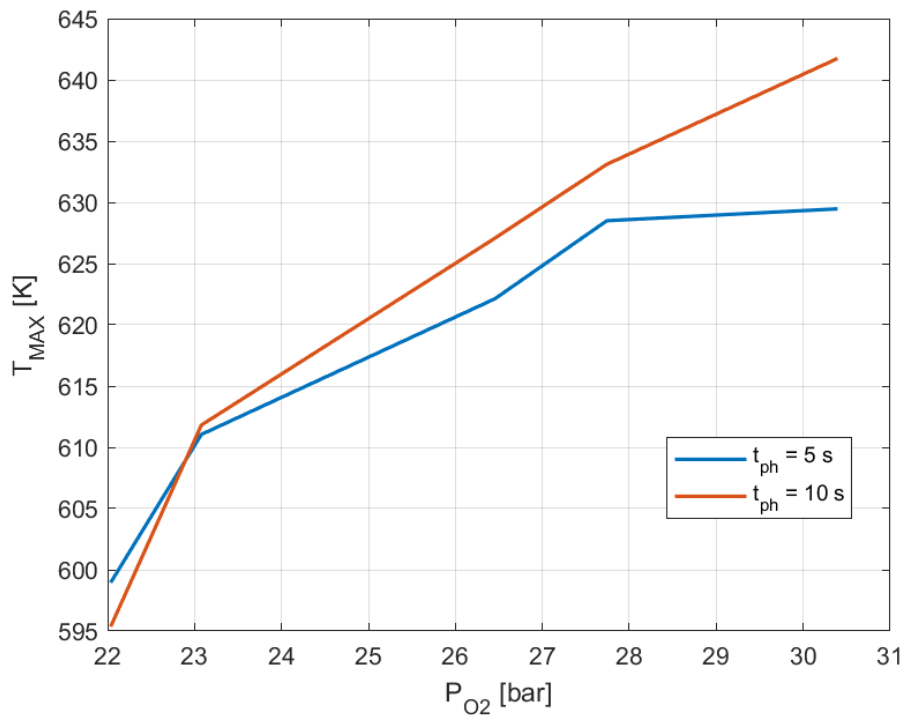


**Figure 4.5:** Resonator maximum temperature over measured pressure

## 4.3 Calculation model validation with experiments

This section is dedicated to validate with the experimental data the theoretical calculation models used in chapter 3 to design fluid system tanks. In particular the purpose is to compare pressure over time trends of the adiabatic and isothermal model to pressure over time trends obtained with blowdown experiments for both oxygen and methane. In this way it is possible to choose initial tanks pressure such to have a certain mass flow to get a proper oxidizer to fuel ratio that allows to achieve ignition.

**Oxygen validation** Oxygen blowdown pressure over time curves have been obtained during blowdown Cold Flow tests.

Comparing the models with experimental data, as it is possible to see in figure 4.6 for an initial tank pressure of 35 bar, the more appropriate model to describe blowdown phenomena is the isothermal one.

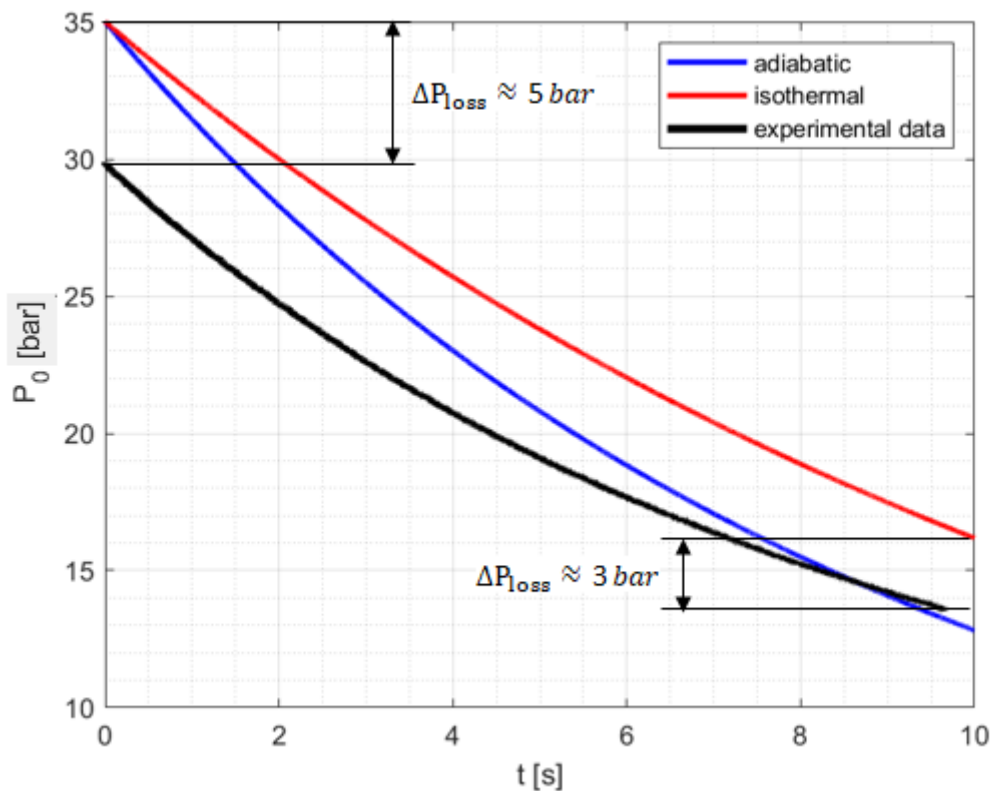


**Figure 4.6:** Blowdown models comparison with experimental data -  $P_0 = 35 \text{ bar}$

Ten seconds represent a slow tank discharge and consequently in not negligible the heat exchange between tank/pipelines and surroundings. The pressure difference ( $\Delta P_{loss}$ ) between isothermal model and experimental data is partially explained by heat exchange with surroundings, but mainly this offset is due to the pressure losses in the pipelines and actuated valve downstream the tank, which are not taken into account in the isothermal model. This pressures losses decrease approximately linearly over time with density: in fact, as it is possible to see in figure 4.6, at the beginning they are about  $\Delta P_{loss} \simeq 5$  bar, while in the end about  $\Delta P_{loss} \simeq 3$  bar. In particular due to sufficiently low gas velocity in propellant lines (Mach  $< 0.3$ ) static pressure and temperature are respectively assumed as equal to total pressure: because of this it is possible correlate dynamic pressure to velocity in both isothermal model and experimental data as follow:

$$\Delta P \propto \frac{1}{2}\rho c^2 \quad (4.1)$$

and so write pressure losses for the pressure over time is obtained that

$$\Delta P_{loss} \propto \Delta P_{isothermal} - \Delta P_{experimental} = \frac{1}{2}\rho(c_{isothermal}^2 - c_{experimental}^2) \propto \frac{1}{2}\rho\Delta V \quad (4.2)$$

The velocity decreases over time, consequently pressure losses due to dynamic pressure decrease over time. The oxygen pipelines volume has been neglected since it represents only the 1.3 % of the whole volume in the oxygen line.

**Methane validation** Methane blowdown test also confirms that the isothermal model is more appropriate than the adiabatic one to study the blowdown tank discharge. Figure 4.7 shows same trend observed with the oxygen, with a pressure offset between the theoretical isothermal model and the experimental data due to pressure losses in pipelines and valve downstream the tank. Here, the discharge time being very short (2 seconds), the curves are almost similar to straight lines and the losses have a constant trend.

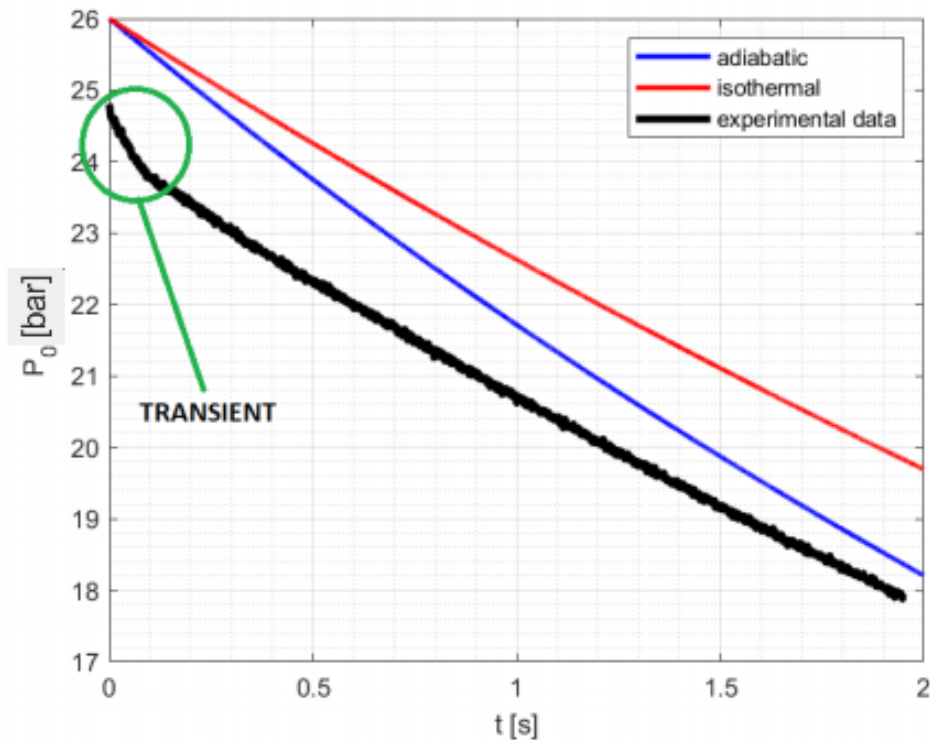


**Figure 4.7:** Blowdown models comparison with experimental data -  $P_0 = 26 \text{ bar}$

In this case the pipelines volume is not negligible being methane pipelines volume half than methane tank. So in the plot represented in figure 4.7 pipelines volume is taken into account. In fact, from the graph it is possible to see that for 1 tenth of a second the curve is steeper due to a transient in which the pipes are filled. In the case of oxygen this transient is not visible because the pipelines represent only 1.3% of the total volume and therefore have a negligible effect during the discharge of the tank.

Also for methane are evaluated several initial tank pressure, and the experimental results are shown in figure 4.8, for 2 second of discharge.

Considering also other initial pressure values, we notice the same phenomenon of an initial transient due to the not negligible volume of the pipes. In addition, it can be seen in the figure 4.11 that as the initial pressure inside the tank increases, the stretch of curve that represents the transient is steeper. This is due to the fact that the higher the initial

pressure is inside the tank, the greater the difference in pressure between the tank and the pipes is. This results in a higher slope of the curve section of the initial transient.

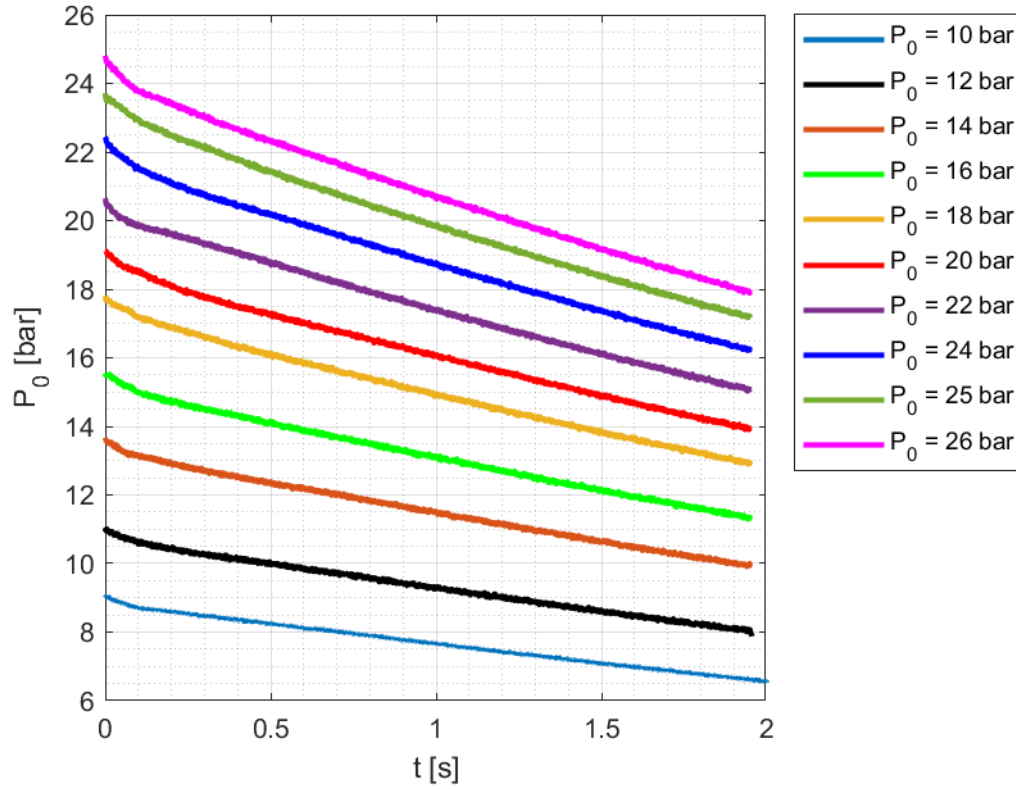
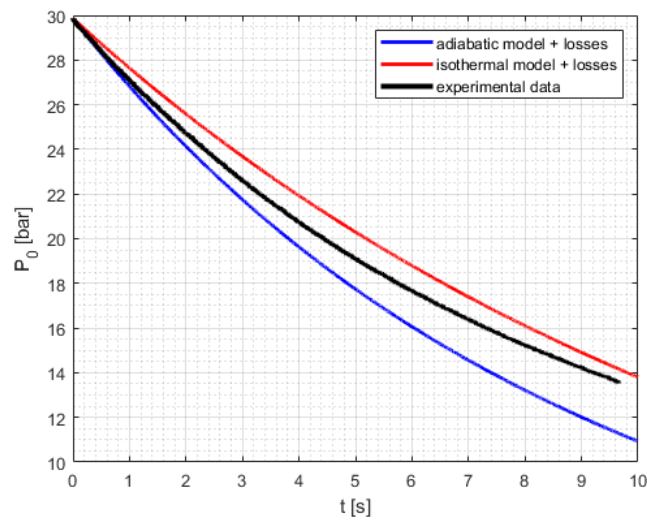
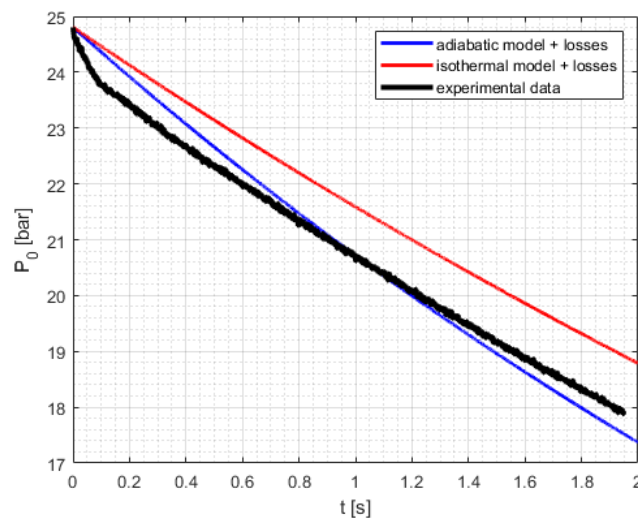


Figure 4.8: Pressure over time - experimental data

**Isothermal model: losses addition** Comparing the experimental data with the isothermal model, an estimate of the losses due to pipes and valves was obtained. Taking now into account the losses in the calculation with the isothermal model, we obtain the following figure 4.9 and 4.10. As far as oxygen is concerned, it is important to see how, considering the losses, the isothermal model roughly follows the experimental data. A slight offset is still present, due to the assumptions of the calculation model (see section 3.2) such as heat perfect gas, one dimensional flow etc. The same is true for methane: for the latter, however, it is possible to observe a higher offset and with a constant trend, due to the fact that the model is almost stationary and does not take into account the transient that occurs because of the volume of the methane pipes (figure 4.10).



**Figure 4.9:** Pressure over time - models comparison plus losses: oxygen



**Figure 4.10:** Pressure over time - models comparison plus losses: methane

### 4.3.1 Oxidizer to fuel ratio calculation

Once the pressure over time for both oxygen and methane are known, and consequently temperature over time it is possible to calculate the mass flow assuming

- isentropic expansion
- flow choked
- ideal gas
- total pressure equal to static pressure (gas velocity low)
- $C_d$  equal to 1

which is equal to

$$\dot{m} = C_d \frac{PA_t}{\sqrt{RT}} \sqrt{k} \left[ \frac{k+1}{2} \right]^{\frac{-(k+1)}{2(k-1)}} \quad (4.3)$$

where  $C_d$  is the discharge coefficient,  $A_t$  is the orifice throat area,  $P$  and  $T$  respectively static pressure and static temperature and  $k$  is the isentropic exponent.

Then the oxidizer to fuel ratio is equal to

$$\frac{O}{F} = \frac{\dot{m}_{O_2}}{\dot{m}_{CH_4}} \quad (4.4)$$

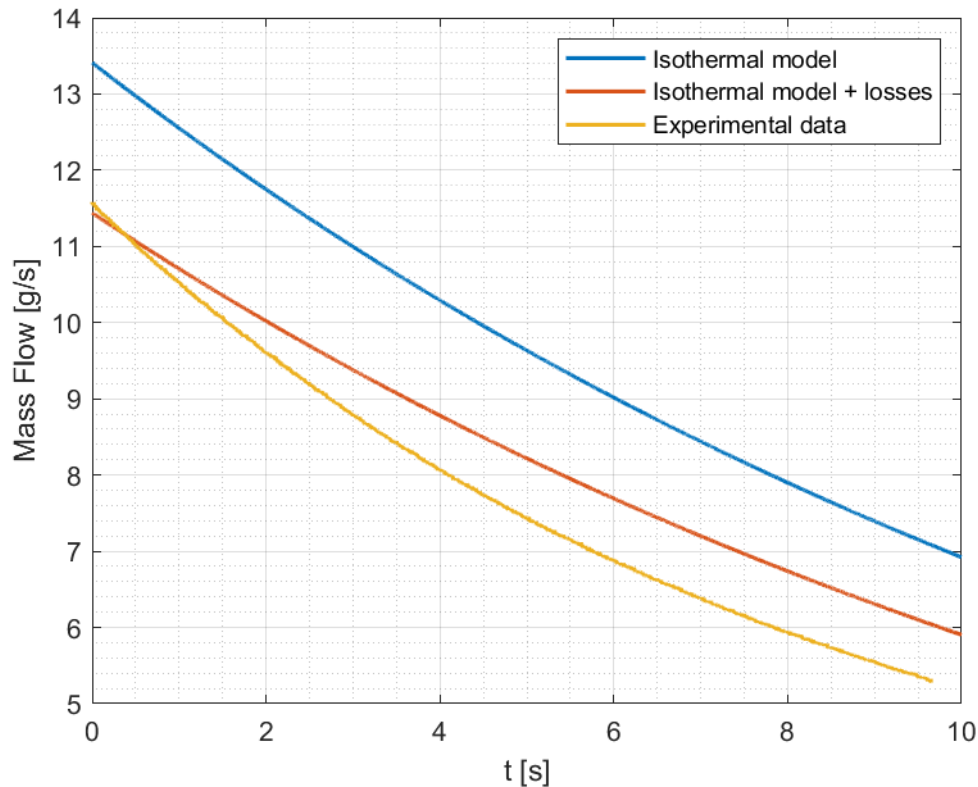
An oxidizer / fuel (O/F) ratio of 30 has been chosen as nominal, for the pressure regulated tests, since it is sufficiently far away from the lean flammability limit of O/F = 36 but still lean enough so that the resulting hot gas temperatures allow for a sufficiently long operating time of the ignition system [2].

In the case of blowdown, the objective is to have a constant or limitless O/F within an acceptable range. For the Z1 igniter it has been defined an envelope in which reliable ignitions are produced, thus defining the operational margins of the ignition system [2]. With regards to the latter, in the present study an O/F between 25 and 30 is chosen. In order to fall within this range, oxygen and methane blowdown pressure over time curve have to be comparable in terms of local slope in order to achieve a roughly constant ratio. The parameters that have been chosen for oxidizer to fuel calculation are presented in table 4.4.

**Table 4.4:** O/F calculation parameters

$t_{ph}$	5 [s]	Preheating time
$t_{oxygen}$	6 [s]	Oxygen run time
$t_{methane}$	1 [s]	Methane run time

Five seconds of preheating time and one second of methane run time are selected on the basis of the actual resonator performances, in particular with regards to blowdown cold flow test campaign. Thus oxygen mass flow and methane mass flow are calculated and a comparison with isothermal model is represented in figure 4.11 and figure 4.12. Also analysing mass flow trend it is possible to highlight how the isothermal model is appropriate to study the phenomena. Moreover is even here present pressure losses offset between the isothermal model and experimental data. As regards the difference between the experimental data and the isothermal model plus the losses, the offset is to be attributed, as described above, to the assumptions on which the model is based.

**Figure 4.11:** Oxygen mass flow comparison

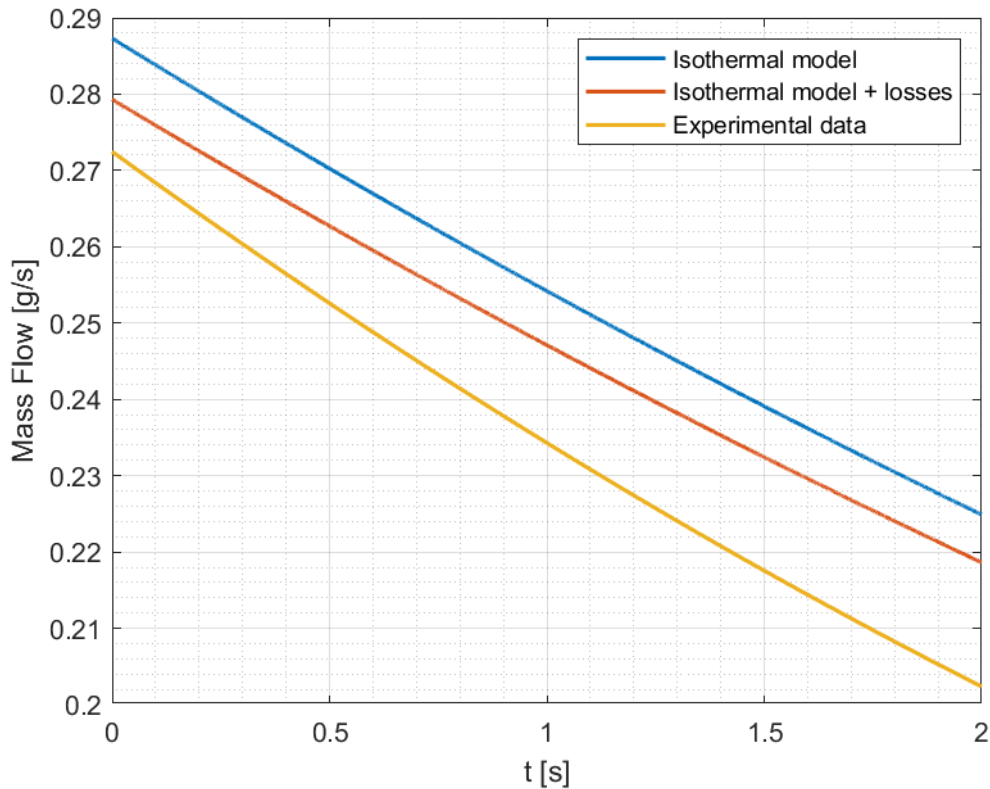


**Figure 4.12:** Methane mass flow comparison

Now that both oxygen and methane mass flow are known from experiments, it is possible to proceed with the oxidizer to fuel ratio calculation. The latter is obtained from pressure values after the preheating time (see figure 4.13), means between  $t = 5\text{ s}$  and  $t = 6\text{ s}$ : in fact after the preheating time methane valve opens and ignition takes place for one second as shown in figure 4.13. The sum of preheating time plus the ignition time forms the range of operation time, which is depicted in figure 4.13 in terms of characteristic blowdown curve pressure over time.

It is important to note how the two curves are quite comparable in terms of local slope: this is a requirement that allows to obtain a O/F trend as much as possible contained in the previously established range.

As a consequence of this O/F, with the boundary conditions chosen, is calculated and presented in figure 4.14. It is possible to see how the ratio tends to increase linearly. Referring to figure 4.13, this is due to the fact that the methane curve is steeper than that of the oxygen approaching  $t = 6\text{ s}$ . The coefficient of discharge  $C_d$  has been assumed equal to 1 for both oxygen and methane. For methane, due to the problems encountered in chapter 2 of the Hot Flow tests, a calibration was carried out which led to the assumption of a discharge coefficient of 1 due to manufacturing tolerances (see subsection 2.4.3).

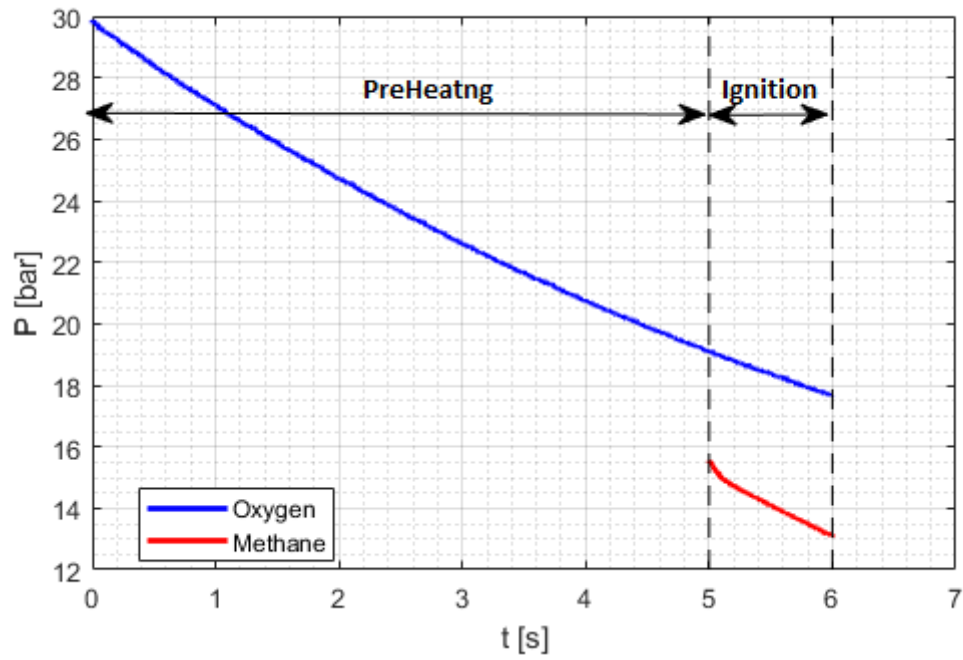


Figure 4.13: Pressure over time during igniter operation time

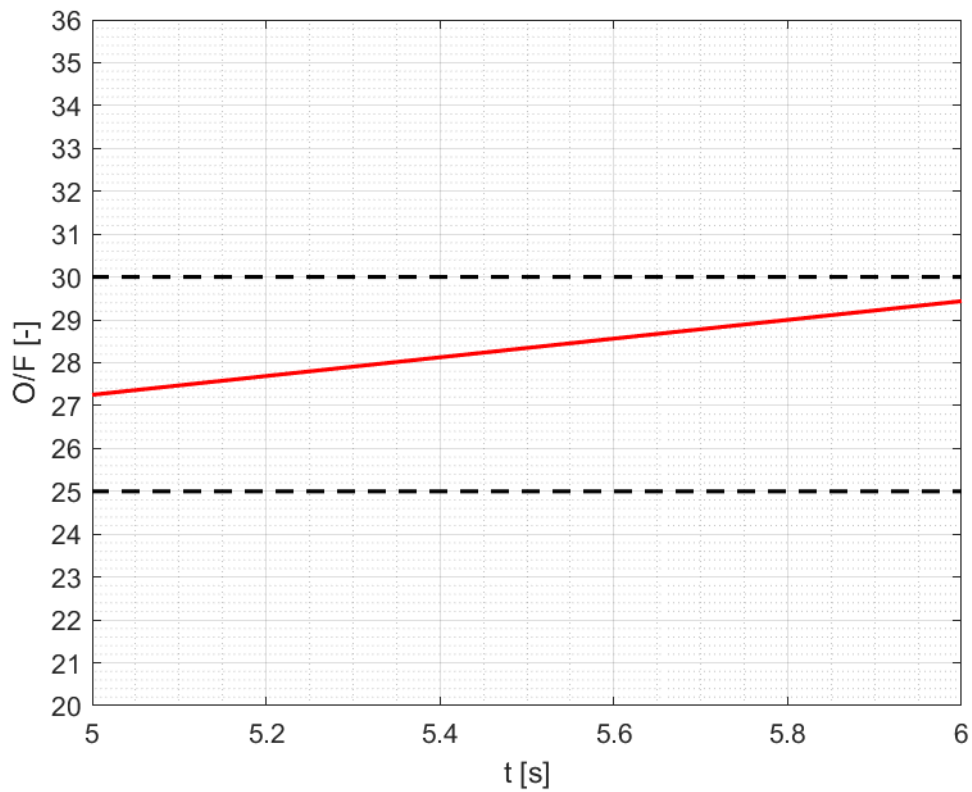


Figure 4.14: Oxidizer to fuel ratio over time

As a result of the calculation of the O/F ratio, the values shown in the table 4.5 have been chosen as oxygen and methane supply pressures. These values were chosen because they provide an O/F ratio within the chosen range for a burning time of 1 second from requirement.

**Table 4.5:** Igniter supply pressure values

$P_{0,oxygen}$	35 [bar]	Oxygen initial pressure in the tank
$P_{0,methane}$	16 [bar]	Methane initial pressure in the tank

## Chapter 5

# Tank design for spacecraft

This chapter aims to design the final tanks using a better model, the isothermal one, which is has been validated thanks to experimental data analysed in chapter 4.

During the pressure regulated test campaign, in particular after hot flow tests, resonator damage occurs. The subsequent cold flow test campaign showed anyway good results in terms of maximum temperature, but it was not possible reduce the preheating time resulting in big tanks for the blowdown test campaign.

Now, expecting resonator is going to perform better in the future due to upgrades, the goal is preheating reduction, resulting in a significant decrease of tank volume and obviously in a considerable weight saving. For the current work the requirement is 1 second of burning time. Therefore this chapter aims to optimize tanks taking into account the burning time requirement and the preheating time requirement of 1 second.

## 5.1 Tank optimisation

The tank optimization, with preheating time reduction, is based on the igniter operating conditions, gathered in the blowdown test campaign. Best performance have been achieved for 35 bar of nominal oxygen supply pressure. By reference to pressure over time plot (see figure 5.1) for that level of pressure it is possible to extrapolate pressure value  $P_2$  at  $t = 5 s$ , i.e after the preheating time.

After this the start value of pressure  $P_1$  is known and it is possible to evaluate the ratio between the latter and  $P_2$ , which correspond to

$$\frac{P_1}{P_2} = \frac{29.85}{19.13} = 1.56 \quad (5.1)$$

As said this value is obtained for a  $\Delta t = 5 s$ . Now the preheating time is reduced to the value from requirement, i.e  $\Delta t = 1 s$ . The matlab isothermal model (A.2), written in the same way as shown in chapter 3, is run with the new boundary conditions.

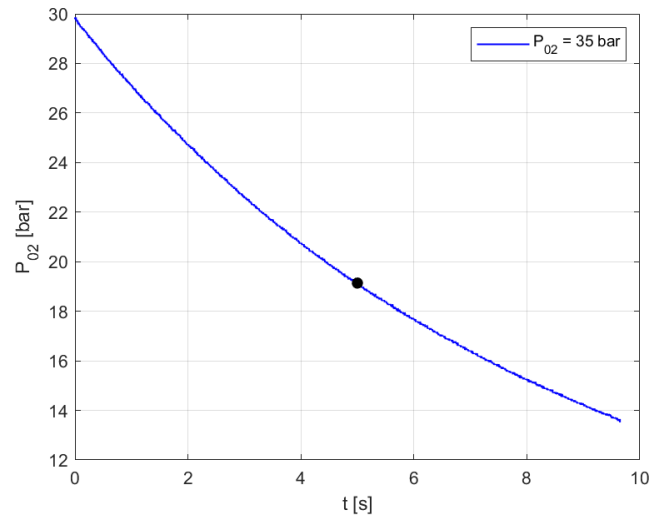


**Figure 5.1:** Temperature over time

With these new conditions ( $P_{up} = 19.13$ ,  $\Delta t = 1 s$ ) the initial pressure of the tank is varied until a value of initial pressure is obtained such that the ratio is equal to  $P_1/P_2$ . Once this ratio has been obtained, the characteristic blowdown curve relative to that ratio is in turn identified in the space of the possible solutions as shown in figure 5.2.

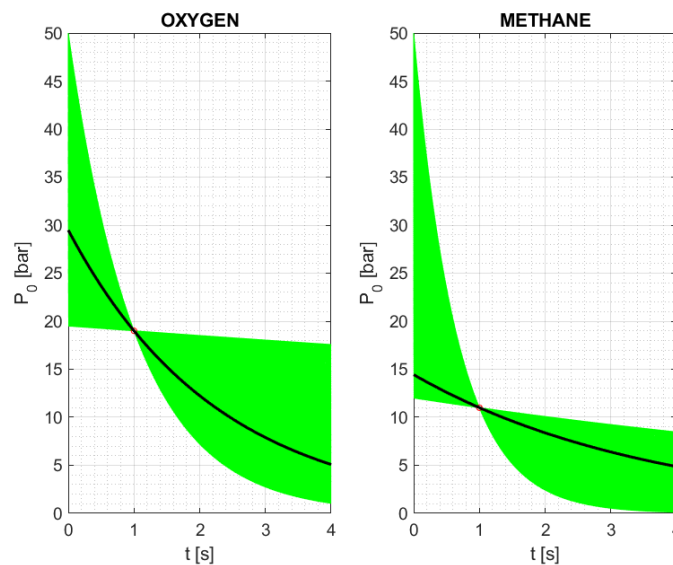


**Figure 5.2:** Pressure over time for different  $P_0$

Consequently are obtained the values of the volume, gas mass and etc for that trend of oxygen pressure.

Following this, the methane tank is sized, choosing the pressure level which gives O/F as much as possible included in the range established in the chapter before.

As a results of this is represented in figure 5.3 pressure over time for both oxygen and methane, during igniter operation. As figure 5.3 shows, the sequence consist of one second of preheating time for oxygen, then methane valve opens and ignition occurs for one second.

Methane volume and initial pressure that offer the best O/F trend is the one represented in figure 5.3.

Consequently the O/F produced is highlighted in figure 5.4. The O/F decrease linearly and approaching two seconds the value the pressure of methane decreases more slowly than the pressure of oxygen. This results in a greater mass flow of methane and a consequent decrease in the oxidizer to fuel ratio.

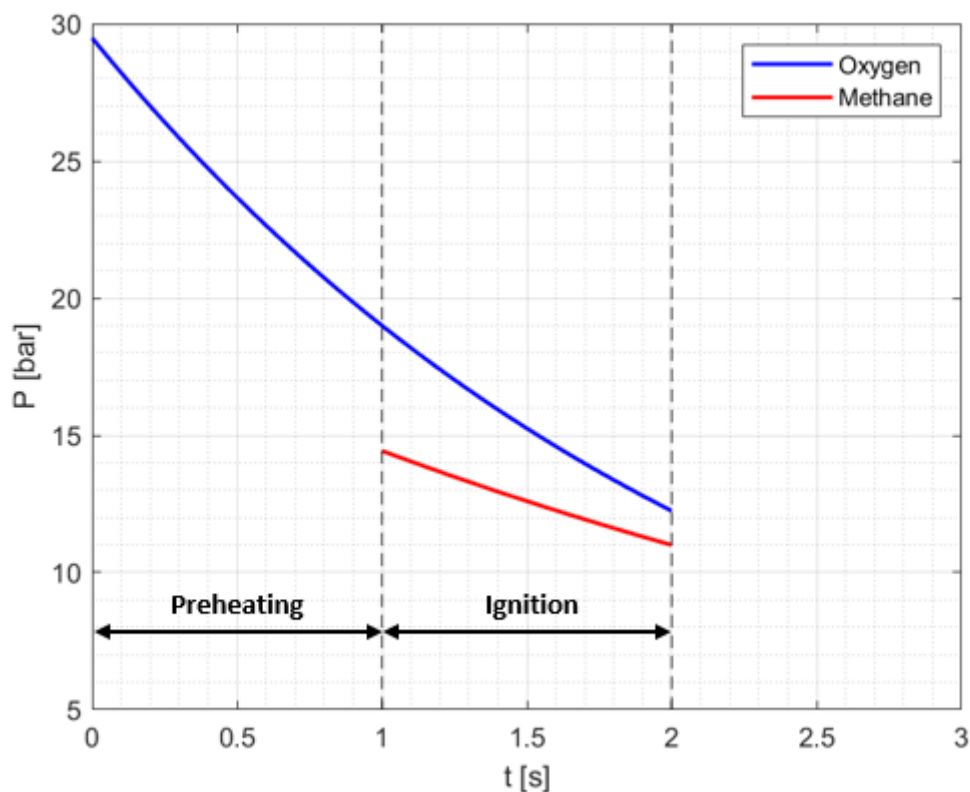


**Figure 5.3:** Pressure over time - igniter operation time

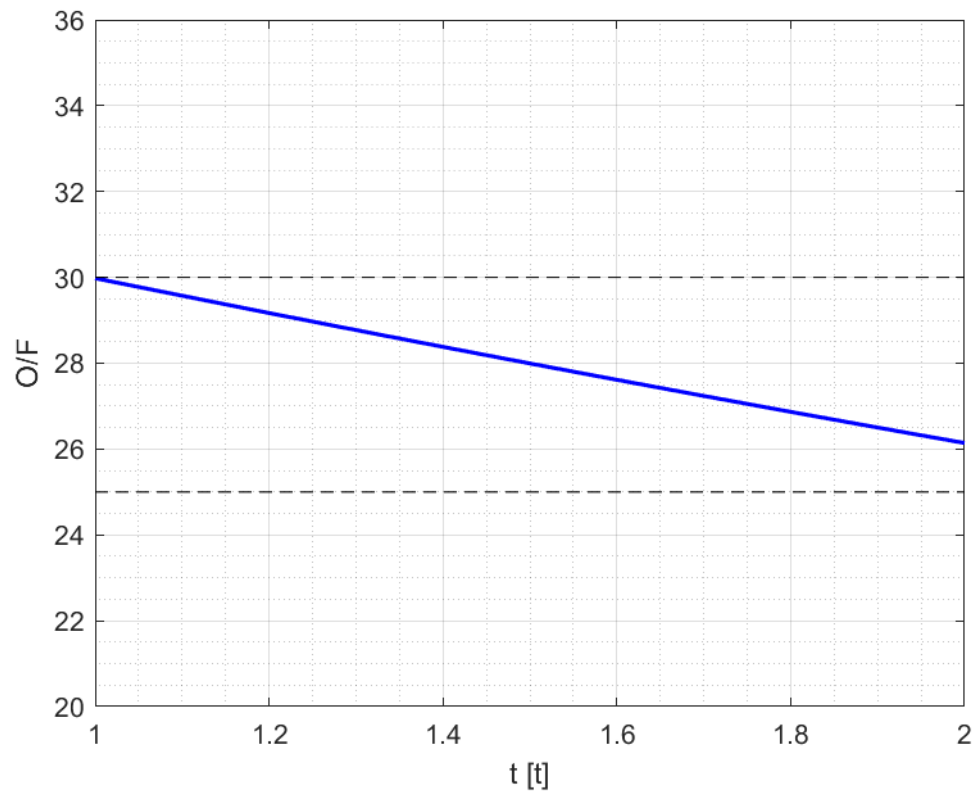


**Figure 5.4:** Oxidizer to fuel ratio

### 5.1.1 Results check

Finally is necessary check if those values chosen constitute points of optimum, in the possible solutions ranges. The aim is weight saving and lowest tanks envelope, never the less gas saving. For this reason, from figure 5.5 to figure 5.7 are brought to light those characteristics over pressure.

Referring to the oxygen, the choice fall in the minimum area, so it means optimum is approximately achieved. On the other hand, methane tank chosen is not in the optimum area: this is due to O/F constraint, which have to included in a predefined range and not allowing to increase more methane pressure. In fact if methane initial pressure is too higher, considering the same conditions for oxygen, oxidizer to ratio decrease since methane mass flow is rising. Expecting new solution for mixing in igniter combustion chamber, other methane pressure levels might be considered in the future. All this has led to the values for the tanks reported in table 5.1.

**Table 5.1:** Tanks design values

		OXYGEN	METHANE
$P_0$	[bar]	29.48	14.43
$V_0$	[L]	0.68	0.10
$T_0$	[K]	298.50	298.50
<i>Gas Mass</i>	[g]	25.78	0.95
$M_{structural}$	[g]	31.89	2.36
$th$	[mm]	0.19	0.05
$r$	[mm]	54.50	29.01
$S_y$	[—]	1.8	1.8
<i>MATERIAL</i>		Ti 6Al-4V	Ti 6Al-4V

Moreover, the methane tank is not in the optimal region because the study of the pressure variation is carried out considering the separate tanks: in the moment in which the coupling of the two is made, the constraint on the O/F must be taken into consideration. On the other hand, however, the methane tank is small compared to the oxygen tank, so it has a small impact on the overall design. In fact, oxygen is the main design drive, while methane has to hold the O/F constraint. This makes it reasonable to accept the values obtained for methane. Referring to the data in the table, as in section 3.4, the wall thickness must be compatible with the manufacturing technology. Therefore, considering a feasible tank,

it will have a greater thickness and will be heavier than that obtained by pure theoretical analysis.

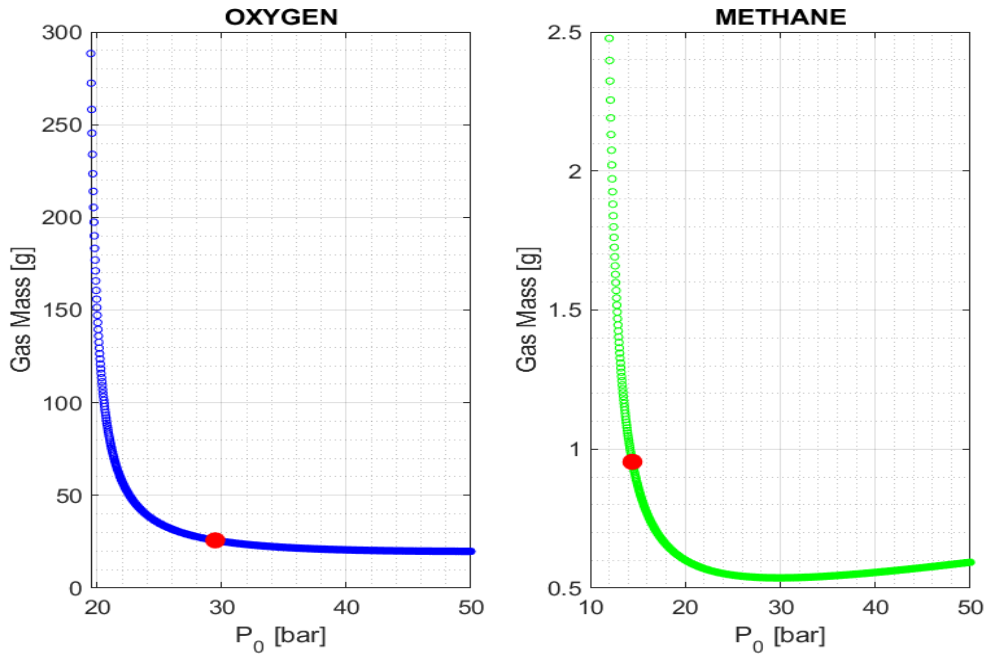


Figure 5.5: Gas mass over initial tank pressure

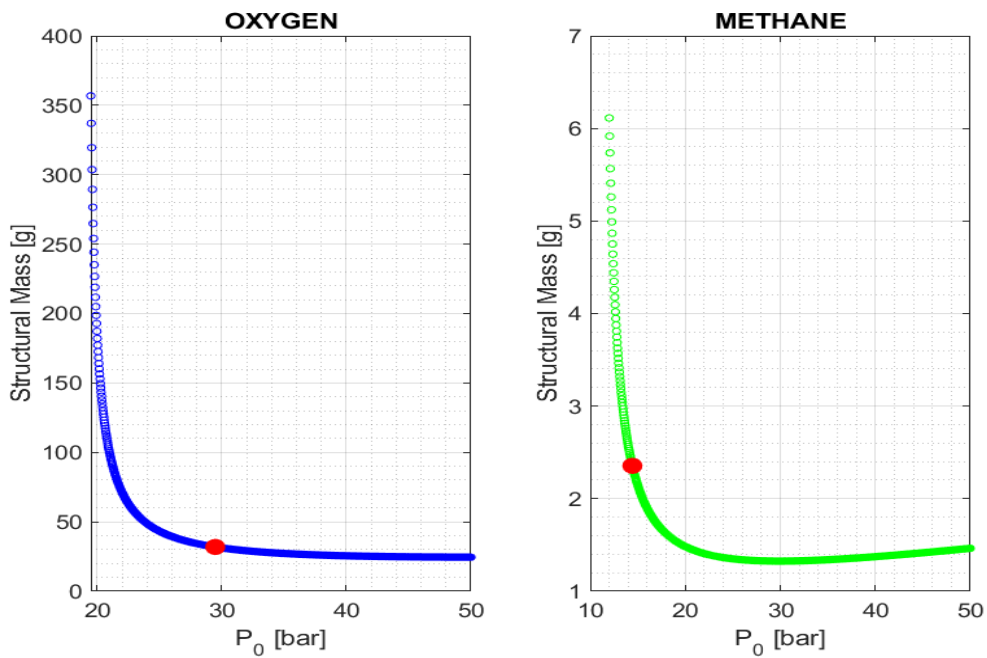
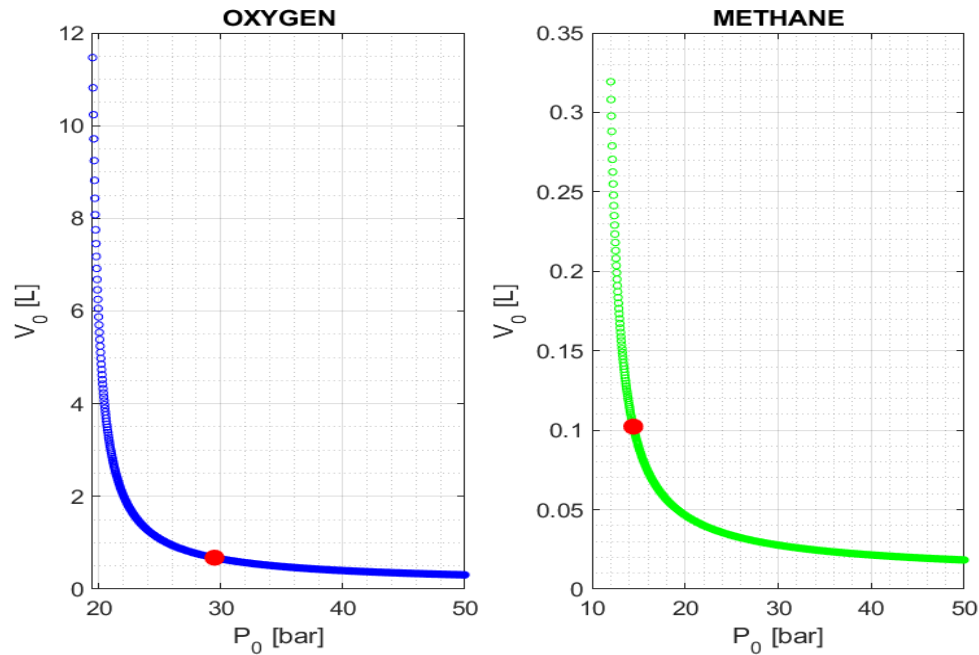


Figure 5.6: Structural mass over initial tank pressure



**Figure 5.7:** Tank volume over initial tank pressure

Furthermore, the igniter is currently not operating at full capacity because it has been damaged. Therefore, it is expected that better performance in terms of resonance heating can be achieved in the future with new solutions in terms of the material used for the construction of the resonator. This will allow further oxygen curves to be obtained. These new curves can be associated with new methane pressure values in order to optimise the tank as much as possible. Concluding in table 5.2 are reported the final values of the tanks design, with the thickness correction in order to take into account manufacturing.

**Table 5.2:** Tanks design values - Thickness correction

		OXYGEN	METHANE
$P_0$	[bar]	29.48	14.43
$V_0$	[L]	0.68	0.10
$T_0$	[K]	298.50	298.50
<i>Gas Mass</i>	[g]	25.78	0.95
$M_{Structural}$	[g]	<b>165.3</b>	<b>46.8</b>
$th$	[mm]	<b>1</b>	<b>1</b>
$r$	[mm]	54.50	29.01
$S_y$	[—]	1.8	1.8
<i>MATERIAL</i>		Ti 6Al-4V	Ti 6Al-4V

## Chapter 6

# Tank heating and filling

Once the tanks parameters are fixed, is therefore a need to integrate tanks and relative fluid system in a spacecraft, with particular regards to the connection with the main propellants tanks. So this chapter aims to:

- 1 Define an heating and filling procedure of the igniter's supply tanks
- 2 Define the method to restore the initial pressure in the igniter's supply tanks

The idea is to equip each tank with an heat exchanger fed with electrical power, as it is possible to see in figure 6.1. With the help of a thermocouple and a pressure sensor, temperature and pressure are detected.

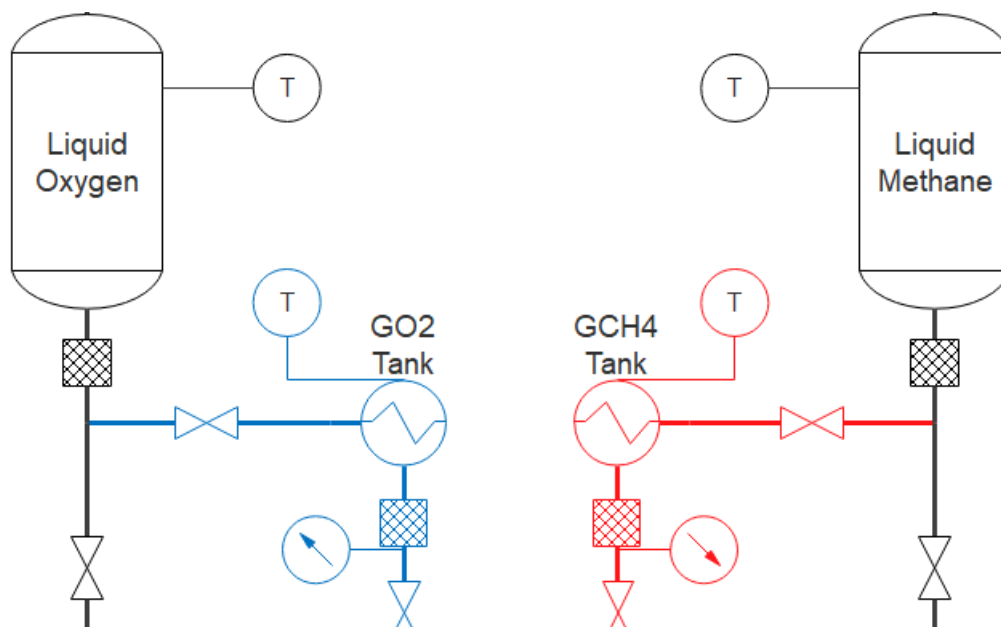


**Figure 6.1:** Extract from fluid system

The procedure consists of open valves upstream GOX and GCH4 and from main tanks fill igniter's vessels with the required amount of propellant. Immediately after that, heat exchangers are activated as long as the desired temperature in the tank is not achieved. The temperature is measured by a thermocouple since in this way, with the method of temperature detection, initial pressure in tanks is re-established. By setting the desired final temperature inside the tank, the enthalpy jump necessary to evaporate the liquid propellant is provided. It is therefore necessary to calculate the enthalpy jump necessary to heat the propellant. This calculation is performed with a function written in matlab (A.4) that gives as output the thermal power necessary to heat up liquid oxygen and methane. By providing the LOX and LCH4 properties as input to the matlab function, thermal power over time is plotted. The output plots are show in figure 6.2 and figure 6.3. The calculation procedure adopted consists of:

- 1 Calculate the pressure of gas inside the tank after ignition is complete: this can be done by evaluating the value of the pressure operating time of the methane and oxygen defined in Chapter 5. These can be read by analysing the pressure curves over time.
- 2 Calculate the temperature in the tanks after ignition
- 3 The residual mass in the tank can be calculated using the pressure, temperature and volume values calculated. Subtracting the latter from the mass initially present, the mass necessary to fill the tank is obtained.

Once the mass necessary is determined, to evaluate the enthalpy necessary to bring the liquid propellant to the desired temperature, the following formula was used:

$$\Delta h = m_p \cdot C_p \cdot (T_f - T_i) \quad (6.1)$$

where  $m_p$  is the propellant mass,  $C_p$  is the specific heat,  $T_f$  is the final temperature and  $T_i$  is the initial temperature. The total enthalpy required will be given by the sum of:

- $\Delta h_1 = m_p \cdot C_p \cdot (T_{boiling} - T_{liquid})$  Enthalpy jump to bring the liquid propellant from the temperature of the main tank to the boiling temperature;
- $\Delta h_2 = \Delta H_{evap} \cdot m_p$  Enthalpy jump to completely evaporate the propellant;
- $\Delta h_3 = m_p \cdot C_p \cdot (T_{design} - T_{boiling})$  Enthalpy jump to bring the gas from the boiling temperature to the desired temperature.

The total enthalpy necessary will be:

$$\Delta h_{tot} = \Delta h_1 + \Delta h_2 + \Delta h_3 \quad (6.2)$$

Then the thermal power TP is obtained as

$$TP = \frac{\Delta h_{tot}}{t_h} \quad (6.3)$$

where  $t_h$  is the heating time. The characteristics of the liquid propellant are reported in table 6.1

**Table 6.1:** Liquid propellant characteristics

		LOX	LCH4
$C_p$	[J/Kg/K]	840	2074
$T_{liquid}$	[K]	80	95
$T_{boiling}$	[K]	134.23	168.27

As a result of this in the table below is reported the enthalpy necessary for the two tanks chosen in chapter 5. The temperature wanted that has to be set is the design temperature, i.e  $T_{design} = 298.5 K$  from requirement. The heating time considered is 10 seconds. Furthermore walls heat losses are assumed be equal to 0. The boiling point of both methane and oxygen was calculated considering main tanks pressurized to 20 bar, with the help of the law of Clausius Clapeyron.

$$\ln\left(\frac{P_B}{P_A}\right) = \frac{\Delta H_{evap}}{R} \left(\frac{1}{T_A} - \frac{1}{T_B}\right) \quad (6.4)$$

**Table 6.2:** Heating results -  $t_h = 10 s$

		Oxygen	Methane
$m_p$	[g]	25.77	0.95
$\Delta h_{tot}$	[kJ]	7.68	0.69
$TP$	[Watt]	767.29	68.74

From the figure 6.2 and figure 6.3 it is possible to see that enthalpy jump increase moving to shorter time of heating. On the other hand, considering longer heating time, it is possible to decrease the enthalpy jump resulting in a thermal power saving.

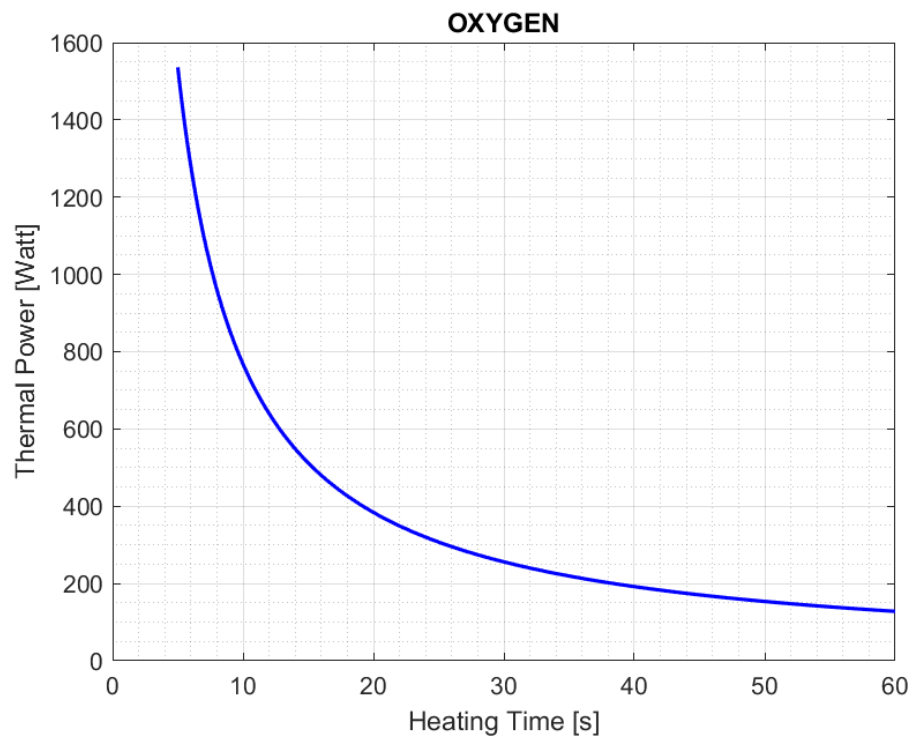


**Figure 6.2:** Thermal power over time -  $t_h = 10$  s

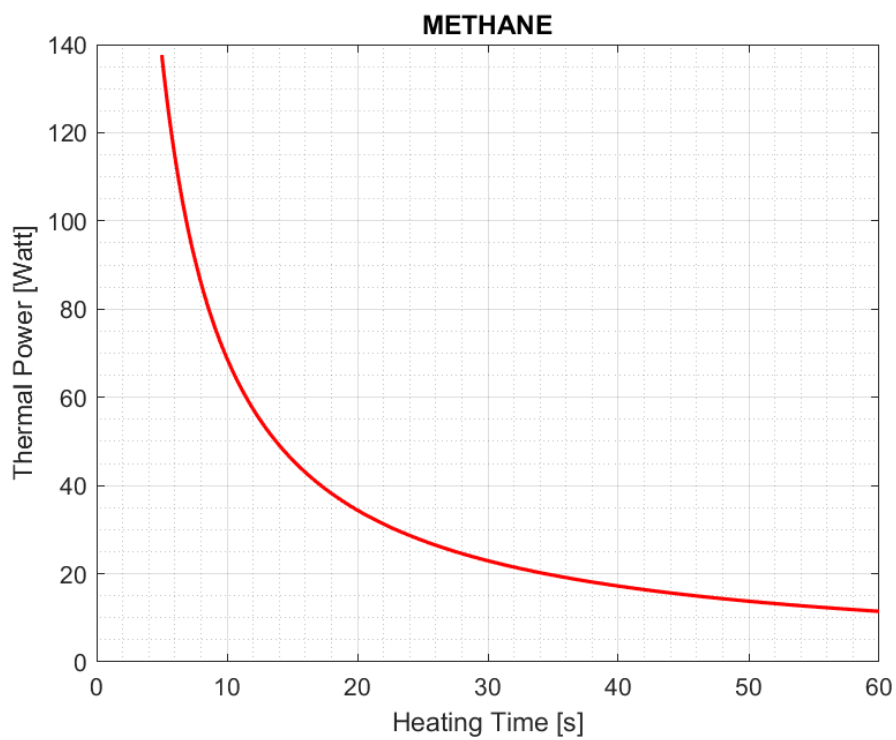


**Figure 6.3:** Thermal power over time -  $t_h = 10$  s

Then it is possible to have a further check if those tanks represent also an optimum in terms of heating. This check is made plotting the thermal power over initial tank pressure. Those are shown in figure 6.4 and 6.5 and, as highlighted in subsection 5.1.1, oxygen fall in a optimum region, in contrast to methane which is not in the range of the best solution. Anyway this was expected since, as said previously, the design driver is the oxygen while methane has to "hold" the O/F constraint.

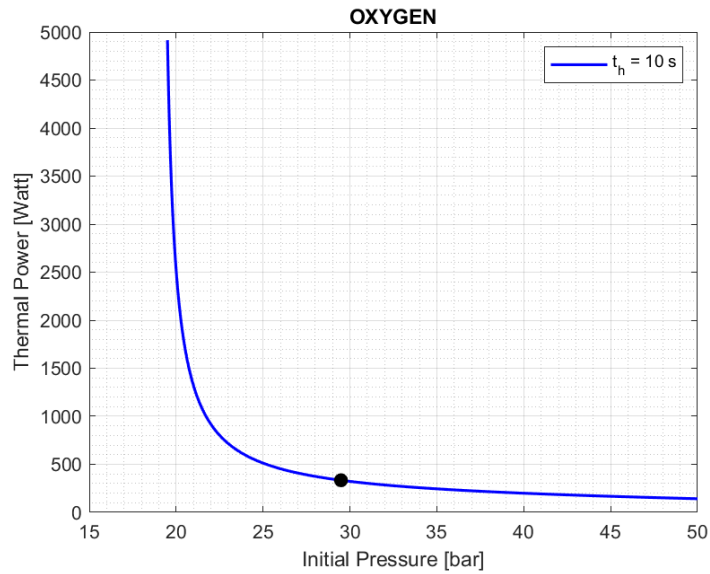


**Figure 6.4:** Thermal power over pressure

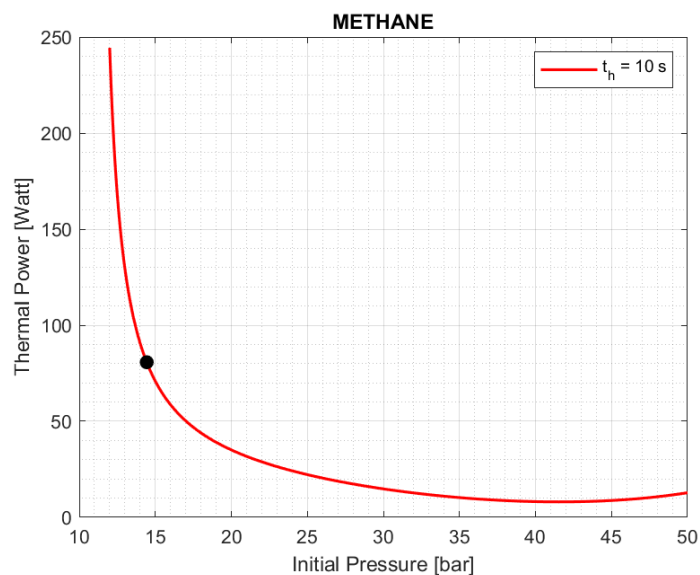


**Figure 6.5:** Thermal power over pressure

Finally, referring to figure 6.6 and figure 6.7, a study of the thermal power depending on the initial pressure of the liquid propellants is investigated. It is possible to see, as expected, that higher temperature in the main propellant tanks correspond to a decrease in thermal power request, since the enthalpy jump is lower.

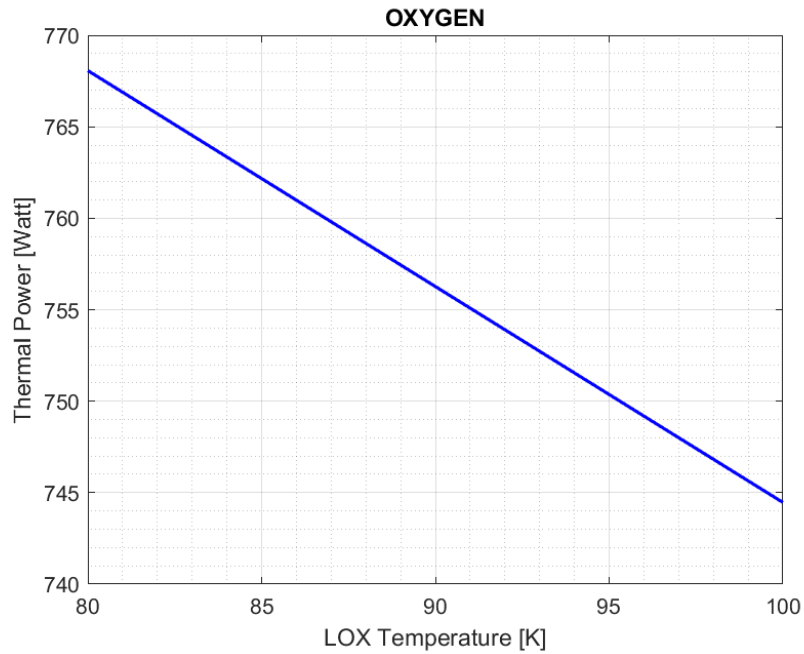


**Figure 6.6:** Thermal power over LOX temperature -  $t_h = 10$  s

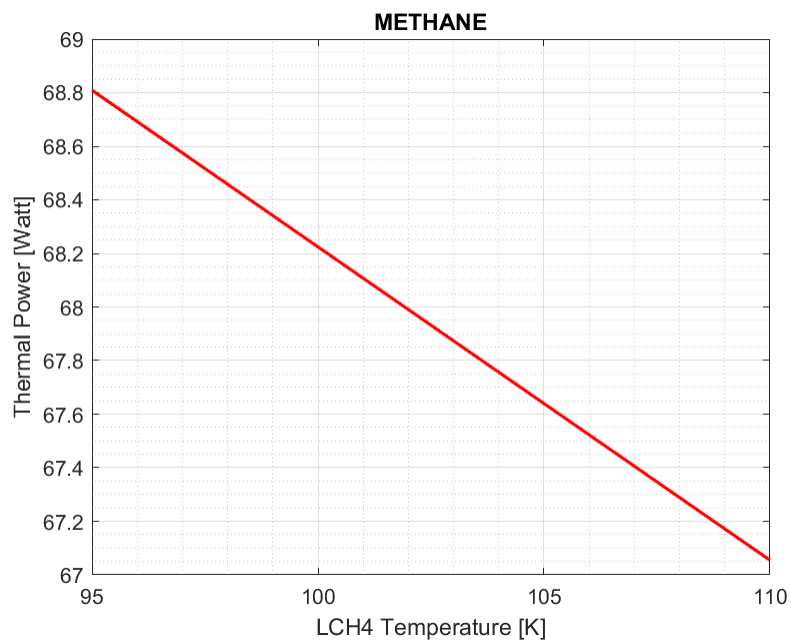


**Figure 6.7:** Thermal power over LCH4 temperature -  $t_h = 10$  s

## Chapter 7

# Conclusions and future prospects

The fluid supply system was designed using tanks operating in blowdown mode. A test campaign with pressure regulator, together with the design data of the igniter, allowed to define an operational envelope. Thanks to this it was possible to study the blowdown system with the adiabatic model: higher pressures mean smaller tanks and an optimum in terms of mass of oxygen and methane was found.

A blowdown test campaign was carried out: good results were found in terms of resonance heating in line with the results obtained in the previous campaign with the pressure regulator. This leads to considering the blowdown system capable of feeding the igniter. In particular, this test campaign allowed to validate the calculation model: it was highlighted that the isothermal model is more relevant to the reality of the phenomenon, unless losses due to the configuration of the system. This allowed to choose the isothermal model for the final design. In this way, with reference to the current performance of the igniter, the thermodynamic characteristics that must have oxygen and methane for an ignition have been defined.

Expecting an improvement in the future of the igniter's performance, on the basis of the validated isothermal model, the preheating time has been reduced for the future calculation in order to optimize the size of the tanks and therefore the overall fluid system dimension reduction. The optimized final tanks were then designed, defined the boundary conditions of oxygen and methane to obtain a mixture ratio capable of achieving an ignition.

Finally, for future spacecraft implementation, the tank filling process was analysed in terms of the power required to evaporate oxygen and liquid methane from the main tanks. An estimate of the power required for the selected tanks led to the conclusion that the optimum in terms of volume brings to have also an optimum in terms of power required.

# Acknowledgements

I would like to thank my supervisor Paul Lungu for his dedicated support, technical advice and review during my thesis work. In particular, I would like to thank him for his continuous availability in clarifications and support during the test session, as thanks to this I was able to grow and improve my technical knowledge.

My thanks are also addressed to Professor Dario G. Pastrone and Professor Oskar J. Haidn for their support and for giving me the opportunity to do this thesis work at the Lehrstuhl für Flugantriebe of the Technische Universität München.

Additionally, my thanks go to my friends who have accompanied me in these years of study at the Politecnico di Torino and especially to those who have shared these six months at the Technische Universität München.

Finally, I want to thank my family for the moral and economic support without which I would not have been able to face and complete this course of study.

# Bibliography

- [1] “U sugli effetti termici nelle valvole di risonanza,” *medie dell’istituto di aerodinamica dell’ETH Zurich*, vol. 21.
- [2] P. Lungu, C. Bauer, and O. J. Haidn, “Operational behaviour investigation of hartmann-sprenger tube based resonance ignition systems for oxygen/methane in-orbit propulsion applications,”
- [3] G. Raman and V. Kibens, “Active flow control using integrated powered resonance tube actuators,” in *15th AIAA Computational Fluid Dynamics Conference*, p. 3024, 2001.
- [4] L. Stabinsky, “Analytical and experimental study of resonance ignition tubes,” 1973.
- [5] C. Bauer and O. J. Haidn, “Design and test of a resonance ignition system for green in-orbit propulsion systems,” in *52nd AIAA/SAE/ASEE Joint Propulsion Conference*, p. 4688, 2016.
- [6] Y.-N. Song, N.-J. Yu, G.-Z. Zhang, M. Bin, W.-L. Zhou, and X. Huang, “Investigation of novel hydrogen/oxygen thruster for orbital maneuver in space station,” *Chinese Journal of Aeronautics*, vol. 18, no. 4, pp. 289–294, 2005.
- [7] A. J. Colozza and L. Kohout, “Hydrogen storage for aircraft applications overview,” 2002.
- [8] C. BAUER, M. HAUSER, and O. J. HAIDN, “Investigation of stabilization effects in hartmann-sprenger tubes,” *TRANSACTIONS OF THE JAPAN SOCIETY FOR AERONAUTICAL AND SPACE SCIENCES, AEROSPACE TECHNOLOGY JAPAN*, vol. 14, no. ists30, pp. Pa\_95–Pa\_100, 2016.
- [9] C. Bauer and O. Haidn, “Numerical investigation of 3d effects in hartmann-sprenger tubes,” in *6th European Conference for Aeronautics and Space Sciences (EUCASS)*, 2015.

- [10] J. Hartmann, "On a new method for the generation of sound-waves," *Physical Review*, vol. 20, no. 6, p. 719, 1922.
- [11] J. Hartmann and B. Trolle, *New investigation on the air jet generator for acoustic waves*. Kongelige Danske videnskabernes selskab, 1926.
- [12] V. Sarohia and L. H. Back, "Experimental investigation of flow and heating in a resonance tube," *Journal of Fluid Mechanics*, vol. 94, no. 4, pp. 649–672, 1979.
- [13] T. J. Smith and A. Powell, "Experiments concerning the hartmann whistle," tech. rep., CALIFORNIA UNIV LOS ANGELES, 1964.
- [14] E. W. Conrad and A. J. Pavli, "A resonance-tube igniter for hydrogen-oxygen rocket engines," 1967.
- [15] B. R. Phillips and A. J. Pavli, "Resonance tube ignition of hydrogen–oxygen mixtures," tech. rep., National Aeronautics and Space Administration, Cleveland, Ohio (USA). Lewis Research Center, 1971.
- [16] J. Kessaev, "Ignition of non-hypergolic propellants," in *Proceedings of the Third International Symposium on Space Propulsion*, pp. 2–4, Beijing, China, 1997.
- [17] Z. Guozhou, S. Yana, Y. Nanjia, T. Xiaoyan, and M. Bin, "Coaxial hydrogen/oxygen gas-dynamic resonance ignition technology for rocket repetitive starting," in *AIAA SPACE 2007 Conference & Exposition*, p. 6157, 2007.
- [18] A. Pavli and B. Phillips, "Resonance tube ignition of hydrogen-oxygen mixtures," 1971.
- [19] M. Niwa, A. Santana, and K. Kessaev, "Development of a resonance igniter for go/kerosene ignition," *Journal of propulsion and power*, vol. 17, no. 5, pp. 995–997, 2001.
- [20] E. Brocher and J.-P. Ardisson, "Heating characteristics of a new type of hartmann-sprenger tube," *International journal of Heat and fluid flow*, vol. 4, no. 2, pp. 97–102, 1983.
- [21] D. K. Huzel, *Modern engineering for design of liquid-propellant rocket engines*, vol. 147. AiAA, 1992.
- [22] J. L. Cannon, "Liquid propulsion: Propellant feed system design," *Encyclopedia of Aerospace Engineering*, 2010.

- [23] A. F. Ardanuy, "Variation of properties during a vessel discharge," *URJ-UCCS: Undergraduate Research Journal at UCCS*, vol. 9, no. 2, pp. 33–40, 2016.
- [24] J. C. Dutton and R. E. Coverdill, "Experiments to study the gaseous discharge and filling of vessels," *International Journal of Engineering Education*, vol. 13, no. 2, pp. 123–134, 1997.
- [25] M. Negahban and the University of Nebraska, "Pressure vessels," 1996.
- [26] D. R. Lide, "Physical constant of inorganic compound," *Handbook of Chemistry and Physics*, vol. 474, 2005.
- [27] N. Valentin Moiseyev, "Titanium alloys. russian aircraft and aerospace application," 2006.
- [28] W. Radtke, "Manufacturing of advanced titanium (lined) propellant tanks and high pressure vessels," in *4th International Spacecraft Propulsion Conference*, vol. 555, 2004.

## Appendix A

## Appendix

### A.1 Function for Cold Flow Blowdown calculations - Adiabatic Model

```
1 function [P_0,mass_gas,t_dim,t_char,P_dim,mass_tank_str,r,th,  
    T_dim,V_0,m_dim,P_up,t_up] = BLOWDOWN_ADIABATIC_CF(R,T_0,  
    P_0,m_dot_req,A_t,k,t_limit,P_e,sigma_y,rho_stru,S,  
    pressure_mesh,time_mesh)  
2  
3  
4 rho_0 = ones(1,pressure_mesh);  
5 v = ones(1,pressure_mesh);  
6 V_0 = ones(1,pressure_mesh);  
7 t_char = ones(1,pressure_mesh);  
8 P_e_dim = ones(1,pressure_mesh);  
9 P_crit_dim = ones(1,pressure_mesh);  
10 t_crit_dim = ones(1,pressure_mesh);  
11 t_dim_upstream = ones(pressure_mesh);  
12 t_dim = ones(pressure_mesh,time_mesh);  
13 P_dim = ones(pressure_mesh,time_mesh);  
14 T_dim = ones(pressure_mesh,time_mesh);  
15 rho_dim = ones(pressure_mesh,time_mesh);  
16 t_unchok = ones(pressure_mesh,time_mesh);  
17 P_dim_unchok = ones(pressure_mesh,time_mesh);  
18 m_dim_unchoked = ones(pressure_mesh,time_mesh);
```

---

```

19 m_dim = ones(pressure_mesh,time_mesh);
20 mass_tank_str = ones(1,pressure_mesh);
21 r = ones(1,pressure_mesh);
22 th = ones(1,pressure_mesh);
23 mass_total = ones(1,pressure_mesh);
24 mass_gas = ones(1,pressure_mesh);
25
26
27 for i = 1:pressure_mesh
28
29     rho_0(i) = P_0(i)/(R*T_0);           % [Kg/m^3] Initial
        gas density in the tank
30     v(i) = 1/rho_0(i);                 % [m^3/Kg]
        Specific volume
31     a_0     = sqrt(k*R*T_0);           % [m/s] Sound
        velocity
32
33
34     t_mass = 0.3;
35     toll = 0.00001;
36     t_up = 0;
37
38     while t_limit - t_up > toll
39
40         t_mass = t_mass + 0.001;
41         mass_gas(i) = m_dot_req*t_mass; % [Kg] Mass of
            Oxidizer for one ignition
42
43         V_0(i) = v(i)*mass_gas(i);     % [m^3] Tank
            volume
44
45         t_char(i) = V_0(i)/(A_t*a_0);  % [s]
            Charchteristic time
46
47         P_e_dim(i) = P_e/P_0(i);      % exit
            pressure dimensionless

```

```

48
49     end_time = 20;
50     t = linspace(0,end_time,time_mesh);           % time
        interval of study
51     t_dim(i,:) = t/t_char(i);                   %
        dimensionless time
52
53
54
55     %%%%%%%%%%%
56     %% OUTPUT %%
57     %%%%%%%%%%%
58
59
60     %% CRITICAL PROPERTIES %%
61     CPR = (2/(k+1))^(k/(k-1));                  % Critical
        pressure ratio P_e/P_crit_dim
62 %     CDR = (2/(k+1))^(1/(k-1));                % Critical
density ratio
63 %     CTR = (2/(k+1));                          % Critical
temperature ratio
64     P_crit_dim(i) = P_e_dim(i)/CPR;           % Pressure
        critical dimensionless
65
66     A = -2*k/(k-1);
67     B = (-k-1)/(2*(k-1));
68     t_crit_dim(i) = ((P_crit_dim(i).^(1/A))-1)/(((k
        -1)/2).*((k+1)./2)^B); % Time critical
        dimensionless (is also the UNchoking time)
69
70     %
        %%%%%%%%%%%
71     P_up = (m_dot_req*sqrt(R*T_0)*(((k+1)/2)^((k+1)
        / (2*(k-1)))))/(A_t*sqrt(k));

```

```

72         t_dim_upsream(i) = (((P_up./P_0(i))^(1/A))-1)/(((
           k-1)/2)*(((k+1)/2))^B);
73         t_up = t_dim_upsream(i)*t_char(i);
74         %
           %%%%%%%%%%%%%%%%%%%%%%%%%%%%%%%%%%%%%%%%%%%%%%%%%%%%%%%%%%%%%%%%%%%%%%%%%%%
75
76         end
77
78     %%% VARIATION OF PROPERTIES OVER TIME IN THE VASSEL %%%
79
80     P_dim(i,:) = (1 + (((k-1)./2).*(((k+1)./2).^((-k-1)./(2*(
           k-1)))))).*t_dim(i,:).^((-2*k)./(k-1));
81     T_dim(i,:) = P_dim(i,:).^((k-1)./k);
82     rho_dim(i,:) = P_dim(i,:).^((1./k));
83
84     %%% CHOKING FLOW %%%                -----> pressure
           ratio lower than CPR
85
86 %     m_dim_choked = sqrt(k)*((k+1)/2)^B;
87
88
89     %%% UNCHOKING FLOW %%%                -----> pressure
           ratio highter than CPR
90
91     t_unchok(i,:) = linspace(t_crit_dim(i),end_time,time_mesh
           );
92     P_dim_unchok(i,:) = (1 + (((k-1)./2).*(((k+1)./2).^((-k
           -1)./(2*(k-1)))))).*t_unchok(i,:).^((-2*k)./(k-1));
93
94     m_dim_unchoked(i,:) = (((2*k)./(k-1))^0.5).*((1-(P_e_dim(
           i)./P_dim_unchok(i,:)).^((k-1)/k)).^0.5).*((P_e_dim(i)
           ./P_dim_unchok(i,:)).^(1./k));
95
96     %%% MASS FLOW RATE %%%
97

```

```

98     m_dim(i,:) = (((2*k)./(k-1))^0.5).*((1-(P_e_dim(i)./P_dim
          (i,:)).^((k-1)/k)).^0.5).*((P_e_dim(i)./P_dim(i,:))
          .^(1./k));
99
100
101     %%%%%%%%%%%
102     %%% TANK SIZING %%%
103     %%%%%%%%%%%
104
105
106     mass_tank_str(i) = (3/2)*S*(rho_stru/sigma_y)*P_0(i)*V_0(
          i);           % [Kg] Structural mass
107     r(i) = (3*V_0(i)/(4*pi))^(1/3);
                                   % [m] Internal
          tank radius
108     th(i) = (S/sigma_y)*(r(i)/2)*P_0(i);
                                   % [m] Thickness
109
110     mass_total(i) = mass_tank_str(i) + mass_gas(i);
                                   % [Kg] Total mass
111
112 end
113 end

```

## A.2 Function for Cold Flow Blowdown calculations - Isothermal Model

```

1 function [P_0,mass_gas,t_dim,t_char,P_dim,mass_tank_str,r,th,
          T_dim,V_0,m_dim,P_up,t_up,rho_dim,rho_0] =
          BLOWDOWN_ISOOTHERMAL_CF(R,T_0,P_0,m_dot_req,A_t,k,t_limit,
          P_e,sigma_y,rho_stru,S,pressure_mesh,time_mesh,p_up)
2
3
4 % rho_0 = ones(1,pressure_mesh);
5 % v = ones(1,pressure_mesh);
6 % V_0 = ones(1,pressure_mesh);

```

```

7 % t_char = ones(1,pressure_mesh);
8 % P_e_dim = ones(1,pressure_mesh);
9 % P_crit_dim = ones(1,pressure_mesh);
10 % t_crit_dim = ones(1,pressure_mesh);
11 % t_dim_upsream = ones(pressure_mesh);
12 % t_dim = ones(pressure_mesh,time_mesh);
13 % P_dim = ones(pressure_mesh,time_mesh);
14 % T_dim = ones(pressure_mesh,time_mesh);
15 % rho_dim = ones(pressure_mesh,time_mesh);
16 % t_unchok = ones(pressure_mesh,time_mesh);
17 % P_dim_unchok = ones(pressure_mesh,time_mesh);
18 % m_dim_unchoked = ones(pressure_mesh,time_mesh);
19 % m_dim = ones(pressure_mesh,time_mesh);
20 % mass_tank_str = ones(1,pressure_mesh);
21 % r = ones(1,pressure_mesh);
22 % th = ones(1,pressure_mesh);
23 % mass_total = ones(1,pressure_mesh);
24 % mass_gas = ones(1,pressure_mesh);
25
26
27 for i = 1:pressure_mesh
28
29     rho_0(i) = P_0(i)/(R*T_0);           % [Kg/m^3] Initial
        gas density in the tank
30     v(i) = 1/rho_0(i);                 % [m^3/Kg]
        Specific volume
31     a_0 = sqrt(k*R*T_0);               % [m/s] Sound
        velocity
32
33
34     t_mass = 0.3;
35     toll = 0.00001;
36     t_up = 0;
37
38     while t_limit - t_up > toll
39

```

```

40         t_mass = t_mass + 0.001;
41         mass_gas(i) = m_dot_req*t_mass;           % [Kg] Mass of
           Oxidizer for one ignition
42
43         V_0(i) = v(i)*mass_gas(i);               % [m^3] Tank
           volume
44
45         t_char(i) = V_0(i)/(A_t*a_0);            % [s]
           Charchteristic time
46
47         P_e_dim(i) = P_e/P_0(i);                % exit
           pressure dimensionless
48
49         end_time = 20;
50         t = 0:time_mesh:end_time;               % time interval
           of study
51         t_dim(i,:) = t/t_char(i);                %
           dimensionless time
52
53
54
55         %%%%%%%%%%%%%%%%%%%%%%%%%%%%%%%%%%%%%%%%%
56         %%% OUTPUT %%%
57         %%%%%%%%%%%%%%%%%%%%%%%%%%%%%%%%%%%%%%%%%
58
59
60         %%% CRITICAL PROPERTIES %%%
61         CPR = (2/(k+1))^(k/(k-1));              % Critical
           pressure ratio P_e/P_crit_dim
62 %         CDR = (2/(k+1))^(1/(k-1));            % Critical
           density ratio
63 %         CTR = (2/(k+1));                      % Critical
           temperature ratio
64         P_crit_dim(i) = P_e_dim(i)/CPR;         % Pressure
           critical dimensionless
65

```

```

66         A = -2*k/(k-1);
67         B = (-k-1)/(2*(k-1));
68         t_crit_dim(i) = log(P_crit_dim(i))/(-((k+1)/2)^B)
           ; % Time critical dimensionless (is also the
             UNchoking time)
69
70         %
           %%%%%%%%%%%%%%%%%%%%%%%%%%%%%%%%%%%%%%%%%%%%%%%%%%%%%%%%%%%%%%%%%%%%%%%%%%%
71         P_up = p_up; %(m_dot_req*sqrt(R*T_0)*(((k+1)/2)
           ^((k+1)/(2*(k-1)))))/(A_t*sqrt(k));
72         t_dim_upsream(i) = log(P_up./P_0(i))/(-((k+1)/2)^
           B);
73         t_up = t_dim_upsream(i)*t_char(i);
74         %
           %%%%%%%%%%%%%%%%%%%%%%%%%%%%%%%%%%%%%%%%%%%%%%%%%%%%%%%%%%%%%%%%%%%%%%%%%%%
75
76         end
77
78         %%% VARIATION OF PROPERTIES OVER TIME IN THE VASSEL %%%
79
80         P_dim(i,:) = exp(-((k+1)./2).^((-k-1)/(2*(k-1))).*t_dim(
           i,:));
81         T_dim(i,:) = P_dim(i,:).^((k-1)./k);
82         rho_dim(i,:) = P_dim(i,:).^((1./k));
83
84         %%% CHOKING FLOW %%%                -----> pressure
           ratio lower than CPR
85
86 %         m_dim_choked = sqrt(k)*((k+1)/2)^B;
87
88
89         %%% UNCHOKING FLOW %%%                -----> pressure
           ratio higher than CPR
90

```

```

91     t_unchok(i,:) = linspace(t_crit_dim(i),end_time,time_mesh
        );
92     P_dim_unchok(i,:) = (1 + (((k-1)./2).*((k+1)./2).^((-k
        -1)/(2*(k-1))))).*t_unchok(i,:).^((-2*k)/(k-1));
93
94     m_dim_unchoked(i,:) = (((2*k)/(k-1))^0.5).*((1-(P_e_dim(
        i)/P_dim_unchok(i,:)).^((k-1)/k)).^0.5).*((P_e_dim(i)
        /P_dim_unchok(i,:)).^(1./k));
95
96     %%% MASS FLOW RATE %%%
97
98     m_dim(i,:) = (((2*k)/(k-1))^0.5).*((1-(P_e_dim(i)/P_dim
        (i,:)).^((k-1)/k)).^0.5).*((P_e_dim(i)/P_dim(i,:))
        .^(1./k));
99
100
101     %%%%%%%%%%%
102     %%% TANK SIZING %%%
103     %%%%%%%%%%%
104
105
106     mass_tank_str(i) = (3/2)*S*(rho_stru/sigma_y)*P_0(i)*V_0(
        i);           % [Kg] Structural mass
107     r(i) = (3*V_0(i)/(4*pi))^(1/3);
                                   % [m] Internal
        tank radius
108     th(i) = (S/sigma_y)*(r(i)/2)*P_0(i);
                                   % [m] Thickness
109
110     mass_total(i) = mass_tank_str(i) + mass_gas(i);
                                   % [Kg] Total mass
111
112 end
113 end

```

## A.3 Function for tanks sizing calculations - Isothermal Model

```

1 function [mass_tank_str,r,th,P_0,V_0] = SIZING(R,T_0,P_0,
      m_dot_req,A_t,k,t_limit,P_e,S,pressure_mesh,time_mesh,yield
      ,density)
2
3
4 rho_0 = ones(1,pressure_mesh);
5 v = ones(1,pressure_mesh);
6 V_0 = ones(1,pressure_mesh);
7 t_char = ones(1,pressure_mesh);
8 P_e_dim = ones(1,pressure_mesh);
9 P_crit_dim = ones(1,pressure_mesh);
10 t_crit_dim = ones(1,pressure_mesh);
11 t_dim_upstream = ones(pressure_mesh);
12 t_dim = ones(pressure_mesh,time_mesh);
13 P_dim = ones(pressure_mesh,time_mesh);
14 T_dim = ones(pressure_mesh,time_mesh);
15 rho_dim = ones(pressure_mesh,time_mesh);
16 t_unchok = ones(pressure_mesh,time_mesh);
17 P_dim_unchok = ones(pressure_mesh,time_mesh);
18 m_dim_unchoked = ones(pressure_mesh,time_mesh);
19 m_dim = ones(pressure_mesh,time_mesh);
20 % mass_tank_str = ones(1,pressure_mesh);
21 % r = ones(1,pressure_mesh);
22 % th = ones(1,pressure_mesh);
23 % mass_total = ones(1,pressure_mesh);
24 % mass_gas = ones(1,pressure_mesh);
25
26
27 for i = 1:pressure_mesh
28
29     rho_0(i) = P_0(i)/(R*T_0);           % [Kg/m^3] Initial
      gas density in the tank

```

```

30     v(i) = 1/rho_0(i);                                % [m^3/Kg]
           Specific volume
31     a_0   = sqrt(k*R*T_0);                            % [m/s] Sound
           velocity
32
33
34     t_mass = 0.3;
35     toll = 0.00001;
36     t_up = 0;
37
38     while t_limit - t_up > toll
39
40         t_mass = t_mass + 0.001;
41         mass_gas(i) = m_dot_req*t_mass;              % [Kg] Mass of
           Oxidizer for one ignition
42
43         V_0(i) = v(i)*mass_gas(i);                   % [m^3] Tank
           volume
44
45         t_char(i) = V_0(i)/(A_t*a_0);                % [s]
           Charchteristic time
46
47         P_e_dim(i) = P_e/P_0(i);                    % exit
           pressure dimensionless
48
49         end_time = 20;
50         t = linspace(0,end_time,time_mesh);         % time
           interval of study
51         t_dim(i,:) = t/t_char(i);                   %
           dimensionless time
52
53
54
55         %%%%%%%%%%%
56         %%% OUTPUT %%%
57         %%%%%%%%%%%

```

```

58
59
60     %% CRITICAL PROPERTIES %%
61     CPR = (2/(k+1))^(k/(k-1));           % Critical
        pressure ratio P_e/P_crit_dim
62 %     CDR = (2/(k+1))^(1/(k-1));       % Critical
density ratio
63 %     CTR = (2/(k+1));                 % Critical
temperature ratio
64     P_crit_dim(i) = P_e_dim(i)/CPR;     % Pressure
        critical dimensionless
65
66     A = -2*k/(k-1);
67     B = (-k-1)/(2*(k-1));
68     t_crit_dim(i) = ((P_crit_dim(i).^(1/A))-1)/(((k
        -1)/2).*((k+1)./2))^B); % Time critical
        dimensionless (is also the UNchoking time)
69
70     %
        %%%%%%%%%%%%%%%%%%%%%%%%%%%%%%%%%%%%%%%%%%%%%%%%%%%%%%%%%%%
71     P_up = (m_dot_req*sqrt(R*T_0)*(((k+1)/2)^((k+1)
        / (2*(k-1)))))/(A_t*sqrt(k));
72     t_dim_upstream(i) = (((P_up./P_0(i))^(1/A))-1)/(((
        k-1)/2)*((k+1)/2))^B);
73     t_up = t_dim_upstream(i)*t_char(i);
74     %
        %%%%%%%%%%%%%%%%%%%%%%%%%%%%%%%%%%%%%%%%%%%%%%%%%%%%%%%%%%%
75
76     end
77
78     %% VARIATION OF PROPERTIES OVER TIME IN THE VASSEL %%
79
80     P_dim(i,:) = (1 + (((k-1)./2).*((k+1)./2).^((-k-1)./(2*(
        k-1))))).*t_dim(i,:)).^((-2*k)./(k-1));

```

---

```

81     T_dim(i,:) = P_dim(i,:).^((k-1)./k);
82     rho_dim(i,:) = P_dim(i,:).^(1./k);
83
84     %%% CHOKING FLOW %%%           -----> pressure
      ratio lower than CPR
85
86 %     m_dim_choked = sqrt(k)*((k+1)/2)^B;
87
88
89     %%% UNCHOKING FLOW %%%       -----> pressure
      ratio higher than CPR
90
91     t_unchok(i,:) = linspace(t_crit_dim(i),end_time,time_mesh
      );
92     P_dim_unchok(i,:) = (1 + (((k-1)./2).*(((k+1)./2).^((-k
      -1)./(2*(k-1))))) .* t_unchok(i,:).^((-2*k)./(k-1));
93
94     m_dim_unchoked(i,:) = (((2*k)./(k-1))^0.5).*((1-(P_e_dim(
      i)./P_dim_unchok(i,:)).^((k-1)/k)).^0.5).*((P_e_dim(i)
      ./P_dim_unchok(i,:)).^(1./k));
95
96     %%% MASS FLOW RATE %%%
97
98     m_dim(i,:) = (((2*k)./(k-1))^0.5).*((1-(P_e_dim(i)./P_dim
      (i,:)).^((k-1)/k)).^0.5).*((P_e_dim(i)./P_dim(i,:))
      .^(1./k));
99
100
101     %%%%%%%%%%%%%%%%%%%%%%%%%%%%%%%%%%%%%%%%%%%%%%%%%%%%%%%%%%%%%%%%%%%%%%%%%
102     %%% TANK SIZING %%%
103     %%%%%%%%%%%%%%%%%%%%%%%%%%%%%%%%%%%%%%%%%%%%%%%%%%%%%%%%%%%%%%%%%%%%%%%%%
104
105
106     mass_tank_str(i,:) = (3/2).*S.*(density./yield).*P_0(i).*
      V_0(i);           % [Kg] Structural mass

```

```

107     r(i,:) = (3.*V_0(i)./(4.*pi)).^(1/3);
                                                % [m] Internal
        tank radius
108     th(i,:) = (S./yield).*(r(i,:)./2).*P_0(i);
                                                % [m] Thickness
109
110 %     mass_total(i) = mass_tank_str(i) + mass_gas(i);
        % [Kg] Total mass
111
112 end
113 end

```

## A.4 Function for Heating calculations

```

1 function [T_boiling_new,index,T_eq,TOTAL,Qtot,TP,m_res] =
    HEATING(mass_gas,R,P_operative,T_operative,P_liquid,
    T_liquid,T_boiling,Lambda,V_0,m_dim,A_t,t_dim,t_char,T_dim,
    t_limit)
2
3 P_standard = 101325; % [Pa]
4 % clausius clapeyron law
5 T_boiling_new = 1/(((R*log(P_standard/20e5))/Lambda)+(1/
    T_boiling)); % Calculation of the new boiling point at the
    different pressure
6
7 if R < 400
8     % oxygen
9     Cpg = (7/2)*R;
10    Cpl = (5/2)*R;
11    Cl = 840;
12    Cg = 918;
13    k = 1.4;
14 else
15    % methane
16    Cpg = 4*R;
17    Cpl = 3*R;

```

```

18     C1 = 2074.1;
19     Cg = 2167.9;
20     k = 1.31;
21 end
22
23 % ADIABATIC WALL WITH RESIDUAL GAS POST-IGNITION
24
25 m_real = real(m_dim.*P_operative'.*A_t./(sqrt(R.*T_operative)
    ));
26 t_real = t_dim.*t_char';
27 T_real = T_dim.*T_operative;
28
29 k = 1;
30 toll = 0.01;
31 t_find = 2;
32 while abs(t_real(1:end,k) - t_find) > toll
33     k = k + 1;
34     index = k;
35 end
36 m_dot_2sec = m_real(1:end,index);
37 T_2sec = T_real(1:end,index);
38 T_res = T_2sec;
39 m_res = m_dot_2sec.*t_limit;
40 m_liq_req = (mass_gas' - m_res);
41
42
43 %%% NO EQUILIBRIUM AT THE BEGINNING %%%
44 for i = 1:length(T_liquid)
45     Q1(:,i) = m_res.*Cpg.*(T_operative - T_res);
46     Q2(:,i) = m_liq_req.*Cpl.*(T_boiling_new - T_liquid(i)) +
        m_liq_req.*Lambda + m_liq_req.*Cpg.*(T_operative -
        T_boiling_new);
47     Qtot(:,i) = Q1(:,i) + Q2(:,i); % [Joule]
48 end
49
50 % termal power

```

---

```

51 heat_time = linspace(5,20,1000); %[second]
52
53 TP = Qtot./heat_time; %[Watt]
54
55 %
    %%%%%%%%%%%%%%%%%%%%%%%%%%%%%%%%%%%%%%%%%%%%%%%%%%%%%%%%%%%%%%%%%%%%%%%%%%%
56
57 % QL = m_liq_req.*Cl.*(T_boiling_new - T_liquid);
58 % QG = m_res.*Cg.*(T_boiling_new - T_res);
59 % Q_vap = m_liq_req.*Lambda;
60 % Q_cond = m_res.*Lambda;
61 %
62 T_eq = 0;%zeros(1,length(T_res));
63 % m_gas = zeros(1,length(T_res));
64 % m_liq = zeros(1,length(T_res));
65 % mx = zeros(1,length(T_res));
66 %
67 %
68 % for i = 1:length(T_res)
69 %     if abs(QG(i)) > abs(QL(i))
70 %         if abs(QG(i)) > (abs(QL(i)) + abs(Q_vap(i)))
71 %             T_eq(i) = (m_liq_req(i).*Cl.*T_liquid -
m_liq_req(i).*Cl.*T_boiling_new + m_liq_req(i).*Cg.*
T_boiling_new - Q_vap(i) + m_res(i).*Cg.*T_res(i))./(
m_liq_req(i).*Cg + m_res(i).*Cg);
72 %             m_gas(i) = m_res(i) + m_liq_req(i);
73 %             m_liq(i) = 0;
74 %         else
75 %             T_eq(i) = T_boiling_new;
76 %             mx(i) = (QL(i) + QG(i))/Lambda;
77 %             m_gas(i) = m_res(i) + mx(i);
78 %             m_liq(i) = m_res(i) - mx(i);
79 %         end
80 %     else
81 %         if abs(QL(i)) > (abs(QG(i)) + abs(Q_cond(i)))

```

```
82 %           T_eq(i) = ( - m_res(i).*Cg.*T_boiling_new +
m_res(i).*Cg.*T_res(i) + Q_cond(i) + m_res(i)*Cl.*
T_boiling_new + m_liq_req(i).*Cl.*T_liquid)./(m_liq_req(i)
.*Cl + m_res(i).*Cl);
83 %           m_gas(i) = 0;
84 %           m_liq(i) = m_liq_req(i) + m_res(i);
85 %       else
86 %           T_eq(i) = T_boiling_new;
87 %           mx(i) = -(QL(i) + QG(i))/Lambda;
88 %           m_gas(i) = m_res(i) - mx(i);
89 %           m_liq(i) = m_res(i) + mx(i);
90 %       end
91 %   end
92 % end
93 %
94 %
95 TOTAL = 0; %[m_gas' m_liq' m_res m_liq_req T_boiling_new*ones
(length(m_res),1) T_res T_eq'];
96
97 end
```